CONDUCTING POLYMERS AS ION TRANSPORT AND SOLID ELECTROLYTE MATERIALS

By

FERNANDO E. LARMAT GONZALEZ

A DISSERTATION PRESENTED TO THE GRADUATE SCHOOL
OF THE UNIVERSITY OF FLORIDA IN PARTIAL FULFILLMENT
OF THE REQUIREMENTS FOR THE DEGREE OF
DOCTOR OF PHILOSOPHY

UNIVERSITY OF FLORIDA

1997

I dedicate this work and dissertation to my parents, brothers, sisters, and wife, who have unconditionally encouraged and supported me throughout all of these years.

ACKNOWLEDGMENTS

I would like to express my sincere thanks to my research advisor Dr. John R. Reynolds, for his encouragement, guidance and support throughout my graduate studies at the University of Florida. He has been a constant source of knowledge and inspiration, and has always made time to give focus and orientation, and at the same time motivation and new ideas to solve scientific problems.

I would also like to thank all the members of the Reynolds' group for their support and discussions throughout all of this time, specially Don Cameron, Peter Balanda, Dr. Seungho Kim, Dr. Balasubramanian Sankaran, Greg Sotzing, David Irvin, Jennifer Irvin, Jerry Reddinger, Dr. Tony Pullen, Shawn Sapp, Dr. Myongho Pyo, Dr. Andrew Child, Dr. Anil Kumar, Dean Welsh and Dr. Mark Morvant.

I would also like to acknowledge the polymer floor members for making my stay enjoyable.

I would also like to thank Dr. Daniel Talham and Candance Seip for collaboration.

Finally, I would also like to thank to Universidad del Valle and Colciencias for their financial support.

This work was supported by grants for the National Science Foundation, AVX Incorporated, and the Air Force Office of Scientific Research.

TABLE OF CONTENTS

LIST OF TABLES

LIST OF FIGURES

Abstract of Dissertation Presented to the Graduate School of the University of Florida in Partial Fulfillment of the Requirements for the Degree of Doctor of Philosophy

CONDUCTING POLYMERS AS ION TRANSPORT AND SOLID ELECTROLYTE MATERIALS

By

Fernando E. Larmat Gonzalez

May, 1997

Chairman: John R. Reynolds
Major Department: Chemistry

The structure-property relationships in a series of poly[1,4-bis(2-heterocycle)-*p*-phenylenes] (PBHPs) and poly[3,12-bis(2-heterocycle)-*p*-dialkylfluorenes] (PBHDFs) as well as the use of polypyrrole (PPy) as solid electrolyte for tantalum capacitors have been investigated.

PBHPs, where the heterocycle is thiophene or pyrrole, and PBHDFs, where the heterocycle is thiophene or ethylenedioxythiophene (EDOT), were synthesized electrochemically and their electrochemical properties studied using cyclic voltammetry. The ion transport characteristics of the polymers were investigated using the electrochemical quartz microbalance (EQCM) while the electronic properties of the polymers were studied using

optoelectrochemical and *in situ* electron paramagnetic resonance (EPR)/electrochemical techniques.

The electrochemical and electronic properties of PBHPs and PBHDFs have been found to be highly dependent on the nature of the heterocycle and on the pendant side groups substituents. Alkoxy substitution on the phenylene rings results in a marked decrease in the monomer and polymer oxidation potentials and a decrease in the electronic band gap. Substitution with long-chain alkoxy groups results in the formation of stable paramagnetic charge carriers at intermediate doping levels. Also, metallic-like character was observed at high doping levels. The presence of electron-rich heterocycles (e.g., pyrrol, EDOT) as terminal electro-polymerizable units on the multi-ring conjugated monomers leads to stabilization of the cation-radical intermediates allowing the electropolymerization to be carried out at low potentials. The ion transport behavior of these polymers under electrochemical switching was found to be anion dominant.

PPy as solid electrolyte for tantalum capacitors was prepared using a combination of chemical and electrochemical methods, antraquinone-2-sulfonate (AQS^-) was used as the dopant ion. The redox properties of PPy were studied by cyclic voltammetry while compositional analysis were carried out using X-ray photoelectron spectroscopy (XPS). UV-Vis spectroscopy was used to check the stability of PPy to spontaneous ion-exchange of AQS^-. The dielectric properties

of the capacitors were measured in order to determine the optimum conditions for PPy deposition.

The capacitors prepared showed excellent high frequency performance up to 100 kHz and long term stability.

CHAPTER 1
INTRODUCTION

1.1 Historical Background

The field of organic conducting polymers began in 1977 with the discovery of the highly conductive doped form of polyacetylene films synthesized by the Shirakawa's method using a Ziegler-Natta polymerization on a glass surface.[1,2] When polyacetylene is oxididatively doped as is shown in Figure 1.1, its conductivity can be systematically and continuously increased over a range of eleven orders of magnitude.

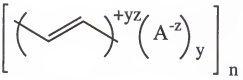

Figure 1.1. Doped polyacetylene.

Although doped polyacetylene has a conductivity which is as high as those of metals on a weight basis, the polymer films are brittle, insoluble, infusible, and unstable in the presence of water and oxygen in both the conducting and insulating forms. This intractability precludes any practical application and limits its usefulness. Despite its environmental instability, polyacetylene is still the simplest conjugated polymer and remains as a model for this

class of materials; thus a significant amount of work has been dedicated to its study.[3]

In order to conduct electricity, a high degree of π overlap is required to allow charge to be delocalized along the polymer chain. In the neutral or undoped form, conjugated polymers are insulators or semiconductors due to the lack of charged carriers. To make them conductive, it is necessary to form mobile charge carriers. This is achieved by the process called redox doping, which is the oxidation or reduction of the polymer using chemical or electrochemical methods. In the presence of an electrical field, these charge carriers move along segments of the conjugated polymer chain and hop between adjacent chains. Charge balance is obtained by the introduction of counter ions (dopant ions) into the polymer matrix. These dopant ions compensate the charges on the polymer and they are immobile throughout the material in the solid state, indicating that conducting polymers are electronic conductors as opposed to ionic conductors.[4]

The driving force behind the development of new conducting polymers has been the possibility of fine tuning their properties; the variety of shapes (films, fibers, powders, *etc.*) in which the polymers can be produced and the weight-based conductivities for the doped polymers can be as high as those of metals. These properties, combined with environmental stability, processability and good mechanical strength, have motivated research in the fields of chemistry, physics, and material science.[5]

The concept of electrical conductivity established for polyacetylene has been extended to a number of polyheterocycle compounds. Monomers such as pyrrole,[6] thiophene,[7] furan,[7a,8] aniline,[9] azulene,[7a,10] indole,[7a,11] carbazole,[12] fluorene,[13] benzene,[14] pyrene,[12,13b,15,] ethylenedioxythiophene (EDOT),[16] and others[17] have been polymerized to yield electrically conducting films which in some instances, exhibit useful environmental stability. Figure 1.2 shows the structures of some of these polymerizable monomers.

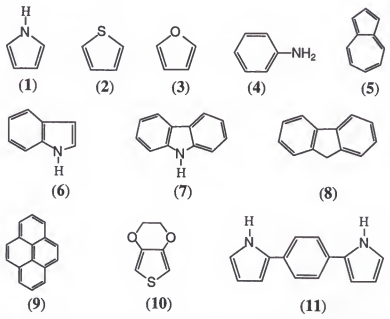

Figure 1.2. Polymerizable monomers. 1) pyrrole, 2) thiophene, 3) furan, 4) aniline, 5) azulene, 6) indole, 7) carbazole, 8) fluorene, 9) pyrene, 10) EDOT, 11) 1,4-bis(pyrrol-2-yl)benzene.

Also, the wide range of possibilities in making heterocycle derivatives has produced a great number of conducting polymers with a variety of properties. This synthetic

flexibility allows the design of polymeric materials in which the polymer properties are controlled at the molecular level. Among the great number of conducting polymers that have been synthesized, polypyrrole, polythiophene and their derivatives are probably the most extensively studied due to their good environmental stability and relatively high conductivity in the oxidized state. Among these heterocycles, thiophene is a structurally versatile molecule, in which long alkyl chains substituted in the 3-position increase the solubility of the polymer without serious detrimental effects on the electronic properties.[18] In the case of poly[1,4-bis(2-heterocycle)-2,5-disubstituted phenylenes], substitution with long alkoxy chains increases the electron density along the π conjugated systems, resulting in a decrease in the monomer and polymer oxidation potentials, and narrowing the electronic band gap relative to unsubstituted or alkyl derivatives.[19] In addition, the use of an electron rich terminal heterocycle (e.g., pyrrole, EDOT) on multi-ring conjugated monomers leads to stabilization of the cation-radical intermediates, allowing the electropolymerization to be carried out at lower potentials.[20] The low polymerization potential eliminates undesirable side reactions (e.g., β-coupling of monomers, crosslinking of the polymer, and overoxidation of the polymer) and allows electrochemical polymerization even in the presence of easily oxidized electrolytes.

Conducting polymers can be prepared by chemical oxidation of the heterocyclic monomer using an oxidizing

agent such as $FeCl_3$, or by electropolymerization in the presence of an electrolyte that supplies the necessary counterions for the charge compensation in the oxidized polymer. A wide range of electrolytes has been used during the electropolymerization of heterocycles.[21] The results indicate that the electrochemical behavior of these conducting polymers depends not only on the type of electrolyte but also on the electropolymerization conditions (solvent, potential, temperature, *etc.*).[22] The main advantages of electropolymerization are that conducting polymer films can be obtained on several conducting substrates (Pt, Au, indium tin oxide, stainless steel, etc.), it is possible to control the film thickness by measuring the deposition charge, and rapid, homogeneous film growth is possible since newly formed polymer contacts a conductive substrate. In addition, the redox doping process is reversible and can be accomplished by switching the potential. The electrochemical switching of a conducting polymer requires ion transport into and out of the film for compensation of the charge carriers on the polymer backbone. It has been demonstrated that the dominant ionic species that migrate during the redox switching can be controlled by the nature of the electrolytes employed in the electropolymerization process.[23] In the case of small anions like Cl^-, ClO_4^-, BF_4^-, *etc.*, these anions will be mobile during subsequent potential switches, and the ion transport mechanism is anion dominant; when the electropolymerization is carried out in the presence of large

anions or polyanions [e.g., poly(styrene sulfonate)], the resulting ion transport mechanism is cation dominant due to the immobility of the dopant. It is important to mention that the ion transport mechanism can be affected by the solution properties of the switching medium, especially the pH of the solution, the solvent, and the presence of other electrolytes.

Polymer electronic and intermolecular structures that are a result of the doping process cause important changes in several polymer properties which are useful for various technological applications.[24] The scope for potential applications includes energy storage as in rechargeable batteries and redox capacitors,[17a,25] electromechanical actuators,[26] electrochromic windows and displays,[27] electromagnetic shielding and antistatic coatings,[28] electrochemically controlled chemical separations and delivery systems,[29] along with sensors and indicators.[30]

Several analytical techniques have been employed to study the properties of conducting polymers. Repeated potential scanning electropolymerization has been employed for the synthesis of polymers, and cyclic voltammetry has been used for the study of the electrochemical properties of the resultant polymers.[6-17] Fast scan cyclic voltammetry has proven to be useful in the study of the electropolymerization mechanism and in the observation of reactive radical-cations at microelectrodes.[31] Spectroelectrochemistry has been used to study the electronic properties of the polymers, especially

to determine the band gap of the polymers.[32] EPR-electrochemistry has been used in the detection of stable paramagnetic charge carriers (polarons) that are formed upon oxidation at intermediate doping levels and their subsequent combination into spinless bipolarons upon complete oxidation.[33] The electrochemical quartz crystal microbalance (EQCM), in combination with impedance analysis has been employed to directly monitor the ion movement into and out of polymer films.[34] In this technique, the frequency change of a gold plated quartz electrode coated with a polymer film is directly related to the mass change caused by the ion movement during potential switches. XPS and SEM have been used to study the effects of electropolymerization conditions (electrolyte, applied potential, current density, *etc.*) on the morphology of the polymer films.[35] The conductivity of polymer films has been generally determined by using the four probe method.[36]

1.2 Electronic Properties of Conducting Polymers

The electronic structure determines the electrical properties of any material and can be explained in terms of band theory.[37] In the solid state, the atomic orbitals of neighboring atoms overlap to form molecular orbitals. These molecular orbitals can be spaced together in a continuous range of energies called energy bands. The difference in energy between the highest occupied molecular orbital (HOMO) in the valence band and the lowest unoccupied molecular

orbital (LUMO) in the conduction band is the band gap (E_g) and is highly dependent on structure. Figure 1.3 illustrates three possibilities that can be obtained depending on how the bands are filled.

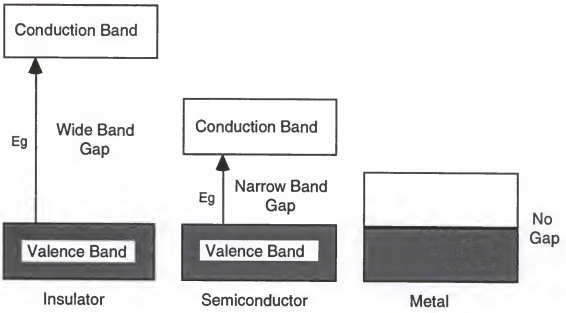

Figure 1.3. Band diagrams according to the band theory.

When the energy gap is too wide, no electrons can cross the gap at room temperature and the solid is an insulator. If the band gap is narrow, electrons can be thermally excited from the valence band to the conduction band giving rise to electrical conductivity, as in the case of classical semiconductors. In the case of metals, the high conductivity is the result of partially occupied bands or a zero band gap. In the case of semiconductors, an increase in conductivity can result from doping by the formation of unfilled electronic bands. When electrons are removed from the top of the valence band during oxidation the process is called p-

type doping, and when electrons are added to the bottom of the conduction band, the process is called n-type doping.

In the case of conducting polymers, electrical conductivity can be obtained without having partially filled or partially empty bands, making conventional band theory inaccurate. In these instances, conductivity has been found to be associated with spinless charge carriers.[38] EPR/electrochemical studies in polyacetylene,[39] polypyrrole,[40] polythiophene,[41] and poly(*p*-phenylene)[42] indicate that the charge carriers are mainly spinless, although the presence of spin carriers has also been found.[43]

Polyacetylene is an special case among the conducting polymers. It has a degenerate ground state (two equivalent resonance forms). In the case of polyheterocycles the resonance forms are not identical and the aromatic structure dominates over the more energetic quinoidal structure as has been demonstrated by theoretical calculations.[44] Figure 1.4 shows the two resonance forms in polyacetylene and the non-degeneracy of polyheterocycles.

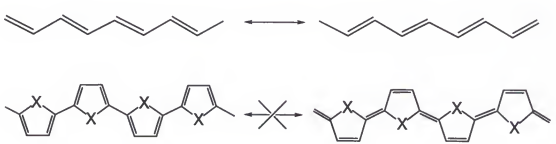

Figure 1.4. Resonance forms of polyacetylene and non-degeneracy of polyheterocycles.

The degeneracy of polyacetylene leads to highly delocalized charge carriers called solitons[38,45] when the polymer is doped by oxidation or reduction as shown in Figure 1.5 for the case of p-doping. The degeneracy in doped poyacetylene also leads to the formation of only one energetic level exactly on the middle of the valence and conduction band. Because the energy of the potential well is the same on both sides of the charge, the soliton is not restricted by deformation energy, as in the case of polyheterocycles, and it is free to move along the polymer chain.

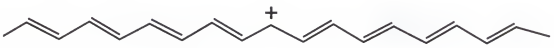

Figure 1.5. Soliton in p-doped polyacetylene.of p-doping.

When a conjugated polymer with a non-degenerate ground state is oxidized by removal of an electron from the top of the valence band, a radical-cation, called a polaron,[38,46] is formed. This polaron is partially delocalized over several monomeric units and a structural deformation produces a localized lattice distortion. Further separation of the radical with the cation is limited because it would generate a further unfavorable lattice distortion. The generation of a polaron also results in a creation of new energy levels, one slightly higher than the valence band and one slightly lower than the conduction band. Removal of another electron from the already oxidized polymer containing a polaron produces a dication, called a bipolaron.[38,46] The formation of polarons and bipolarons during redox switching is illustrated in

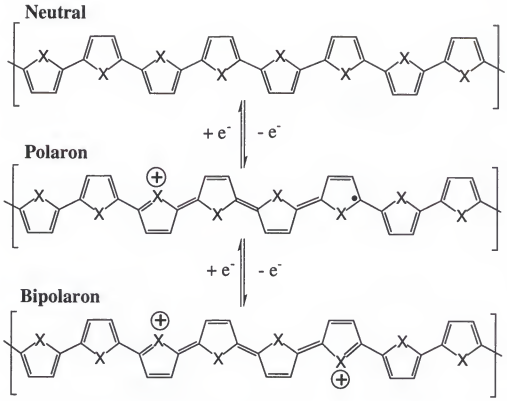

Figure 1.6. Formation of charge carries on polyheterocycles during redox switching (X = S, O, NH).

Figure 1.6 for polyheterocycles. As the oxidation level of the polymer is increased, many bipolarons are formed, and the energies of the bipolaronic states overlap, creating bipolaronic bands. Therefore, at intermediate and high levels of oxidation, it is possible to excite an electron from the valence band to the bipolaronic bands, thus producing electrical conductivity.

The band diagrams for conducting polymers with a non-degenerate ground state are shown in Figure 1.7. In doped polyheterocycles, the more energetic quinoidal form of the bipolaronic species shown in Figure 1.4 will try to return to the aromatic form bringing the positive charges closer to

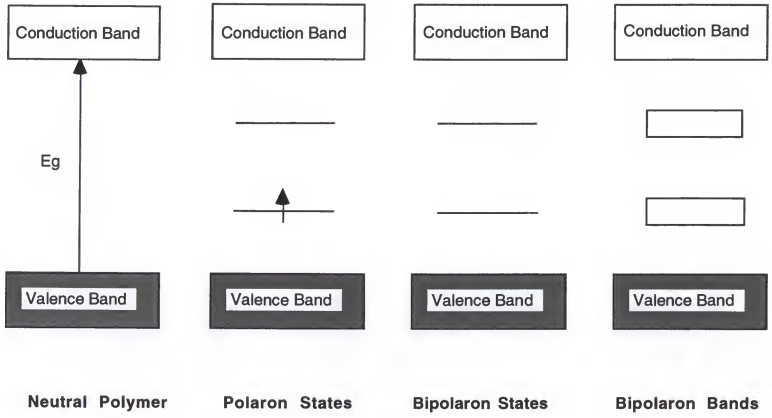

Figure 1.7. Band diagram for conducting polyheterocycles.

each other. The opposite effect of the repulsive force of similar charges and the tendency towards an aromatic structure ultimately determined the number of aromatic rings between any two charges in a polymer chain of a conducting aromatic polymer.

1.3 Electrochemical Polymerization

Conducting polymers can be synthesized by both chemical and electrochemical methods. Chemical polymerizations to form soluble polymers allow processing to free-standing films. Most unsubstituted conjugated polymers though are completely insoluble, precluding the use of these methods. In these cases, powders[47] or films of poor quality[48] are obtained, and they are less ordered than electrochemically prepared films as was shown by X-ray diffraction and transmission electron microscopy.[49] Electrochemical synthesis can produce well-adhered films of insoluble conducting polymers to the electrode surface that are easy to peel off to obtain free standing films. Their properties can be easily studied using several electrochemical techniques, and these modified electrodes can be used in several technological applications.[50] Another advantage of electrochemical polymerization is that the conducting polymer films can be obtained on a variety of electrode materials. The working electrode material must be inert under the anodic conditions used to produce the films. Thus, most conducting polymers are prepared on platinum or gold electrodes. However, films can

also be obtained on other materials such as indium tin oxide (ITO), stainless steel, and graphite. The electropolymerization of heterocycles are achieved at relatively low anodic potentials by using an electrochemical cell containing a solution of the monomer and supporting electrolyte. The polymerization is generally performed using three different methods, each of particular interest. Using constant current conditions, a controlled rate of reaction is ensured and a simple two electrode configuration is used. However, as the polymerization proceeds the potential at the working electrode changes and other electrochemical processes may occur affecting the properties of the polymer. Constant potential conditions are conducted with a three electrode cell consisting of a working, reference and counter electrode, and in this case, the dopant levels tend to be constant throughout the polymerization. Usually, the conductivity of the films varies with the applied potential and there is an optimum potential for producing highly conductive films.[51] The polymerization potential should be adjusted to avoid overoxidation of the polymer,[52] because this process breaks the conjugation along the π system and decrease the conductivity.[53] Finally the polymerization can be achieved by continuously cycling the potential between values at which no polymerization occurs and values at which the monomer is oxidized to form the polymer. This method usually produces more compact films with good electroactive properties, as the formed polymer is continuously switched

between its reduced and oxidized states, and because the concentration of the monomer near the electrode surface remains constant during the time that the electropolymerization is taking place.[9a]

1.3.1 Effect of Solvent and Electrolyte

The selection of solvent and electrolyte affects several aspects of electrochemical polymerizations. Because a conducting medium is necessary for the passage of current, a soluble supporting electrolyte is required. In addition, the polymer has to be insoluble in the solvent while the monomer is soluble in order to allow precipitation from the solution to coat the electrode to produce a polymer film. The solvent must be chemically compatible with the polymerization reaction, and in the case of electropolymerizations at relatively high potentials the sensitivity of the reaction towards nucleophiles must to be considered. The best solvents for the preparation of conducting polymers are aprotic solvents because the nucleophilicity can be maintained at a low level. Acetonitrile is probably the most common solvent for electropymerization, but propylene carbonate, methylene choride, benzonitrile, and nitrobenzene are commonly used. On the other hand, nucleophilic solvents, such as pyridine, dimethylsulfoxide, and dimethylformamide, inhibit the formation of films. Water has also been used in the polymerization of pyrrole,[6,51,54] aniline,[9,55] and EDOT,[16,56] but its use is generally limited due to the insolubility of

the monomers. In some instances, it has been found that small amounts of water influence the rate of polymerization and the properties of polypyrrole films.[57] In the case of thiophene, water inhibits the formation of polymer films by reacting with the as-made polymer, decreasing its conductivity and forming a passivating layer on the electrode.[57b]

The supporting electrolyte not only serves to increase the conductivity of the polymerization medium by providing a high ionic concentration but also serves as the source of dopant ions to compensate the charge carries on the polymer backbone. A high concentration of electrolyte ensures that diffusion of the monomer to the electrode surface controls the polymerization rate and that diffusion limited currents are only a function of the bulk concentration of the monomer. Again the most important considerations in the selection of the electrolyte are solubility, nucleophilicity, and degree of ionization. In aprotic solvents, the most frequently used electrolytes are tetraalkylammonium salts, e.g., tetrabutylammonium perchlorate (TBAP), tetrabutylammoium hexafluorophosphate ($TBAPF_6$), tetrabutylammonium tetrafluoroborate ($TBABF_4$), and tetraethylammoium tosylate, (TEATOS). Nucleophilic anions such as hydroxide, alkoxyde, cyanide, acetate, and benzoate affect the polymerization reaction and give rise to the production of soluble side products that change the composition of the electrolyte solution.[58] The anion of the electrolyte has little effect on the oxidation potential of the monomers, but has a more

important influence on the resultant polymer's electrochemistry,[59] ion transport properties,[23,60] conductivity,[61] morphology,[62] and tensile strength.[59,63]

1.3.2 Mechanism of Electropolymerization

The mechanism of electropolymerization of heterocyclic monomers has been extensively studied but has still not been completely elucidated. The most accepted mechanism is presented in Figure 1.8. The first step involves the oxidation of the monomer at the surface of the electrode to produce the radical cation.[64] With time, the concentration of the radical-cations becomes higher than the neutral monomer at the surface, favoring the radical coupling mechanism as shown in the second step. A competing reaction which involves the coupling between a radical-cation and neutral monomer is also possible.[65] However, the fact that the growth of the polymer is interrupted when the potential applied is decreased below the oxidation potential of the monomer, also supported by theoretical calculations,[66] suggests that coupling of radical-cations is the most probable route.[67] The dication obtained by the coupling of two radical cations subsequently deprotonates to produce the dimer as shown in the third step. This dimer is then oxidized, coupled with a monomeric radical-cation, and deprotonated to form the trimer as presented in the fourth step. As this process continues, oligomers are formed which eventually precipitate onto the

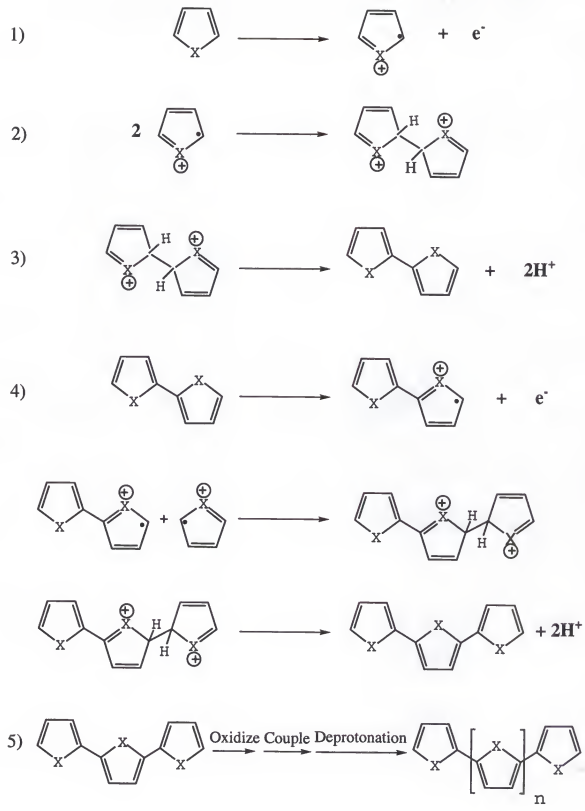

Figure 1.8. Mechanism of electropolymerization of heterocycles.

electrode surface when the solubility limit is exceeded.[68] The presence of soluble oligomers has been detected as well as the proton release during the electropolymerization.[68,69] The precipitated oligomers serve as nucleation sites for polymers to grow.[6e,70] This one-dimensional growth of the film perpendicular to the electrode surface leads to a large numbers of polymer chains and, ultimately, to a more compact and uniform film.[71]

1.4 Ion Transport in Conducting Polymers

Conducting polymers can be reversibly switched between their neutral (insulating) and oxidized (conducting) states. This electrochemical switching requires ion transport into and out of the polymer film to compensate the charge carriers created on the polymer backbone. Some polymers, such as polyacetylene and poly(*p*-pheneylene), can be reduced (n-doped) to generate negative charge carriers or oxidized (p-doped) to produce positive charges through the backbone.[72] In the case of polyheterocycles, p-doping is most common as the reduced forms are quite unstable.

The nature of the electrolytes used during the electropolymerization process determines the dominant ionic species that migrate during redox switching of the polymer.[24,61b,61c] Usually, when the electrolyte contains small anions such as Cl^-, ClO_4^-, BF_4^-, PF_6^-, *etc.*, these anions will be mobile during subsequent redox switches.[60b,73] This mechanism is called anion dominant transport and is shown in

Figure 1.9a. When the electropolymerization is performed in electrolytes containing very large, multivalent anions or polyelectrolytes, such as poly(styrene sulfonate),[61a] poly(vinyl sulfonate),[61a] dodecyl sulfate,[60b] Nafion,[60b] Heparin,[74] copper pththalocyanide tetrasulfonate,[75] etc., the resulting ion transport mechanism is called cation dominant as illustrated in Figure 1.9b. In this case, cations will penetrate the polymer film to compensate the immobilized

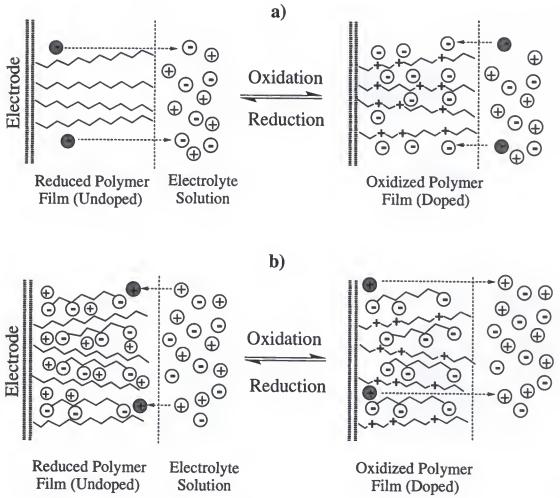

Figure 1.9. Ion transport in conducting polymers: a) Anion dominant transport. b) Cation dominant transport.

multi-anions in the reduced polymer, and they will move out the film during oxidation. Specific ionic transport in conducting polymers is not always the case. In some instances, it has been shown that both anion and cation transport occurs during redox switching.[21,76,77] In addition to electrochemically driven ion transport, spontaneous exchange of dopant anions with anions from the electrolyte solution occurs. The results indicate that the anion incorporated into the polymer during the electropolymerization can be replaced by a variety of anions from the solution.[78]

1.5 Analytical Methods for the Characterization of Conducting Polymers

1.5.1 Standard Electrochemical Methods

1.5.1.1 Cyclic voltammetry

Cyclic voltammetry has been used extensively in the study and characterization of the redox events that occur during electropolymerization and during the electrochemical switching of conducting polymers.[6,17,79] Cyclic voltammetry is an extension of linear sweep voltammetry where a triangular waveform is applied to an electrode immersed in an unstirred solution of freely diffusing electroactive species and the resulting current is measured.[80] The potential is increased linearly until a current maximum (oxidation peak) is obtained and then the potential scan is reversed after the current

maximum has been passed. The scan rate is generally < 100 V/s for conventional electrodes (1-10^{-2} cm^2) and can be > 1000 V/s for microelectrodes (10^{-6}-10^{-8} cm^2). After the peak, the current decays as the surface concentration of the reduced species becomes negligible and further species to be oxidized diffuse from the solution to the electrode surface. This process gives rise to the tailing decrease in the current after the peak. During the reverse scan, the reduction of the recently oxidized species occurs and the current response is again controlled by diffusion. A cyclic voltammogram is characterized by the peak potentials (cathodic, $E_{p,c}$; anodic, $E_{p,a}$), the corresponding peak currents ($i_{p,c}$; $i_{p,a}$), and the difference between the peak potential values (ΔE_p). When the redox process is reversible, the peak current is given by the Randles-Sevcik equation:[81]

$$i_p = (2.69 \times 10^5) n^{3/2} A D^{1/2} C^* \nu \qquad (1\text{-}1)$$

where n is the electron stoichiometry, A is the electrode area (cm^2), D is the diffusion coefficient (cm^2/s), C^* is the bulk concentration (mol/cm^3), and ν is the scan rate (V/s). According to this equation i_p is a linear function of $\nu^{1/2}$ (n,A,D,C^* are constants for a particular case). For a reversible redox process (Nerstian equilibrium), the ratio of the peak currents is equal to unity ($i_{p,c} = i_{p,a}$) and the difference in peak potentials (ΔE_p) is given by $\Delta E_p = E_{p,a} - E_{p,c} = 0.059/n$, which provides an easy way to determine the value of n. Also, the formal reduction potentials, $E^{0'}$ for a reversible couple is the average of the peak potentials,

$E^{0'} = (E_{p,c} + E_{p,a})/2$. Deviations from these values indicate complications related to slow electron exchange of the redox species with the working electrode (kinetic effect) or instability of one of the redox states due to a fast following reaction (chemical effect). For irreversible systems the ΔE_p increase with the scan rate, and in the extreme case of a totally irreversible system, no reduction peak is observed.

The cyclic voltammograms of conducting polymers films on electrode surfaces are different from those of species in solution. The ideal case results when the electrode is coated with a monolayer of an electroactive material. In this case, there is no diffusion of electroactive species to the electrode surface because they are already adhered to the electrode. This situation gives rise to a sharp and symmetrical response, where the decrease of the current response after the peak is as rapid as the increase before the peak, and the ratio of current peaks will be equal to one. For a reversible system, peak to peak separation will be zero, and the increase of this value is an indication of slow electron transfer.

The peak current according to the theory of surface immobilized redox centers is given by[82]

$$i_p = n^2F^2A\Gamma\nu/4RT \qquad (1\text{-}2)$$

where Γ is the total amount of electroactive species present on the electrode surface. According to equation (1-2), the peak current is proportional to the scan rate and not to $\nu^{1/2}$

as in the case of species in solution. Also, the area under the current peaks corresponds to the charge associated with the oxidation or reduction of the adsorbed layer. The surface coverage can be obtain by

$$\Gamma = Q/nF \qquad (1\text{-}3)$$

In the case of non-interacting electroactive sites within the film, the full width at half-maximum, FWHM, of the current peaks should be equal to 90.6/n mV. Increased values of FWHM indicate repulsive interactions between the electroactive sites, while decreased values of FWHM indicate attractive or stabilizing interactions.[83] Also the broadening of the peaks has been explained in terms of small differences in structure, solvation, environment, *etc.* that cause a range of $E^{0'}$ values for the immobilized layer of electroactive sites.[83,84]

Conducting polymer films coated on electrodes represent a non-ideal case because the amount of adsorbed polymer is much larger than a monolayer and the surface coverage is far from uniform. The situation is made more complex due to the large differences in conductivity between the oxidized and reduced states of the polymer. This situation affects the rate of electron transfer and transport through the film, especially when the polymer film is being reduced because electrons must be transferred through reduced and insulating material to reach the electroactive sites that are far away from the electrode surface. This can create isolated regions of oxidized polymer that are difficult to reduce

electrochemically. Therefore, the cyclic voltammograms of conducting polymers are characterized by a significant peak to peak separation that is dependent on film thickness.

Another situation that affect the voltammetric waveshape is the movement of counterions into and out of the polymer film during electrochemical switching. These ions must diffuse to and from the solution to maintain charge neutrality. Therefore, the current response in a cyclic voltammogram will be the combination of effects from the electroactive sites on the film and the diffusion of counter ions. The application of the laws of diffusion to the ion transport through polymer films has been useful for the evaluation of the apparent diffusion coefficients, D_{app}.[60a,85] In the case of large values of D_{app}, low scan rates, or very thin films, the cyclic voltammogram obtained is close to the ideal case of a monolayer film. For the situation of small D_{app}, fast scan rates or thick films, the cyclic voltammogram is more diffusion controlled as the counterions' mobility becomes more important.

Despite the complexity of the situation, cyclic voltammetry has been used extensively in the study of conducting polymers.[6-17] It is a very useful technique for the determination of the redox potential of the polymers, and their stability to redox switching.

1.5.1.2 Chronoamperometry and chronocoulometry

Potential step methods such as chronoamperometry, in which the potential is changed instantaneously between a potential E_1 where no Faradaic process occurs and a potential E_2 where a redox process of interest takes place and the resulting current is recorded as a function of time, have proven useful for the study of polymer redox processes. Also, it is possible to record the charge as a function of time in a potential step process, and in this case the experiment is called chronocoulometry.

During a potential step experiment with electroactive species in solution, the Faradaic process that occurs at potential E_2 decreases the concentration of the reactive species at the electrode surface to zero. This situation creates a concentration gradient that produces, in turn, a mass transport from the bulk solution to the electrode surface that is controlled by diffusion. The expresion for the current that results from semi-infinite linear diffusion is described by the Cottrell equation:[81]

$$i = nFAC^*D^{1/2}/\pi^{1/2}t^{1/2} \qquad (1\text{-}4)$$

According to this equation, the current response is directly proportional to $t^{-1/2}$ with intercept at the origin (test for diffusion control). Also, the diffusion coefficient can be obtained from the slope of the curve.

The charge-time behavior can be obtaineded from the integrated Cottrell equation:[86]

$$Q = 2nFAC^{*}D^{1/2}t^{1/2}/\pi^{1/2} \qquad (1\text{-}5)$$

where Q is the amount of charge (coulombs) that has passed at time, t, since the potential step was applied. A plot of Q vs $t^{1/2}$ will be linear, and again the diffusion coefficient can be obtained from the slope.

The potential step method is useful for the study of electrochemical polymerization, where the charge passed during the oxidation of the monomer is used to estimate the thickness of the polymer film.[87] The potential step method is also used for the study of the redox processes of electroactive polymers. In this case, chronocoulometry is used to calculate apparent diffusion coefficients.[60a,86] This approach has been successful because, after a potential step, equilibrium is reached rapidly at the coated electrode and the counterions follow the semi-infinite linear diffusion conditions within the polymer film.

1.5.2 Optoelectrochemistry

In order to study the electronic properties of conducting polymers, optical spectroscopy has been coupled with electrochemistry in an *in situ* technique called optoelectrochemistry.[88] This technique is very useful in the study of the evolution of the band structure of conducting polymers during electrochemical switching.[89] Due to the extensive π conjugation along the polymer backbone, conducting polymers are highly colored. Thus, optical spectroscopy is an important tool for the characterization of

the electronic structure changes that take place in the polymer during the electrochemical doping. These changes have played an important role in the elucidation of the mechanism of doping and the nature of the charge carrier species in the polymer.[88]

In this technique, a three electrode cell is mounted in a spectrophotometric cuvette. The conducting polymer is coated (either by solution casting or electrochemical methods) on an ITO coated conducting transparent glass. Another piece of ITO glass without polymer film is used in the reference compartment of the spectrophotometer for subtraction of the background absorption. The electrode potential is set to the desired value, and after equilibration, the spectrum is taken. This process is repeated at different potentials until the complete doping range is covered.

The electronic transition between the bands (valence and conduction) and the intragap transitions fall within the UV-Vis-NIR region of the electromagnetic spectra. The electronic transitions allowed in polyheterocycles are presented in Figure 1.10. In the fully reduced state, polyheterocycles have a single absorption band corresponding to the interband transition ($h\nu_1$). The onset energy of this transition is termed the band gap, E_g, in comparison with inorganic semiconductors. As the oxidation of the polymer proceeds, charge carriers are created on the polymer backbone, and new transitions appear. When polarons are created, three more

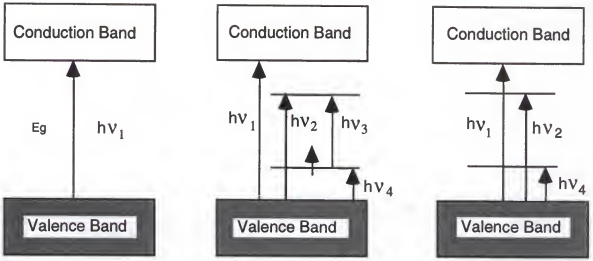

Figure 1.10. Electronic transitions in conducting polyheterocycles.

transitions ($h\nu_2$, $h\nu_3$, $h\nu_4$) are possible. However, in most cases only two more transitions ($h\nu_2$ and $h\nu_4$) are observed due to the formation of bipolaronic states. As the oxidation of the polymer increases, the intensity of the intragap transitions increase, while the intergap transition intensity decreases. In addition, the band gap increases because the bipolaronic energy levels are taken from the band edges.

1.5.3 EPR/Electrochemistry

The simultaneous application of electron paramagnetic resonance, EPR, and electrochemistry has been well established as an important tool in the study of redox processes involving electrochemical generation of active paramagnetic species.[90] EPR is based on detection of the absorption of microwave frequency by species possessing electrons with unpaired spins in the presence of a magnetic

field. The magnetic field produces a splitting of the unpaired electron energy levels. Different energy levels arise from the interactions of the unpaired electron spin moments ($m_s = \pm 1/2$) with the magnetic field (Zeeman effect). The transition energy between the two levels is given by

$$\Delta E = h\nu = g\beta H \qquad (1\text{-}6)$$

where g is the spectroscopic splitting, or g factor (which depends on the orbital and the electronic environment of the electron, for a free electron $g_e = 2.00232$), and β is the electron Bohr magneton, $eh/2m_ec$, which has the value 9.274096×10^{-21} erg/gauss. Hyperfine structure is found in EPR spectra due to additional splitting of the energy levels caused by interaction of the unpaired electrons with the magnetic moments of protons and other nuclei present in the molecule.[91]

In situ EPR/electrochemistry experiments with conducting polymers typically involve deposition of the polymer on a Pt wire, which is inserted in an EPR quartz flat cell bearing a Pt wire counter electrode and a silver wire quasi-reference electrode. This cell is mounted inside the microwave cavity of an EPR spectrometer.[88d,89a,89b] After the electrode potential is allowed to come to equilibrium, the EPR signal is recorded using signal averaging to improve the signal-to-noise ratio. The spin density in the polymer film is determined by double integration of the EPR signal and the use of a reference standard such as α,α-diphenyl-β-picrylhydrazyl, DPPH.

In situ EPR/electrochemistry studies in conducting polymers have been an important tool for the investigation of the relationship between magnetism and redox state, and for the identification of the charge carriers responsible for the polymer conductivity.[92] The observation of the EPR signal intensity while switching the film from neutral to fully oxidized has shown that polarons (charge carriers with spin 1/2) are first formed upon charge injection. Subsequently, the spin concentration decreases as spin pairing occurs in the polaron to bipolaron conversion at higher potentials. Studies of polypyrrole,[93] polyaniline,[94] and polythiophene[95] have found that there is no direct relationship between conductivity and spin concentration at high doping levels. Therefore, it has been concluded that while the magnetic properties are due to polarons, both polarons and diamagnetic bipolarons are involved in the charge transport at intermediate doping levels, and that a higher doping levels bipolarons are the main charge carriers.

1.5.4 Electrochemical Quartz Crystal Microbalance and Impedance Analysis

The quartz crystal microbalance (QCM) is a piezoelectric device used in the detection of very small changes of mass. In the QCM, a thin quartz crystal is sandwiched between two metallic electrodes and a high frequency electric field is applied between them producing a mechanical oscillation of the crystal at its resonant frequency. This resonant

frequency is highly dependent on mass changes of the composite resonator (crystal and electrodes), and also depends on the material properties of any foreign material deposited on the electrodes.[96]

The coupling of the QCM technology with electrochemical techniques is called the electrochemical quartz crystal microbalance, EQCM. In this case, one of the electrodes is used as a working electrode in an electrochemical cell. The EQCM has been used for the detection of minute mass changes during several types of deposition processes such as adsorption of gas phase analytes,[97] and immunological interactions between analytes and complementary antibodies immobilized on the piezoelectric transducer.[98] The EQCM format has been very useful in the study of the mechanism of metal film deposition and dissolution,[99] electrocrystallization,[100] and electropolymerization.[101] Perhaps the most active area of application of the EQCM to electrochemical problems has been the study of compositional and mass changes that occur during the redox switching of electroactive polymers, specifically in the elucidation of the ion transport mechanism of this class of materials.[23,60,102]

The QCM technology is based on the converse piezoelectric effect in which application of a voltage across a crystal with non-centrosymmetric groups produce a corresponding mechanical strain.[96d] The shear motion of the AT-cut quartz resonator, which is obtained by cutting wafers of quartz at *ca.* 35^0 from the z-axis, is produced by

application of an alternating electrical field across the thickness of the crystal. This results in a shear vibration in the x-axis direction parallel to the electric field and propagation of a transverse shear wave through the crystal in the thickness direction. This is represented in Figure 1.11.[96d]

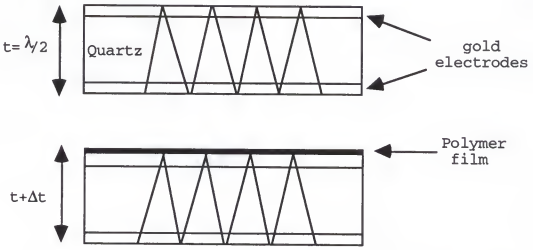

Figure 1.11. Transverse wave in a quartz resonator.

The electric field, the piezoelectric effect, and vibration of the quartz, is therefore confined to the area between the electrodes. As a result, a standing wave condition is established with an acoustic wavelength equal to two times the thickness of the crystal, t_q. The frequency of the acoustic wave in the resonant condition is given by

$$f_0 = v_{tr} / 2t_q = (\mu_q^{1/2} / \rho_q^{1/2}) / 2t_q \qquad (1\text{-}7)$$

where v_{tr} is the transverse velocity of sound in AT-cut quartz, μ_q is the shear modulus (2.947×10^{11} dyne/cm^2), and ρ_q is the density of quartz (2.648 g/cm^3). Increasing the quartz crystal thickness results in an increase in the wavelength ($\lambda=2t_q$) and decrease in the fundamental frequency, f_0. Also,

when a mass is deposited on the crystal that does not increase the effective thickness of the crystal, the density and consequently the frequency decreases. This mass-frequency relationship was established by Sauerbrey and his equation is given by[103]

$$\Delta f = -2f_0^2 \Delta m / A(\rho_p \mu_q)^{1/2} \quad (1\text{-}8)$$

where Δf is the measured frequency shift, Δm is the mass change, and A is the active area of the piezoelectric crystal. Therefore, an increase in the mass per unit area, results in a corresponding decrease in frequency.

The derivation of the mass-frequency relationship relies on the assumption that any deposited material exists only at the antinode of the standing wave, so that the deposit could be treated as an extension of the quartz crystal. The Sauerbrey equation also assumes that there is an uniform distribution of mass on the entire electrode and consequently, a uniform frequency response over the electrode area. This is important since it has been demonstrated that the sensitivity to mass changes decreases from the center to the electrode edge in a monotonic Gaussian mode.[103,104]

The Sauebrey equation is rigorously valid only for infinitesimally thin films that have acoustic impedances identical to that of quartz. In practice it is valid up to loading of *ca.* 10% of the crystal mass.

An impedance analysis method has been developed to compensate for the different acoustic properties of quartz and deposited material.[96d,105] In order to use impedance

analysis, the mechanical model of electroacoustic devices such as AT-cut quartz resonators must be described as an electrical network consisting of inductive, capacitive, and resistive components in series as is shown in Figure 1.12.

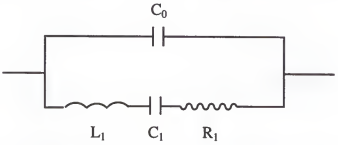

Figure 1.12. Electrial representation of an EQCM resonator.

Here L_1 is the inertial component related to displaced mass during oscillation, C_1 is the compliance for the quartz element representing the energy stored during oscillation, C_0 is the static capacitance of the quartz resonator, and R_1 is the energy dissipation during oscillation due to internal friction, mechanical losses, and acoustic losses due to the surrounding environment. In this model, the maximum surface displacement of a quartz crystal is equivalent to the capacitor charged at its maximum, and the minimum displacement is equivalent to the LCR circuit with a discharged capacitor, and maximum current through the inductor. These parameters become important when the resonator is in contact with a viscoelastic fluid or polymer film. In these cases, C_1 will decrease by increasing the shear modulus, R_1 will increase as a result of increasing the viscosity, and L_1 will increase as a result of increasing the

mass. The properties of the system can be described by the impedance (or admittance) of the resonator:

$$Z = 1/Y, \quad Y = G + jB, \text{ and } |Y| = (G^2 + B^2)^{1/2} \quad (1\text{-}9)$$

where Y is the impedance, Z is the admittance, G is the conductance, and B is the susceptance. The frequency dependent properties of the resonator can be obtained from impedance (or admittance) plots, in which the ordinate represents the imaginary component of the impedance and the abscissa represents the real part. As the frequency is increased, the imaginary part of the admittance (jB) reaches a maximum value at f_1. Upon increasing the frequency further, the real part of the admittance (G) reaches a maximum. This maximum is the point of the resonant frequency of the system. Finally, at frequency f_2, the imaginary part of the admittance reaches a minimum. Although admittance plots are useful, cartesian plots of Z (or Y), B, and G vs frequency are more important for the understanding of the properties of quartz crystals. Figure 1.13 illustrates a typical B-G plot in the resonance region of a AT-cut quartz resonator. The values of f_{Gmax} and f_{Gmin} coincide with f_1 and f_2, the half-power points on the G plot. This plot shows clearly that current flows most easily through the resonator only at frequencies closes to f_{Gmax}. This indicates that quartz crystals behave as bandpass filters, and the bandwidth of the filter (f_2-f_1), also called full width at half height (FWHH), can be used as diagnostic criteria. The conductance spectrum is a useful tool because an increase in f_{Gmax} indicates

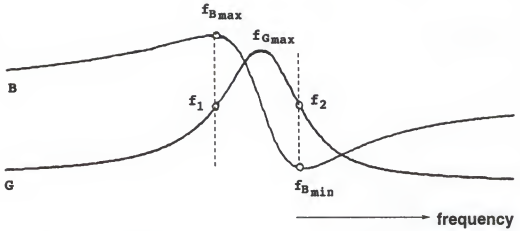

Figure 1.13. Typical B-G plots in the resonance region of a quartz crystal resonator.

changes in the mass at the surface of the quartz crystal while changes in energy dissipation can be obtained from the bandwidth. When an EQCM electrode is immersed in liquid, coated with polymer, or both, a mechanical impedance is introduced, and the corresponding electrical impedance can be obtained. The dependence of the frequency on the density and viscosity of liquids contacting the quartz crystal was found by Kanazawa and Gordon[106] and Bruckenstein and Shay,[107] and their contribution can be incorporated into the Sauerbrey equation to give

$$\Delta f = -2f_0^2(\mu_q\rho_q)^{1/2}\left[(\Delta m)/A + (\rho_L\eta_L/4\pi f_0)^{1/2}\right] \qquad (1\text{-}10)$$

where η_L and ρ_L are the viscosity and density of the liquid respectively. If the product $\eta_L\rho_L$ is constant during an EQCM experiment, the direct relationship between Δf and Δm is still valid. However, polymer films are usually viscoelastic and the contributions of the film viscosity (η_F), film density (ρ_F), and film elasticity (μ_F) to the resonant

frequency must be considered. If the polymer film is rigid during an EQCM experiment, the contributions of $\rho_F\eta_F$ can be neglected. On the other hand, changes in $\rho_F\eta_F$ will affect Δf, G_{max}, and f_2-f_1. Therefore,the extent of the viscous coupling to the polymer film can be qualitatively obtained from the change in the bandwidth.[108]

In summary, the Sauerbrey equation must be used with caution when interpreting frequency changes, especially in the case of polymer films. In this case, ΔF measurement is not sufficient, and contributions from $\rho_F\eta_F$ and film elasticity should be considered. These contributions become more important as the film thickness is increased.[96]

The first application of the EQCM were in the study of electrodeposition of metals onto electrode surfaces,[107] and the determination of the coulombic efficiencies of electrodeposition.[109] The electrochemical dissolution of metal films were examined, showing that the EQCM is an important tool in the study of corrosion processes.[99b,110] The EQCM has also been used to measure the adsorption of electrolytes on the electrode surface,[111] the formation of hydrogen bubbles on thin metal films,[112] the elctrocrystallization of charge transfer salts of several organic cations and anions,[113] the catalytic effect of thin films,[114] and the adsorption and desorption of self-assembled monolayers of organic and organometallic species.[115]

In the field of electroactive polymers, the EQCM has been used extensively since the first report of ion transport

in polypyrrole by Kaufman.[116] Several other redox polymers have been investigated with the EQCM, including poly(vinylferrocene)[117], poly(thionine)[117b,118], and Prussian blue.[119] The electropolymerization and ion transport of conducting polymers have also been the focus of EQCM studies. Reynolds and co-workers[61a,101,102b,120] have studied the electropolymerization of pyrrole and the ion transport behavior during redox switching and cycling of polypyrrole films in different supporting electrolytes. Other polyheterocycles, such as polyaniline,[102a,121] and polythiophene and its derivatives[102c,122] have also been investigated in order to elucidate the ion transport mechanism and the contribution of solvent to the overall mass change. Finally, it has become apparent that impedance analysis plays an important role in EQCM studies, especially those involving viscoelestic films and viscous fluids.[108,123]

1.1.5 Scanning Electron Microscopy

Scanning electron microscopy (SEM) is a widely used analytical technique to obtain images and magnify details that are not visible with an optical microscope. The resolution of a microscope is approximately equal to one-half the wavelength of the radiation used to view the specimen. In the case of a light microscope, the best resolution using light with λ = 400 mn is, therefore 200 nm. SEM uses electrons, as opposed to visible light, as a source of radiation and since electrons are of shorter wavelength (*ca.*

0.1 nm) they are able to produce images with better resolution. With present technology, SEM is able to produce images with resolution on the order of 0.2 nm.[124]

SEM images are obtained by irradiating a sample with a beam of electrons produced by an electron gun. The electrons are accelerated by a high voltage (5-25 kV) and focused on the specimen by electron lenses (electromagnets). The image is constructed from radiation emitted from the specimen during rastering of the specimen by the electron beam. Secondary and backscattered electrons are usually used to image the specimen, although X-rays, Auger electrons, and cathodeluminiscence can also be used.[125] The image produced by SEM can then be manipulated by image-processing techniques to maximize the information obtained. The sample preparation requires that the specimen be placed in a high vacuum before examination in order to remove any volatile materials. Also, when non-conducting specimens are examined, they tend to collect electrons on their surfaces and become negatively charged. As the charge builds up, it repels or deflects the incident electron beam causing image defects. To overcome this problem, samples are usually sputtered with a thin layer (*ca.* 100 Å) of gold or palladium.

SEM is generally used in the study of conducting polymers to obtain information about the surface morphology as a function of the film thickness,[126] the nature of the dopant ions,[62,127] the electrode material,[128] or the redox state of the polymer.[129] The results indicate that polymer

morphology is strongly influenced by the supporting electrolyte used during the synthesis, and by the current density passed during the electropolymerization.[62] Also, film thickness is a determinant parameter of the surface morphology. In the case of thin films (< 10^3 Å) the surface is generally homogeneous, but when the thickness is increased to *ca.* 1 μm, surface defects appear. When the polymer thickness is increased to several microns, usually powdery deposits rather than films are obtained.[126] These structural defects can result as consequence of crosslinking, β-coupling, overoxidation, *etc.*

1.5.6 Conductivity

Electrical conductivity, σ, or its reciprocal, resistivity, ρ, are characteristic parameters of any material and represent the proportionality between current density and the electric field in terms of the Ohm's law. In order to determine the conductivity of a polymer film, a voltage difference between contact probes is measured when a known constant current is passed through the material. Mechanical measurements are also required to determine the dimensions of the film (thickness and width), and the distance between probes.

Conductivity measurements in polymer films are usually made by the two-probe method or the four probe-method.[130] The former is useful for materials with low conductivities in which the resistance of the sample is much larger than the

resistance of the contacts and the measured total resistance is, therefore, the resistance of the sample. In the case of conducting polymers, the four-probe method is preferred because the effect of the contact resistance is minimized. In this method a constant current (e.g., 10^{-6} A) is passed between the external wires and the voltage difference across the internal wires are measured as is illustrated in Figure 1.14.

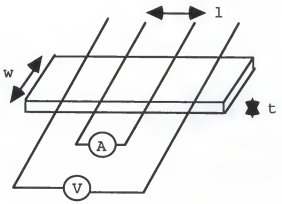

Figure 1.14. Four probe method for conductivity measurements.

The conductivity of the film is given by

$$\sigma(S/cm) = il/Vtw \qquad (1-11)$$

where i is the applied current, V is the measured voltage, l is the distance between the internal wires, w is the width of the sample, and t is the thickness of the film. Conductivity measurements are routinely employed in the characterization of conducting polymers and can be found in almost any paper related to this field.

1.6 Electrochemical Applications of Conducting Polymers

Due to the major changes in a conducting polymer molecular and electronic structure during redox switching, dramatic changes result in several properties which are useful for practical applications. The most important effects for device applications are changes in electronic (optical spectra and conductivity), ion diffusion rates, redox potentials, mechanical moduli and strength, and physical dimensions.

The scope of practical applications includes electrochromic devices (smart windows and displays),[27] rechargeable batteries and redox capacitors,[17a,25] electromagnetic shielding and antistatic coatings,[28] electrochemical sensors and indicators,[30] ion-exchange and separation membranes,[29a-c] conductive textiles,[131] field effect transistors,[132] drug release devices,[29d] electromechanical actuators,[26] and light emitting diodes.[133]

1.6.1 Solid Electrolyte

A very promising application of conducting polymers is their use as solid electrolytes in metal oxide capacitors. Electrolytic capacitors are composed of a very thin film of dielectric oxide anodically formed on the so-called valve metals (Al, Ta, Nb, Zr, *etc.*) and a liquid electrolyte. The electrolyte works as a protecting layer for the dielectric oxide by minimizing the leakage current of the capacitor

through electrochemical oxidation of the metal at any defect of the oxide layer. However, most of the commercial available aluminum electrolytic capacitors have some disadvantages, such as high equivalent series resistance, high impedance at high frequencies and low temperatures, poor thermal stability, and relatively short operation lifetimes, which are a consequence of the use of an ionic solution as an electrolyte with a low conductivity of *ca.* 10^{-2} S/cm. Conventional solid electrolyte capacitors utilize manganese dioxide (MnO_2)[134] as the solid electrolyte layer in contact with the dielectric oxide. The MnO_2 based capacitors still have poor frequency properties due to the low conductivity of MnO_2 (10^{-1} S/cm). Also the organic semiconductor TCNQ has been used.[135] The higher conductivity of TCNQ (*ca.* 1-10 S/cm) results in much better properties at high frequencies, but the process of forming the layer is complex and expensive.

In order to improve the performance of solid electrolyte capacitors at high frequencies (> 10 kHz), the former compounds have to be replaced by a material with higher conductivity. Conducting polymers based on heterocycles have been proposed as excellent candidates for this application because they are inexpensive, more conducting, easy to prepare, and less toxic. Recently, several studies have been published regarding the application of conducting polymers as solid electrolytes in aluminum and tantalum capacitors.[136] Polypyrrole doped with several counterions has been applied as a solid electrolyte using a combination of chemical and

electrochemical synthetic conditions.[136a-b] In addition, capacitors prepared using a combination of MnO_2 and polypyrrole have been studied.[136c]

Despite the progress made in the preparation of conducting polymer capacitors, a better understanding of the interaction between the dielectric layer and the conducting polymer is needed in order to develop a solid electrolyte with optimum properties.

1.6.2 Rechargeable Batteries

Rechargeable batteries were the first commercial products based on conducting polymers. The reasons for this include the facts that conducting polymers have lower densities than metals, exhibit good mechanical properties, and have easily accessed charging and discharging reactions due to the redox doping and undoping of the polymer. During switching there is no dissolution and redeposition of the electrode material and therefore they are dimensionally stable. The main disadvantages of conducting polymers are their lower charge densities compared to metals and their relatively low long term stability when they are deeply discharged and recharged.

Usually, the rechargeable batteries based on conducting polymers utilize polypyrrole, polyaniline, or polythiophene as the cathode material, lithium or a lithium/aluminum alloy as the anode material, and $LiClO_4$ or $LiBF_4$ in propylene carbonate as the electrolyte solution. During battery

discharge, electrons move from the anode to the cathode through an external circuit and reduce the p-doped polymer to the undoped state (neutral). The dopant anions are released from the polymer to the electrolyte solution, at the same time lithium ions are produced at the anode and enter the electrolyte phase. During the charging process, an opposite potential is applied to the electrode causing reoxidation of the polymer along with reinsertion of the dopant ions from the electrolyte while lithium ions are redeposited at the anode as lithium metal.

Various cell configurations have been studied, depending on the kind of polymer used, and the mobile ionic species. The pioneering work of MacDiarmid and Heeger focused on polyacetylene.[137] Later, Bridgestone-Seiko developed button cell batteries based on polyaniline.[25b,138] Varta-BASF investigated polypyrrole based batteries,[139] and Allied-Signal have combined inorganic and conducting polymers as electrode materials.[25a] They also demonstrated functioning rechargeable batteries using n-doped polyphenylene as the anode material, and p-doped polymers such as polypyrrole, polythiophene and polyaniline as the cathode material.[140]

1.6.3 Electrochromic Devices

Electrochromism is the reversible change in color in a material produced during an electrochemical process. The electrochemical doping process that produces the changes in the optical properties of conducting polymers (color and

extinction coefficient) is the removal or addition of π electrons from the polymer backbone and the associated ion transport into and out of the polymer to compensate the electronic charges. Thus, by controlling the doping process, it is possible to control the color of the polymeric material. The optical contrast between the doped and undoped states of a conducting polymer depends on its electronic band gap (E_g) which in turns depends on its molecular structure. When the Eg > 3 eV, the polymer is almost transparent in the undoped state and highly colored in the doped form, but when Eg < 1.7 eV, the polymer is highly colored in undoped form and slightly colored in the doped form.[27d]

Due to the large number of possible molecular structures possible with conducting polymers, a great variety of colors and contrasts have been obtained which make them suitable for electrochromic devices such as smart windows and displays.[27e] The most important parameters to be considered in this application are the optical contrast (difference in the percent transmittance of the oxidized and reduced forms), the electrochromic efficiency (ratio of the variation of the optical density to the injection charge), the switching time (time necessary to switch from one state to the other), and the switching lifetime (number of possible cycles).

An electrochromic display is an electrochemical cell in which the electrochromic electrode and the counter electrode are separated by an electrolyte solution. Because the electrochromic display works in the diffuse reflactance mode,

the counterelectrode can be any material (e.g., lithium) and the electrolyte can be any solution that contains the dopant ions. Since the switching time in an electrochromic display varies from milliseconds, as in the case of watches, to seconds as in the case of information panels, a large number of possibilities are allowed.

In the case of smart windows, which change color in response to temperature or sunlight changes, both electrodes have to be transparent and the electrochromic material colors block or reflect the sunlight as a potential is applied.

The electrochromic properties of many polyheterocycles such as N-substituted pyrroles,[141] polyaniline,[142] polythiophenes and their derivatives[143] have been studied. More recently, a series of EDOT[144] based polymers have been synthesized which have a wide range of colors and useful properties to be used as materials for electrochromic devices.

1.6.4 Electrochemical Sensors

Electrochemical sensors are based on changes in current (amperometric), potential (potentiometric), or conductivity (conductimetric) of the sensing device as a result of the interaction of the analyzed species and the electrode surface.[145] The electrochemical sensing process usually consists of two steps: analyte recognition and signal generation. Conducting polymers are versatile materials in which molecular analyte recognition can be achieved in a

number of different ways. This includes the incorporation of counterions that introduce selective interactions, using the inherent ion-exchange properties of the conducting polymers; the addition of functional groups to the monomers; the codeposition of metals within the polymer, and the incorporation of biorecognition sites such as enzymes, antibodies, and nucleotides. The electroactivity of these materials, as well as their conducting properties, also provides the basis for the signal generation step. Therefore, the changes in electronic properties accompanying any molecular interaction can be readily monitored.

In the case of amperometric sensors, a significant amount of work has been devoted to the development of enzyme biosensors.[146] Particularly, to the detection of glucose by glucose oxidase. The enzyme have been immobilized on the sensor surface by entrapment within electrochemically grown polypyrrole,[147] or by covalent binding of the enzyme to functionalized conducting polymers.[148] The disadvantage with these two approaches is that the amperometric signal is dependent on the shuttling of electrons with the aid of freely-diffusing redox mediators such as oxygen. The third generation of biosensors is based on the covalent binding of enzymes and redox mediators in conducting polymers, in this case a direct communication is established between the enzyme and the electrode via the polymer-bound redox relays (osmium-bipyridine complex or ferroce moieties).[149] Amperometric

sensors for electroinactive anions based on polypyrrole and polyaniline have also been developed.[150]

In the field of potentiometric sensors, both anions and cation selective electrodes have been prepared.[151] They have nernstian and fast response, good reproducibility, and detection limits of *ca.* 10^{-5} M.

Finally, the third kind of electrochemical sensors which utilize conducting polymers are those based on microelectrode arrays in which microband electrodes separated by small gaps are used to construct microelectrochemical transistors.[152] In this case, the microelectrodes are connected by a conducting polymer and any chemical that causes a change in the conductivity of the channel material will cause a change in the drain current at a fixed drain voltage, and thus can be sensed. Several redox switches based on polypyrrole, polyaniline, and poly(3-methylthiophene) have been made for the detection of oxidant anions and oxygen.[153] A more interesting application of the electrochemical transistors is in the preparation of enzyme switches, where the presence of enzymes entrapped in the conducting polymer supplies the required selectivity, in contrast to the poor selectivity found in redox switches. Enzyme switches sensitive to NADH,[154] glucose,[155] pH,[156] and penicillin[156] have been successfully prepared.

1.6.5 Drug Release Devices

The redox properties of conducting polyheterocycles can be used for the electrically controlled binding and release of ions of interest. In the charged or ionic state, the polymer can be loaded with bioactive counterions (ionic drugs). When the polymer is neutralized, the counterions are released into the surrounding medium to perform their pharmaceutical activity. The drug release device would comprise the drug-loaded electrode in contact with a physiological medium (blood, lymph, cerebrospinal fluid, *etc.*), the skin, and a second electrode placed on the skin nearby the first. The amount of ionic drug that is released form the polymer is controlled by the charge passed through the electrical circuit. Other ions (Na^+, Cl^-) will carry the current in the body and back through the skin.[157]

Conducting polyheterocycles can be loaded with anionic drugs by oxidizing the polymer in the presence of the dissolved anionic compounds. Once loaded, cathodic pulses can be used to electrically neutralize the polymer and partially release the bioactive counterions. In order to control the uptake and release of cationic drugs, it is necessary to modify the ion transport properties of the polymer. This is achieved by preparing conducting composite polymers by doping the polyheterocycle with polyanionic electrolytes such as poly(styrenesulfonate), nafion, *etc.* during the synthesis. These composite polymer materials have cation exchange

properties and can act as a binder and releaser of cationic drugs.[158]

The pioneering work in the field of drug release has been made by Miller and co-workers. They have incorporated and released several anions such as glutamate, salycilate, ferrocyanide, TCNQ-, *etc.* from polypyrrole and poly(3-methoxythiophene).[29d,159] Also, the release of cationic drugs such as protonated dopamime, protonated dimethyldopamine, 1-benzylnicotinamine, $Ru(bpy)_3^{+2}$, protonated procaine, methyl viologen, *etc.* have been accomplished by using polymer composites of poly(N-methylpyrrole)/poly(styrenesulfonate) and poly(N-methylpyrrole)/nafion.[160] More recently, Hepel *et al.*[161] have prepared composite polypyrrole films with the biopolymer melanin that incorporates and, subsequently, release a variety of neuroleptic drugs such as chlorpromazine, thiriodizine, trifluoropromazine, and the tricyclic antidepressant imipramine. Also, the controlled released of ATP from polypyrrole films and bilayers of polypyrrole/ATP:poly(N-methylpyrrole)/Heparine have been studied by Pyo *et al.*[74b,162] Although this is a promising application of conducting polymers, the problem of spontaneous release needs to be solved.

1.6.6 Electromechanical Actuators

In order to develop microscopic machines it is necessary to synthesize and characterize materials capable of performing electromechanical work as a result of

conformational changes at a molecular level. A relatively new potential application of conducting polymers has been proposed by Baughman,[27] in which the electrical energy is directly converted into mechanical energy. This application is based on the large dimensional changes that occur in conducting polymers when they are electrochemically doped. Dimensional changes larger than 10% can be obtained by applying voltages on the order of 1 V. The dimensional changes are lower than those of polyelectrolyte gels (up to 50%), but much larger than those obtained with piezoelectric polymers (*ca.* 0.1%) both of which require voltages on the order of 100 V. Conducting polymers can generate much larger stresses than gels or piezoelectric polymers. Conducting polymers can develop forces of 10^2-10^3 kgf/cm^2 that are about two order of magnitude higher than those generated by the other polymeric materials.[24,163]

The possible applications of conducting polymers as electromechanical actuators include microtweezers, microvalves, micropositioners, artificial muscles, *etc.*[164] The main disadvantage of conducting polymers compared to piezoelectric polymers are shorter cycle lifetimes and cycle rates, which are less than 10^6 cycles and in the order of seconds respectively. These parameters can be optimized by the use of very thin films, possibly leading to the development of microactuators based on conducting polymers.

1.7 Outline of Work

The research to be described in this dissertation has been divided into two different projects. In the first project, the structure-property relationships in a series of conducting polymers containing bisheterocycle/*p*-phenylene and bisheterocycle/*p*-dialkylfluorene units were studied. The effect of the heterocycle and pendant side-chain structure on the electronic and electrochemical properties of the polymers was the primary focus of this study. Poly[1,4-bis(2-heterocycle)-p-phenylenes], PBHPs, where the heterocycle is thiophene or pyrrole, and poly[3,12-bis-(2-heterocycle)-9,9-didecylfluorenes], PBHDFs, where the heterocycle is thiophene or EDOT were studied using a combination of electrochemical, spectroscopic, EQCM, and EPR techniques.

The polymers were synthesized electrochemically, and the electrochemical properties were studied using cyclic voltammetry. The redox properties of the polymers were studied in several solvents and electrolytes. The current and mass transport characteristics of the polymers were investigated using the EQCM. Also, conductance spectra were taken in order to confirm the rigid behavior of the films and the validity of the Sauerbrey equation.

Optoelectrochemistry experiments were carried out in order to determine the band gap of the polymers and the evolution of the charge carriers as a function of voltage. *In situ* EPR/electrochemistry was used to detect the presence of

spin-bearing polarons charge carriers at intermediate doping levels.

In the second project, tantalum/tantalum pentoxide (Ta/Ta_2O_5) based capacitors, in which polypyrrole is used as solid electrolyte coating, were prepared and their dielectric properties were analyzed. The polypyrrole was synthesized by combination of chemical and electrochemical polymerization methods. The redox properties of polypyrrole were studied by cyclic voltammetry. Compositional analysis of the polypyrrole coatings were carried out using XPS before and after the re-anodization process used in the capacitors preparation. UV-Vis spectroscopy was used to check the stability of the polypyrrole to spontaneous ion exchange during the re-anodization process. For the chemical polymerization, different synthetic conditions were employed in order to improve the conductivity of the polypyrrole and to reduce the equivalent series resistance (ESR) of the capacitor. The dielectric properties of the capacitors (capacitance, dissipation factor, ESR, and leakage current were measured.

CHAPTER 2
EXPERIMENTAL

2.1 Electrochemical Techniques

In order to study the electropolymerization and redox properties of conducting polymers, several electrochemical techniques were used. In these experiments, a defined potential waveform is applied by using a potentiostat and the resulting current or charge is measured.

2.1.1 Electrochemical Cells and Electrodes

A standard three electrode cell was used in most of the electrochemical experiments carried out during this study. The cell is illustrated in Figure 2.1.

The three electrodes were connected to a potentiostat which controlled the potential of the working electrode relative to a reference electrode which was positioned with its tip near the working electrode. Due to the high input impedance of the potentiostat, the current flows between the working and the counter electrode and a negligible current is drawn through the reference electrode. Since no current is passed through the reference electrode, its potential remains constant and the iR drop between the working and reference electrode is negligible. The counter electrode used in all

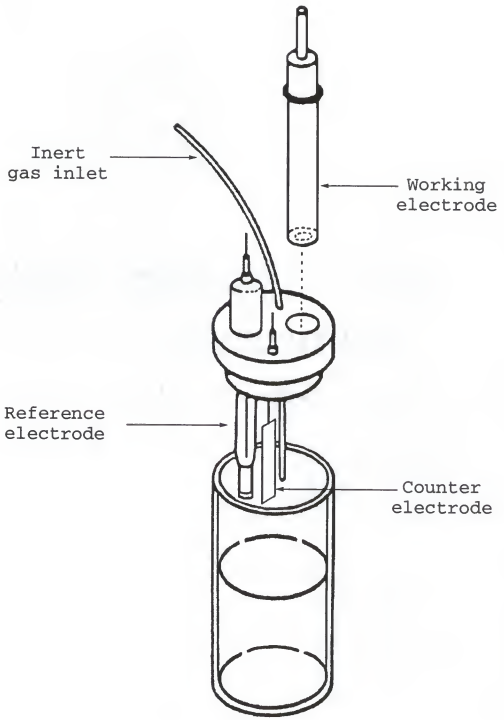

Figure 2.1. Three electrode cell.

cases was a platinum plate (Aldrich). A Ag/Ag^+ reference electrode was used for non-aqueous solutions. This electrode consists of a silver wire immersed in a 0.01 M solution of $AgNO_3$ (Fisher), and 0.1 M tetrabutylammonium perchlorate (TBAP) (Aldrich), separated from the external electrolyte solution by a wafer of vicor porous glass attached with teflon heatshrink tubing (Bionalytical Systems). The standard electrode potential of Ag/Ag^+ is 0.473 V vs standard hydrogen electrode, SHE, the electrode was calibrated using a ferrocene standard solution (0.2 M $LiClO_4$ and 5 mM ferrocene). In the case of aqueous solutions (e.g., electropolymerization of pyrrole), a Ag/AgCl reference electrode was used. This electrode consists of a silver wire coated with AgCl immersed in a 3 M KCl solution and separated from the external electrolyte solution by a vicor tip (Bioanalytical Systems). The standard electrode potential of Ag/AgCl is 0.223 V vs SHE. For *in situ* measurements (e.g., optoelectrochemistry and EPR/electrochemistry) a silver wire quasi-reference electrode was used due to size limitations in both cells. A silver wire has a 0.3 V lower electrode potential than Ag/Ag^+ in a 0.1 M $TBAP/CH_3CN$ solution.

The working electrodes used in this study were Pt, Au, and ITO. Their specific characteristics depend on the type of experiment. For electrochemical polymerization and study of the redox properties of the conducting polymers, Pt button electrodes with an area of 0.02 cm^2 (Bioanalytical Systems) were used. The electrodes were cleaned by polishing them with

fine grind Cerium Oxide Polish (Janos), sonicated in pure CH_3CN for 2 minutes, washed with pure CH_3CN, and dried. A Pt plate (0.2 mm thick and 2 cm^2 of area from Aldrich) were used to prepare thick films for conductivity measurements. These electrodes were cleaned by flaming with a propane torch followed by rinsing with solvent and drying. Pt wire (0.1 mm diameter from Aldrich) was used as the working electrode in EPR/electrochemistry experiments. ITO glass slides (50x7x0.7 mm and resistance of *ca.* 40 Ω from Delta Technologies) were used as working electrodes to obtain thin films for the optolectrochemistry experiments. They were cleaned with acetone after a copper lead was attached using silver paint (Delta Technologies) to ensure good electrical contact. Au electrodes (Valpey-Fisher) were used for the EQCM studies. These special electrodes consist of an AT-cut quartz crystal sandwiched between two gold electrodes that have been evaporated on a previously chromium coated quartz crystal surface in a key hole configuration. The top gold surface is used as a working electrode in a typical three electrode cell configuration. The gold electrode area is 0.71 cm^2. These electrodes were cleaned with concentrated H_2SO_4, then washed with distilled water and rinsed with acetone.

2.1.2 Preparation of Films

Conducting polymer films were prepared on a Pt button electrode by multiple scanning electropolymerization. The initial potential was selected such that no oxidation of the

monomer occurs, at least 0.5 V below the monomer oxidation peak. The potential was increased linearly to 50 mV beyond the monomer oxidation peak and then decreased to the initial potential with a constant scan rate, usually 100 mV/S. Generally, 5-10 scans were allowed to obtain a thin polymer film on the electrode surface.

Polymer films were electrochemically prepared (for conductivity measurements) on a platinum plate using constant potential electropolymerization at the monomer peak oxidation potential. The concentration of the monomer was usually 0.01 M and the concentration of the electrolyte 0.1 M. The potential was held until the desired amount of charge was passed, generally 1-2 C/cm^2 in order to allow for films of proper thickness, typically 5-10 μm.

For optoelectrochemistry experiments, polymer thin films were obtained potentiostatically at the monomer peak potential on ITO plates. The charge passed was typically 5 mC/cm^2 in order to obtain transparent films, in all cases they were checked by visual inspection.

For XPS experiments in the capacitor project, polypyrrole films were chemically prepared on Ta/Ta_2O_5 foils. Polypyrrole was synthesized chemically by mixing 0.03 M pyrrole, 0.07 M $FeCl_3$ and 0.1 M of various aromatic sulfonate salts in deionized water.

After the films were prepared, they were thoroughly washed with pure solvent and dried at room temperature.

2.1.3 Cyclic Voltammetry

Cyclic voltammetry was used to determine the oxidation potential of the monomers and the redox properties of the polymers obtained. Usually, a solution containing 0.01 M monomer and 0.1 M electrolyte was used in these experiments. The monomer oxidation was observed as a large, irreversible anodic current peak.

In order to study the redox properties of the polymers, the films were washed with pure solvent and placed in monomer free electrolyte solution. The initial potential was selected such that no redox reactions occur, usually 0.5 V below the reduction peak of the polymer. The final potential was usually 0.2 V beyond the oxidation peak in order to avoid overoxidation of the polymer. Cyclic voltammograms of the electroactive polymers were obtained in various electrolyte solutions and characterized by comparing their anodic and cathodic peak potentials, the peak separation, and the corresponding peak currents. Due to the surface bound nature of these polymer films, the current at the peak potentials is often given by equation (1-1) and is linearly related with the scan rate as a consequence of a non-diffusion controlled surface bound reaction. The scan rate dependence of the peak currents was measured and used as a diagnostic tool to check the surface adherence of these polymers. Cyclic voltammograms were taken after the polymer films were stabilized at each scan rate by cycling the potential until a reproducible

current response was obtained. The scan rate was increased by 25 mV/s increments, starting at a scan rate of 25 mV/s and usually increased up to 150 mV/s.

Cyclic voltammetry and electropolymerizations were carried out using a Princeton Applied Research EG&G 273 potentiostat/galvanostat. The voltammograms were recorded on a Houston Instruments model 200 or a Graphitec model WX4000 X-Y-T recorder.

2.1.4 Potential Step Method

The potential step method was used in the potentiostatic preparation of conducting polymers and also in the study of the electrochemical and electronic properties of the conducting polymers. In various experiments, a potential difference is applied between the reference and working electrode and either the changes in current, charge, mass, absorbance, or EPR intensity were measured.

During the constant potential preparation of conducting polymers, the potential was stepped from a value where no redox reaction occur (e.g., 0.5 V lower than $E_{p,m}$) to the monomer oxidation potential. The polymerization was stopped when the charge passed reached the desired value as was mentioned above. After the polymer films were obtained, they were equilibrated by cycling them between their reduced and oxidized states (*ca.* 10 times) in monomer free electrolyte solution in order to break in the polymer film and obtain a reproducible current response. This approach was used in the

synthesis of polymer films for conductivity measurements, optoelectrochemistry, EQCM studies, and EPR/electrochemistry.

The potential step method was also used in the study of the redox processes that occur in conducting polymers. After the polymer films were broken in by cycling, an initial potential was applied for an adequate time (*ca.* 30-60 seconds) to reduce the film completely and to assure that no faradaic processes occur. The potential was subsequently stepped to a value in which the redox reaction of interest took place. Different parameters were measured depending on the nature of the experiment. The potential step method was used in optoelectrochemistry and *in situ* EPR/electrochemistry in order to study the evolution of charge carriers as the polymer was oxidized. Also, potential step experiments were combined with the EQCM to investigate the ion transport behavior during redox switching.

2.1.5 Constant Current Electropolymerization

Galvanostatic electropolymerizations were also used to prepare polymer films for conductivity measurements. A current density of 2-5 mA/cm^2 was generally used in these experiments, the current was allowed to pass until polymer films with a thickness of *ca.* 5-10 μm were obtained.

Constant current electropolymerization was also used to synthesize polypyrrole during the preparation of capacitors. The current density used was 2 mA/anode. In this case, an external electrode was used to contact a previously

chemically deposited layer of polypyrrole. The electropolymerizations were carried out until the anodes were fully coated with polypyrrole.

2.2 Electrochemical Quartz Crystal Microbalance and Impedance Measurements

The electrochemical quartz crystal microbalance is the instrument that results from the coupling of the QCM with a typical three electrode cell. With this device, it is possible to simultaneously measure the changes in the current and mass that occur at the working electrode during any redox reaction. The fundamentals of the EQCM were discussed in chapter 1. The design of the EQCM used in this study is shown in Figure 2.2. An At-cut quartz crystal sandwiched between two gold electrodes was use as a resonator. The top gold electrode on the quartz was used as a working electrode in the electrochemical cell. An alternating voltage is applied between the gold electrodes causing the quartz crystal to oscillate at its resonant frequency (*ca.* 5 MHz).

According to the Sauerbrey equation (equation 1-9), there is a direct relationship between the changes in the oscillation frequency and the mass deposited on the electrode surface. The sensitivity of the quartz resonator used is 18 $ngHz^{-1}cm^{-2}$. The quartz resonator was mounted in the electrochemical cell and sealed by O-rings. The working electrode area was determined for the inner diameter of the O-ring and was 0.71 cm^2. The EQCM used through this study was

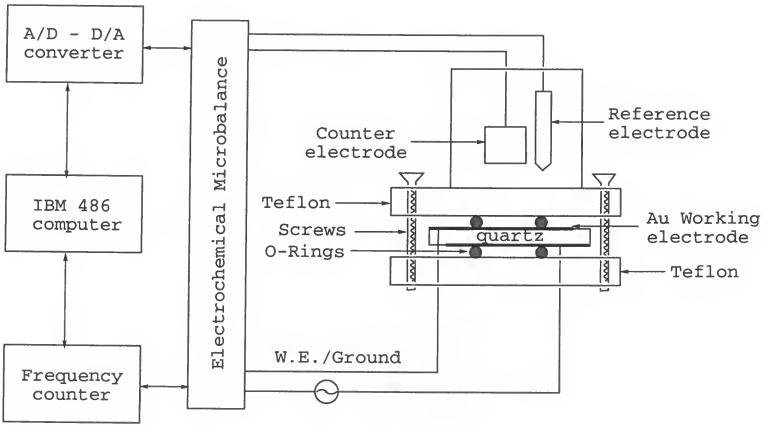

Figure 2.2. Diagram of the EQCM.

designed at IBM and built in the electronics shop of The University of Texas at Arlington. The frequency changes of the quartz crystal resonator during redox events were measured by a Phillips PM6654 frequency counter. The data was collected by a 486 IBM computer using a National Instruments AT-MIO-16X multifunction I/O board, The data acquisition program was written in C language using a National Instrument Lab Windows software package.

In order to check the rigidity of the polymer films, conductance spectra were taken in both the reduced and oxidized form of the polymers. The conductance spectra of the quartz/polymer film composite resonators were measured with a Hewlett Packard 4192A impedance analyzer.

2.3 Optoelectrochemistry

Optoelectrochemistry experiments were carried out to study the electronic properties and the change in the optical spectra during the electrochemical switching of the conducting polymers.

The polymer coated ITO electrodes were placed in a standard 1 cm path length spectrophotometric quartz windows cuvette (NSG Precision Cells, Inc.) with a silver wire quasi-reference electrode as shown in Figure 2.3. A hole with 0.5 cm diameter was made in a platinum plate counter electrode to allow light to be transmitted through the electrode. Another clean ITO slide in electrolyte solution was placed in another cuvette and was used in the reference compartment of the

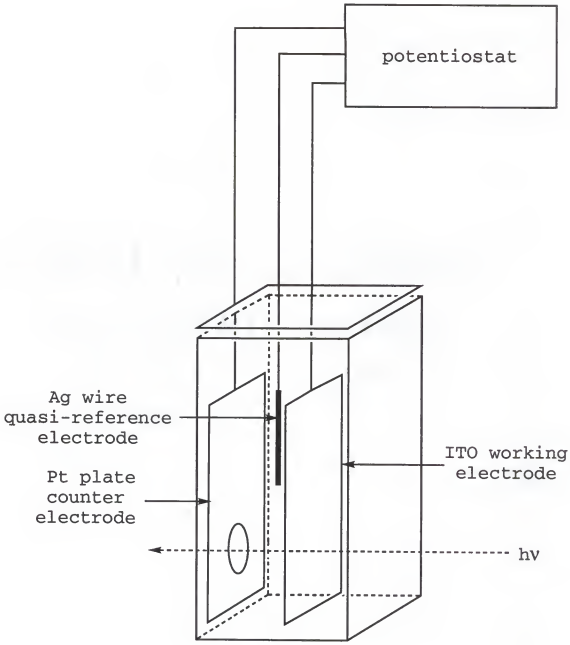

Figure 2.3. Cell design for optoelectrochemistry experiments.

spectrophotometer to subtract the background absorption of the ITO glass and electrolyte. The electrode potential was held at a value in which the polymer is completely reduced(*ca.* 0.5 V below the reduction peak) and the spectrum recorded. The electrode potential was subsequently increased by 50 mV increments and the spectrum recorded at each potential until the complete doping range was covered. The optical spectra were taken with a Varian Analytical Instruments Cary 5E UV-Vis-NIR spectrophotometer and the potential was controlled by the EG&G potentiostat described above.

2.4 EPR/electrochemistry

In situ EPR/electrochemistry was used to investigate the evolution of paramagnetic species during the redox switching of the conducting polymers. The EPR spectra were taken with a Bruker model ER-200D-SRC electron paramagnetic resonance spectrometer and the potentials were controlled by the EG&G potentiostat mentioned above.

The polymer samples were obtained by potentiostatic electropolymerization on a Pt wire from a 0.01 M monomer and 0.1 M TBAP/CH_3CN solution. The counter electrode was a Pt wire, and a Ag wire was used as a quasi-reference electrode. The three wires were placed in a 30 cm test tube, and the electropolymerization was carried out until the desired charge was passed, usually 50 mC. The polymers were subsequently reduced by holding the potential at *ca.* 0.5 V

below the reduction peak of the polymer, rinsed with pure acetonitrile and placed in a special electrochemical EPR cell obtained from Wilmad Glass. This cell is illustrated in Figure 2.4. In order to minimize the absorption of microwave radiation by the electrolyte, this cell has a special configuration in which the flat part contains a very small amount of electrolyte solution, and for this reason counter electrodes were necessary at the top and bottom of the flat part to assure good electrical contact during the redox switching of the polymers. The cell was filled with monomer free electrolyte solution and placed in the EPR cavity of the spectrometer. The potential was initially held at a value were the polymer was fully reduced and the EPR signal was recorded. The potential was subsequently increased by 50 mV increments and the EPR signal recorded at each potential until the polymer was fully oxidized.

The g values of the polymers can be calculated by the equation (1-7). However, due to the lack of precision in measuring the microwave power, α-α-biphenyl-β-picrylhydrzyl, DPPH (Aldrich), was used as the standard with g = 2.0037 ± 0.0002 to obtain the g value of the polymers. The g value was obtained using the equation:

$$g_{(sample)}H_{(sample)} = g_{(standard)}H_{(standard)} \qquad (2\text{-}1)$$

DPPH was also used as a spin concentration calibration standard. A calibration plot was obtained by preparing several samples of known amounts (7.5, 15.0, 20.0 and 30.0 mg) of DPPH dispersed in KBr (IR grade, Aldrich). The

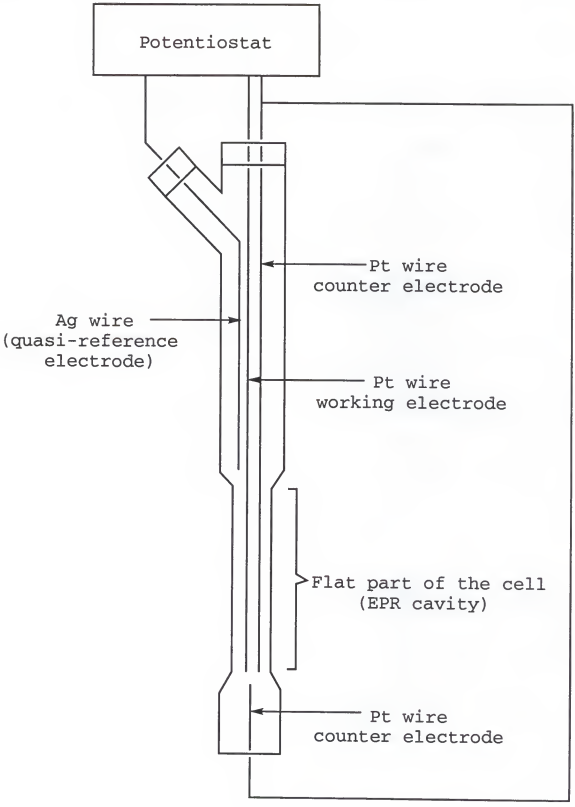

Figure 2.4. EPR/electrochemistry cell.

corresponding amount of DPPH was dispersed in 2.0 g KBr using a wiggle bug. The dispersion was then poured into an standard EPR tube and the EPR signal recorded. The EPR tube was filled with the dispersion assuring that the sample was present throughout the EPR cavity. The intensity of the EPR signal was obtained by electronic double integration of the absorption curve. The length of the EPR tube containing the dispersion was measured and the number of spins/cm present in the cavity responsible for the EPR signal was calculated. The number of moles of repeat units present on the Pt wire were calculated from the charge passed during the electropolymerization, and the polymer coated wire was placed in the EPR cavity in the same manner as the DPPH standard. The number of spins in the polymer sample was obtained by the equation:[93a]

$$N_p = H_s P_s^{1/2} G_s N_s I_p S_p^2 / H_p P_p^{1/2} G_p I_s S_s^2 \qquad (2\text{-}2)$$

where the subscripts s and p indicates standard and polymer respectively, N is the number of spins, P is the microwave power, H is the modulation amplitude, G is the spectrophotometer gain, I is the double integral, and S is the sweep width.

2.5 Conductivity Measurements

Polymer films for conductivity measurements were potentiostatically synthesized on a platinum plate, washed thoroughly with pure acetonitrile and dried at room temperature. The films were removed from the electrode using

transparent adhesive tape and were subsequently fixed on a glass slide and secured with double sided adhesive tape with the polymer film side facing up. The integrity of the films were checked out by using an optical microscope. Four nickel-chromium wires were placed across the film, parallel to each other and at equal distances, and electrical contact between the films and the wires were made using silver paint (Delta Technologies). The Conductivity of the films was measured using the four-probe method as was shown in Figure 1.14. The conductivity of the polymer films were calculated using the equation (1-18).

Constant current was obtained with a Keithly Instruments model 224 programmable current source and the voltage drops were measured with a Keithly Instruments model 197 autoranging multimeter.

2.6 Miscellaneous Techniques

X-ray photoelectron spectroscopy (XPS) spectra were taken for polypyrrole films in order to obtain the doping level of the polypyrrole and to check if spontaneous ion exchange occurred during the re-anodization process used in the preparation of the capacitors. The polypyrrole films were deposited on Ta/Ta_2O_5 foils and the XPS spectra taken before and after the re-anodization process. The XPS spectra were obtained on a Perkin-Elmer PHI 5100 ESCA system.

Scanning electron microscopy (SEM) was used to investigate the polymer film morphology. Polymer films were

electrochemically synthesized on ITO glass electrodes. After the films were washed and dried, they were covered with a thin layer of gold and the SEM images taken. SEM images were obtained with a JEOL JSN-6400 system.

Polymer film thickness for the conductivity measurements were obtained with a Sloan Dektak II profilometer.

2.7 Chemicals

The organic solvents used in this study (CH_3CN and CH_2Cl_2) were distilled over P_2O_5 and under N_2 prior to use. They were used immediately after distillation, purged with argon to degassed, and under an Ar blanket to avoid moisture and oxygen from air. Propylene carbonate (PC) was vacuum distilled before use and store over molecular sieves.

The water used during this study was double distilled using a Millipore Milli-Q-Water system, having a resistance of 18 MΩ.

Pyrrole (Aldrich) was purified immediately before use by passing it through activated alumina until a colorless liquid was obtained.

The electrolytes were recrystallized and stored under N_2 atmosphere until use. TBAP and $TBAFP_6$ (Aldrich) were recrystallized from ethanol. Lithium trifluoromethylsulfonimide (LiImide) was used as received from 3M. $NaB(Ph)_4$ (Aldrich) was used as received from Aldrich. $LiClO_4$, $NaClO_4$ and $CsClO_4$, NaTosilate, and tetraethylammounium tosilate

(TEATOS) (Aldrich) were dehydrated under vacuum and stored under N_2.

The experimental details will be described in the corresponding chapter.

CHAPTER 3
ELECTRONIC AND ELECTROCHEMICAL PROPERTIES OF CONDUCTING POLYMERS CONTAINING BISHETEROCYCLE/*p*-PHENYLENE AND BISHETEROCYCLE/*p*-DIALKYLFLUORENE

3.1 Introduction

The electrochemical synthesis of conducting polymers from multi-ring aromatic monomers with electron rich terminal heterocycles has attracted considerable attention. This is due to their significantly lower oxidation potential than the corresponding parent heterocycle caused by the higher extent of conjugation of the multi-ring system.[165] It is well known that the polymers electronic and electrochemical properties depend strongly on the molecular structure as has been demonstrated for several substituted derivatives of poly(*p*-phenylene)[166], polypyrrole[167] and polythiophene.[18a-b,168] Long alkyl chains have been attached to the 3-position of polythiophenes[18a,18c,167b,168a] and polypyrroles[167b] to increase their solubility and allow processability. The introduction of the alkyl chains has also been useful in inducing fusibility into poly(3-alkylthiophenes)[18c] and poly(9,9-dialkylfluorenes).[13b,13c,169] Attachment of alkoxy substituents directly onto the conjugated chain increases the electron density along the π system, decreasing the monomer and polymer oxidation potentials, and reducing the electronic

band gap of the polymer.[19,170] In addition to the electronic and electrochemical effects, pendant substituents have also been shown to have a strong steric effect on the conformation of the polymer backbone. These steric interactions between pendant groups on adjacent rings increases the energy barrier to planarity of the π system. This effect was demonstrated for poly[1,4-bis(2-thienyl)-2,5-dimethylphenylene], where the thiophene-phenylene torsional angle was found to be significantly larger than the unsubstituted or dimethoxy analogues.[19]

The motivation for the study of poly[1,4-bis(2-heterocycle)-*p*-phenylenes] (PBHPs) in the Reynolds group has been the the ability to control the physical and optoelectronic properties of *p*-phenylene-containing polymers. These polymers exhibit the desirable electronic properties of the polyheterocycles combined with the ease of substitution of the phenylene ring. Due to the broad range of substitution possibilities on phenylene rings, a large number of derivatives has been made possible. An additional benefit of these polymers is that the polymers can be symmetrically derivatized to yield isoregic polymers.[171] It is well established that higher degrees of long-range order can lead to significant enhancements in electrical conductivity.[172] The studies of the PBHPs in our group, have found that, while the parent polyheterocycle properties are largely retained, some unique electrochemical phenomena are observed in both monomers and polymers.

This chapter reports the electrochemical synthesis of a series of polymers containing bis(2-heterocycle)-*p*-phenylene and bis(2-heterocycle)-*p*-dialkylfluorene units. The effect of the heterocycle and the pendant side-chain structure on the electrochemical and electronic properties of the polymers was the main focus of this study.

3.2 Poly[1,4-bis(2-thienyl)phenylene] and its Derivatives

Polymers were electrosynthesized from 1,4-bis(2-thienyl)benzene monomers containing methoxy, hepthoxy, cyclohexylmethyloxy, and dodecyloxy pendant groups. The Monomers structures are shown in Figure 3.1.

The monomers were synthesized in our group by the coupling of the appropriate 2,5-disubstituted-1,4-dihalogenated-benzene with a 2-metallated thiophene.[19,171]

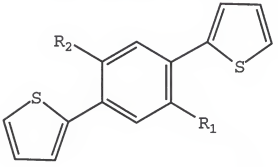

(12) $R_1 = R_2 = H$

(13) $R_1 = R_2 = OCH_3$

(14) $R_1 = OCH_3$, $R_2 = OC_7H_{15}$

(15) $R_1 = R_2 =$ 

(16) $R_1 = OCH_3$, $R_2 = OC_{12}CH_{25}$

Figure 3.1. Monomer structures of 1,4-bis(2-thienyl)benzene and its derivatives.

3.2.1 Electropolymerization

Repeated potential scanning electropolymerization was used for the preparation of electrode supported films.

Table 3-1. Oxidation potentials of monomer **12** obtained by cyclic voltammetry in 0.1 M electrolyte and 0.01 M monomer solution.

	$E_{p,m}$ (V)*	
Electrolyte	CH_3CN	PC
TBAP	0.91	0.91
$TBAF_6$	0.93	0.93
$LiN(SO_2CF_3)_2$	0.93	0.95
$LiClO_4$	0.90	-
$CsClO_4$	0.98	-

* All potentials reported vs. Ag/Ag^+.

Solutions 0.01 M of each monomer in 0.1 M electrolyte were used in each case. Prior to electropolymerization, all solutions were purged with argon and during experimentation an argon blanket was held above the solution. Figure 3.2 shows a series of multiple scanning electropolymerization experiments for the unsubstituted monomer **12** in TBAP/CH_3CN, TBAP/PC, LiImide/CH_3CN, LiImide/PC, $LiClO_4/CH_3CN$, and $CsClO_4/CH_3CN$. Table 3-1 summarizes the results obtained during the polymerization of monomer **12**.

During the first scan, monomer **12** exhibits an irreversible anodic peak at *ca.* 0.9 V (vs. Ag/Ag^+) due to the formation of radical-cations. These radical cations react rapidly to form a polymer film on the electrode surface as was explained in Chapter 1. Two poorly resolved cathodic peaks are observed (in all cases) on the return scans due to

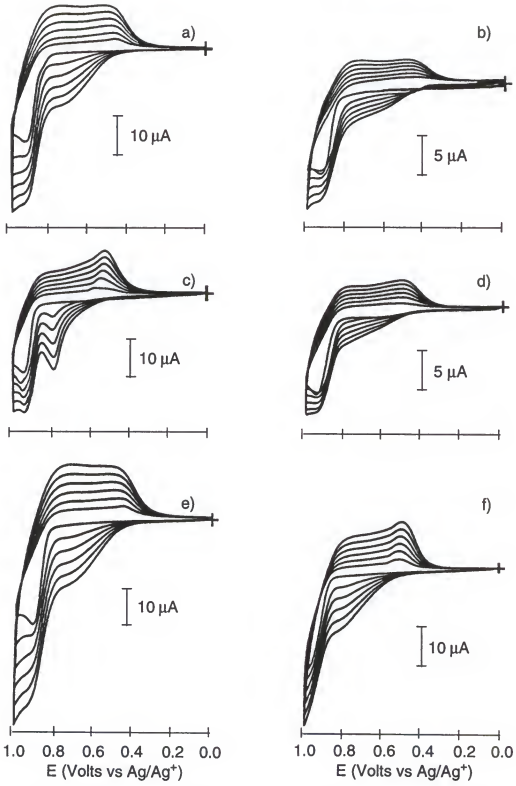

Figure 3.2. Multiple scanning electropolymerization of monomer **12** at 100 mV/s in 0.1 M solution of a) TBAP/CH_3CN, b) TBAP/PC, c) LiImide/CH_3CN, d) LiImide/CH_3CN, e) $LiClO_4$/CH_3CN, and f) $CsClO_4$/CH_3CN.

Table 3-2. Oxidation potential of monomers **12**-**16** obtained by cyclic voltammetry in 0.1 M TBAP/CH_3CN and 0.1 M monomer solution.

Monomer	$E_{p,m}$ (V)*
12	0.91
13	0.71
14	0.70
15[a]	0.80
16	0.72

* All potentials reported vs. Ag/Ag^+.
[a] Obtained in 0.1 M TBAP/CH_2Cl_2 due to its insolubility in CH_3CN.

reduction of the as-made oxidized polymer. The second and subsequent scans show an anodic current response beginning at *ca.* 0.45 V as the reduced polymer on the electrode surface reoxidizes, followed by a higher current during further monomer oxidation at *ca.* 0.9 V. The increase in current with repetitive scanning is due to the fact that the depositing conducting polymer is increasing the effective surface area on the electrode.

The effect of alkoxy substituents on the monomer oxidation potential can be obtained from the cyclic voltammograms of monomers **13**, **14**, **15**, **16** as shown in Figure 3.3. The oxidation potentials of the alkoxy substituted monomers are summarized in Table 3-2. The increased electron donating ability of the alkoxy groups relative to the unsubstituted monomer results in a reduction of the monomer oxidation potential by *ca.* 200 mV. It is well established

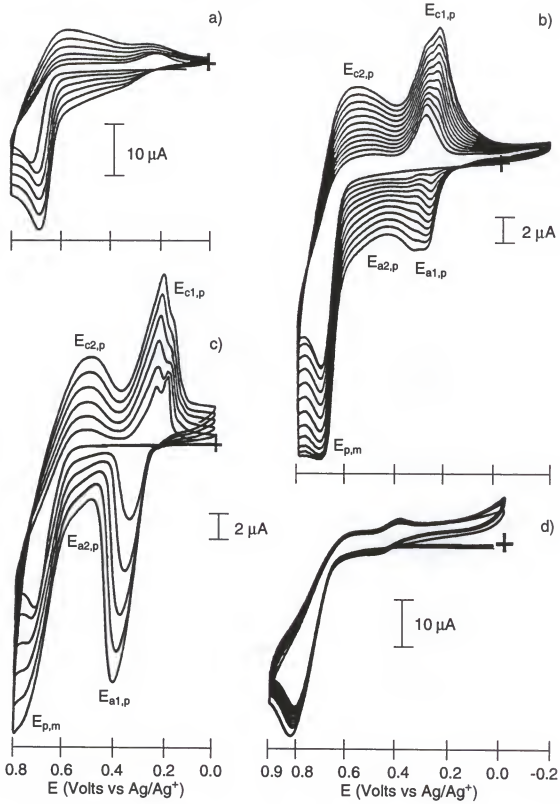

Figure 3.3. Multiple scanning electropolymerization at 100 mV/s of monomers: a) **13**, b) **14**, and c) **16** in 0.1 M TBAP/CH_3CN, and d) **15** in 0.1 M TBAP/CH_2Cl_2.

that alkoxy substituents activate aromatic rings to electrophilic substitution due to resonance effects. In this situation, the alkoxy substituents stabilize the cation-radical by delocalizing the positive charge over a larger area as shown in Figure 3.4.

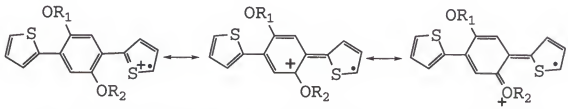

Figure 3.4. Stabilization of radical-cation by resonance.

Cyclic voltammetric scanning electropolymerization of these bis(2-thienyl)benzene monomers is characterized by the observation of polymer cathodic processes during the reverse scan. Multiple scans up to, or slightly beyond, $E_{p,m}$ then yields cyclic voltammograms (CVs) where both the anodic and cathodic polymer redox processes grow in at potentials significantly lower than $E_{p,m}$. In contrast, the bis[(cyclohexylmethyl)oxy]-substituted monomer (**15**) exhibits a different behavior. Scanning to 0.9 V (Figure 3.3c) results in an $E_{p,m}$ at 0.80 V similar in nature to the other systems investigated. Repeated scanning, however, shows a very slow film growth under these conditions. Extending the anodic scan to 1.1 V as shown in Figure 3.5 reveals a second oxidation ($E_{2,m}$) with an onset at 1.0 V. Repeated scanning under these conditions leads to the rapid development of cathodic processes ($E_{c2,p}$ and $E_{c1,p}$) at 0.55 and 0.35 V, along with an

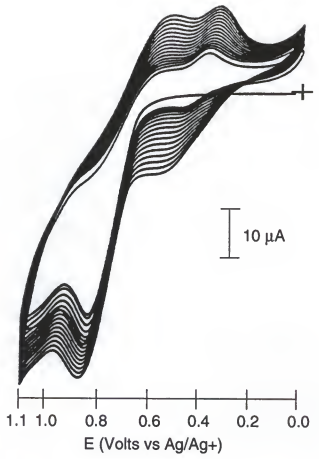

Figure 3.5. Multiple scanning electropolymerization at 100 mV/s of monomer **15** in 0.1 M TBAP/CH_2Cl_2 with scanning to 1.1 V.

anodic process ($E_{a,p}$) at 0.5 V. During this excursion to higher potential, rapid electroactive film growth is observed. This slow growth behavior can be attributed to the solubility of oxidized oligomers which form at low potentials in the CH_2Cl_2 based electrolyte, where the coupling products diffuse away from the electrode preventing formation of polymer on the electrode surface. This phenomenon has also been observed for the highly soluble PBHP derivatives with the longest alkoxy substituents (e.g., $OC_{16}H_{33}$ and $OC_{20}H_{41}$) where the solubility of the oligomers precluded

electrochemical polymerization.[171] The second oxidation of **15** results in rapid electroactive film deposition. It is possible that this second process is due to the reaction of a coupled product to form a new radical-cation. Since the result of this oxidation is rapid coupling, cross-linking of the polymer as it forms is likely.

To examine the potential dependence of this deposition further, the EQCM was used to monitor the mass change during electropolymerization of **15** as shown in Figure 3.6.

Scanning to 0.9 V results in a mass increase as expected for electropolymerization. During the return scan, the mass decreases as the polymer formed dedopes and anions are lost. A small net mass change is observed at 0.0 V indicating that

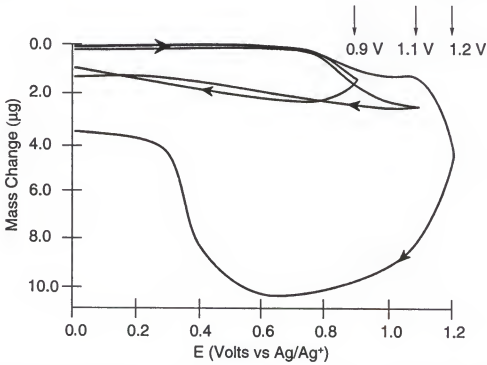

Figure 3.6. EQCM monitored mass shifts during deposition of **P15** in 0.1 M TBAP/CH_2Cl_2 with varied switching potentials.

a small amount of polymer has permanently adhered to the electrode surface during this initial scan. Scanning with a switching potential change of 1.1 V, a plateau is observed in the mass change as deposition occurs at a relatively slow rate on the polymer covered electrode. Again the reverse scan shows a small irreversible mass change as a small amount of polymer deposition has occurred. Scanning beyond the second oxidation to 1.2 V results in a significantly larger mass increase and rapid mass deposition as electroactive polymer forms on the working electrode. The return scan shows a mass decrease, again indicative of the expulsion of counterions during polymer reduction, but the larger net mass increase at 0.0 V indicates a significant amount of polymer has deposited during this single scan.

By examining electropolymerizable bis(2-thienyl)benzenes with well-behaved polymerization characteristics at $E_{p,m}$, it was found that this second redox process is found not only in **15** but in other monomers as well. Figures 3.3b and 3.3c show the well-behaved electropolymerization of the methoxy/heptoxy (**14**), and the methoxy/dodecyloxy (**16**) substituted bis(2-thienyl) monomers respectively with scanning to 0.8 V. Repeated scanning leads to the development of two polymer cathodic ($E_{c1,p}$ and $E_{c2,p}$) processes as electrically conductive and electroactive polymer deposits onto the working electrode. The electropolymerization behavior of **14** and **16** with scanning to 1.0 V is shown in Figure 3.7. A second oxidation ($E_{2,m}$) is now evident, and there are

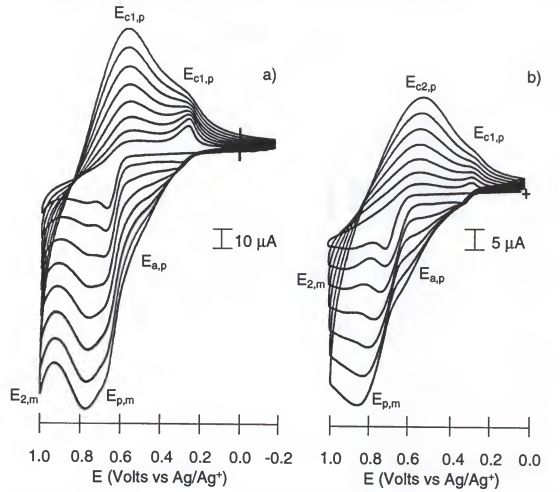

Figure 3.7. Multiple scanning electropolymerization at 100 mV/s of monomers: a) **14** and b) **16** in 0.1 M TBAP/CH_3CN with scanning to 1.0 V.

distinct changes in the electroactivity of the polymers. With scanning to $E_{p,m}$ (Figures 3.3b and 3.3c) two anodic processes are visible, one as a distinct peak at *ca.* 0.35 V and the other as a shoulder at *ca.* 0.5 V. Scanning to higher potential during electropolymerization eliminates the $E_{a1,p}$, and all anodic redox activity is found at higher potential. The upper limit of the polymerization potential also has an impact on the polymer's cathodic redox processes. While scanning to $E_{p,m}$ yields two distinct cathodic processes and a

higher peak current for $E_{c1,p}$ compared to $E_{c2,p}$, scanning to higher potential increases the relative current for $E_{c2,p}$. At the same time, there is a general broadening of the peaks and loss of resolution. This is explained in the following section (see page 91).

3.2.2 Polymer Electrochemistry

Polymer films obtained by multiple scanning electropolymerization of the monomers were washed with pure solvent (CH_3CN, PC or CH_2Cl_2) and placed in a 0.1 M monomer free electrolyte solution. The cyclic voltammograms of **P12** in several solvent and electrolyte solutions are shown in Figure 3.8. In all cases (except for LiImide/PC) the peak of the polymer oxidation is just beyond the potential window of the polymer. The linear dependence of the peak currents on the scan rate indicates that the electroactive species are electrode bound.

In order to study the effect of the alkoxy substituents on the electrochemical properties of these polymers, films of **P12**, **P13**, **P14**, and **P16** were prepared by multiple scanning electropolymerization up to $E_{p,m}$ in a 0.1 M solution of the corresponding monomer containing 0.1 M TBAP/CH_3CN. The polymers were rinsed with CH_3CN, and their redox processes examined in monomer free 0.1 M TBAP/CH_3CN electrolyte solution by cyclic voltammetry. Figure 3.9 shows the CV behavior of these polymers and the redox results for all

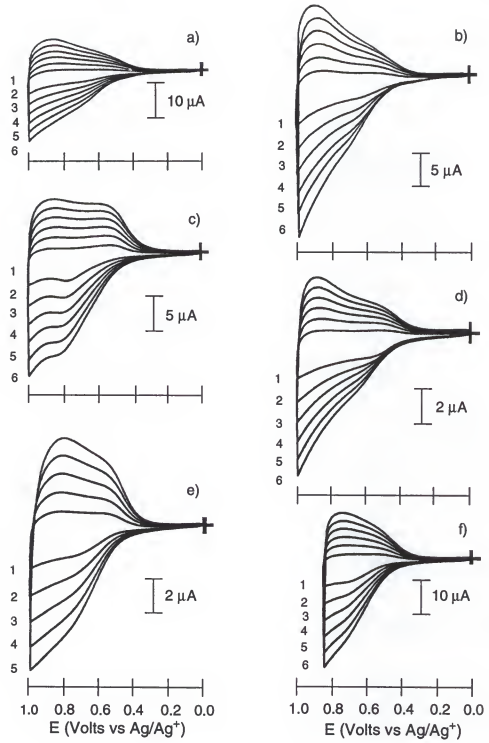

Figure 3.8. Cyclic voltammograms of **P12** electrosynthesized by scanning to $E_{p,m}$, in 0.1 M solution of a) TBAP/CH_3CN, b) TBAP/PC, c) LiImide/CH_3CN, d) LiImide/PC, e) $LiClO_4$/CH3CN, and f) $CsClO_4$/CH_3CN, carried as a function of scan rate: 1) 25, 2) 50, 3) 75, 4) 100, 5) 125 mV/s, and 6) 150 mV/s.

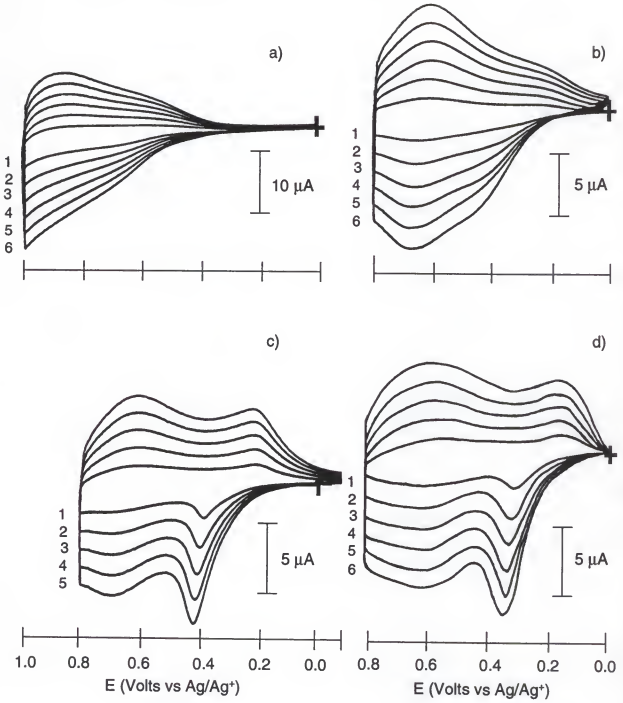

Figue 3.9. Cyclic voltammograms of a) **P12**, b) **P13**, c) **P14**, and d) **P16** electrosynthesized by scanning to $E_{p,m}$, in 0.1 M TBAP/CH_3CN, carried as a function of scan rate: 1) 25, 2) 50, 3) 75, 4) 100, 5) 125 mV/s, and 6) 150 mV/s.

Table 3-3. Electrochemical results for polymers **P12-P16** obtained by cyclic voltammetry in 0.1 M TBAP/CH_3CN.

Polymer	$E_{p,a}$ (V)*	$E_{p,c}$ (V)	$E_{1/2}$ (V)
P12	> 1.0	0.84	-
P13	0.46, 0.67	0.22, 0.61	0.34, 0.64
P14	0.42, 0.69	0.22, 0.62	0.32, 0.67
P15[a]	0.38, 0.65	0.35, 0.55	0.37, 0.62
P16	0.30, 0.60	0.14, 0.58	0.22, 0.59

* All potentials reported vs. Ag/Ag^+.
[a] Cycled in 0.1 M TBAP/CH_2Cl_2.

polymers prepared under similar conditions are summarized in Table 3-3. Again the magnitude of the peak current (i_p) scales linearly with the scan rate in all cases which indicates that the polymers are bound to the electrode surface. The oxidation potential of the polymers follow a trend similar to that observed for the monomers due to the electronic effect discussed earlier.

In the polymers containing long-chain alkoxy substituents (**P14** and **P16**), a well-resolved low-potential redox couple is observed in addition to the major broad process at higher potential. The presence of these two redox couples has been attributed to the separation of the neutral-to-polaron and polaron-to-bipolaron charge-carrier formation events based on previous *in-situ* EPR studies in poly[1,4-bis(2-furanyl)-2,5-diheptoxyphenylene] and poly[1,4-bis(2-thienyl)-2,5-diheptoxyphenylene].[33b] This behavior has also been observed previously in poly(3-alkylthiophenes), where

the extent of separation depends on the length of the alkyl chain,[173] and in alkoxy-substituted polythiophenes.[18b,174]

The separation of the redox processes is more pronounced in the long-chain substituted derivatives and, since the heptoxy and dodecyloxy groups exert a similar electron donating effect as methoxy groups, this suggests a morphology component to this phenomenon. The decreased monomer oxidation potential of the alkoxy-substituted monomers leads to polymers with a lower degree of cross-linking and β-coupling, and likely, a higher degree of swelling in the switching electrolyte. For example, the CV of polythiophene, electrosynthesized from bithiophene, displays two cathodic current responses, whereas the higher monomer oxidation potential of thiophene leads to films with a single redox couple.[95] Noting the CV switching potential effect on the polymer's redox processes of **P14** and **P16** during film growth illustrated in Figures 3.3b and 3.3c, and 3.7a and 3.7b, a comparison of the electroactivity of **P14** and **P16** prepared with varied switching potentials in monomer free electrolyte was made. Figure 3.10 shows that the CVs for **P14** and **P16** polymerized by repeated scanning to the higher potential redox process are drastically altered with almost complete elimination of the low-potential process ($E_{a1,p}$ and $E_{c1,p}$). The chemistry occurring at this high potential limits the electroactivity by producing a polymer which is highly cross-linked, thereby inhibiting counterion mobility. An overall decrease in electroactivity is observed which may be due to

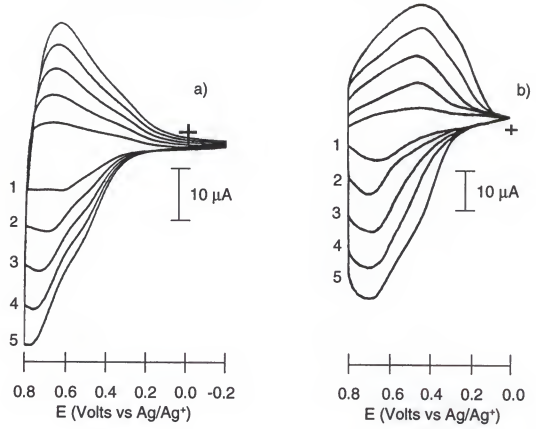

Figure 3.10. Cyclic voltammograms of a) **P14** and b) **P16** electrosynthesized by scanning to 1.1 V, carried as a function of scan rate: 1) 25, 2) 50, c) 75, d) 100, and 125 mV/s.

trapped sites which become isolated and inaccessible to counterion transport. To examine this effect on the high switching potential further, the (cyclohexylmethyl)oxy-substituted monomer, **15**, was polymerized by repeated scanning to 1.1 V, and its CV response measured in CH_2Cl_2 and CH_3CN as shown in Figure 3.11. The CV of the polymer lacks the first, low potential couple when cycled in CH_3CN (Figure 3.11a) but displays two couples in CH_2Cl_2 (Figure 3.11b). The linear alkoxy-substituted polymers are more highly soluble in CH_2Cl_2 compared to CH_3CN, suggesting it more effectively swells the

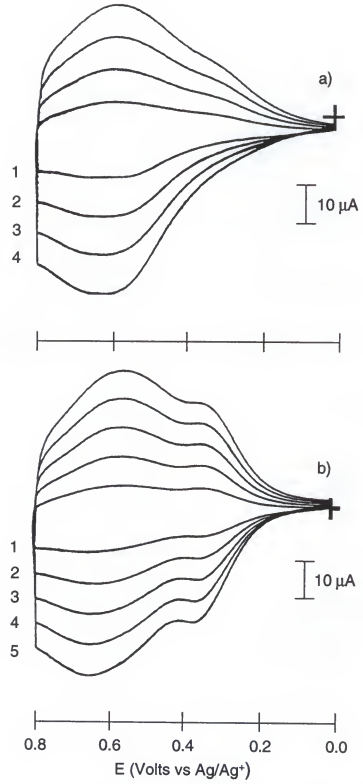

Figure 3.11. Cyclic voltammograms of **P15** electrosynthesized by scanning to 1.1 V in a) 0.1 M TBAP/CH_3CN, and b) 0.1 M TBAP/CH_2Cl_2, carried as a function of scan rate: 1) 25, 2) 50, 3) 75, 4) 100, and 5) 125 mV/s.

insoluble **P15** and facilitates counterion insertion. The above results suggest that the energy required for counterion insertion is an important factor in determining the stability of intermediate charge-carriers.[95] The potential necessary to insert counterions into films of unsubstituted or cross-linked polymers is greater than or equal to the potential for bipolaron formation; therefore, a single two-electron oxidation results. The polymers which exhibit two couples allow facile counterion insertion due to the low oxidation potentials of their monomers (resulting in minimal cross-linking during electropolymerization at $E_{p,m}$) and solvation effects induced by long side chains. Two electrochemical properties support the suggestion that polarons are formed at the first redox couple of these polymers. First, the peak widths of the first couple are narrow with respect to the second couple. Several polythiophene derivatives containing ether groups at the 3-position have been shown to display two distinct redox couples in their CVs, and the presence of a relatively sharp initial couple is characteristic of these systems.[18b,174] The width of the current responses in the cyclic voltammograms of surface bound species is ideally a constant value of 90.6/n mV, where n is the number of electrons transferred. Larger values are indicative of repulsive interactions within the film.[79b] Because polarons posses only a single charge and bipolarons contain two positive charges, repulsive interactions are expected to cause a larger peak broadening effect in the formation of

bipolarons. The FWHH of the first anodic peak in **P14** and **P16** are *ca.* 130 mV at 100 mV/s. The FWHH of the second oxidation of these polymers and the single oxidation of **P12** and **P13** are difficult to determine due to interference of non-faradaic current, but can be estimated to be larger than 250 mV. The narrow current responses in the low-potential couple of these systems suggests that monovalent charge carriers rather than dicationic carriers are present. The large increase in peak width suggests that repulsive charge interactions are much more important in the polymer after the second oxidation. Secondly, the peak separation (ΔE_p) of the second couple is smaller in the polymers with two couples than in the polymers which undergo a single, two-electron process. This separation is greater than 200 mV for polymer **P12**, and only *ca.* 70 mV for the second couple in **P14** and **P16**. The large-peak separation traditionally observed in conducting polymers has been ascribed to the large differences in conductivity between the oxidized and reduced states.[79b] In these polymers where intermediate charge-carriers (polarons) are formed at a lower potential the conductivity difference before and after the second oxidation is greatly reduced, resulting in a small separation between the anodic and cathodic current responses for the second couple.

3.2.3 Optoelectrochemistry

The electronic band structure of **P12**, **P13**, and **P15** were investigated using the optoelectrochemistry technique described in Chapter 2. The partial solubility of the reduced form of **P14** and **P16** in CH_3CN precluded their study due to the long-term exposure to solvent required during this experiment. The electronic band gaps (E_g) were determined from the onset of π to π^* transition. The optoelectrochemical spectra of **P12** is shown in Figure 3.12. The band gap of **P12** is 2.3 eV. Upon electrochemical doping, two new transitions are observed at 0.95 and 2.0 eV at low doping levels which shift toward higher energies (1.05 and 2.1 eV respectively) at high doping levels. This behavior is commonly observed in conducting polymers with nondegenerate ground states as was explained in Chapter 1.[38,88b,89b] At each subsequent doping level the absorption intensity increases for the low-energy transitions and decreases for the high-energy intergap transition, indicating increasing charge carrier concentration.

The alkoxy substituted polymers **P13** and **P15** have a band gap of 2.1 eV as can be observed in Figures 3.13a and 3.14a. The alkoxy substitution lower the energy gap by 0.2 eV following the trend expected considering the electronic effect discussed above. Again upon oxidation, two new transitions are observed in both **P13** and **P15** at 1.0 and 2.0eV, and 0.82 and 1.89 eV respectively as intragap

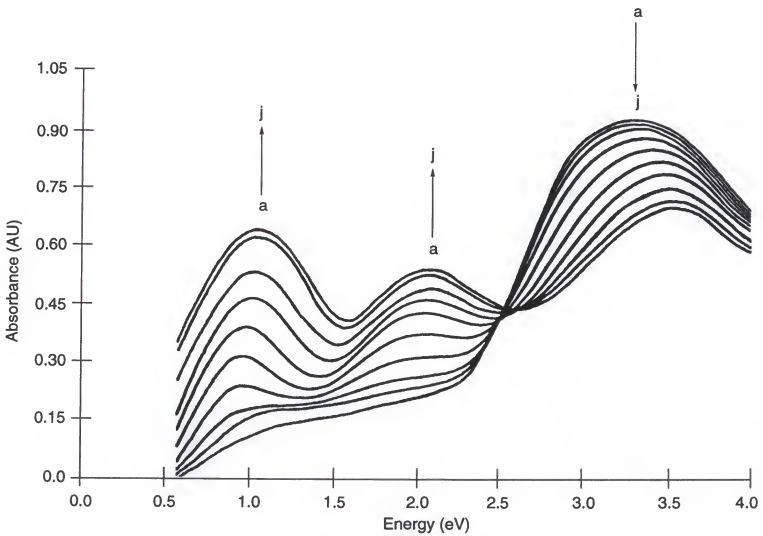

Figure 3.12. Optoelectrochemical spectra of **P12** equilibrated in 0.1 M TBAP/CH_3CN at : a) 0.0, b) 0.5, c) 0.8, d) 0.9, e) 0.95, f) 1.0, g) 1.05, h) 1.1, i) 1.15, and j) 1.2 V.

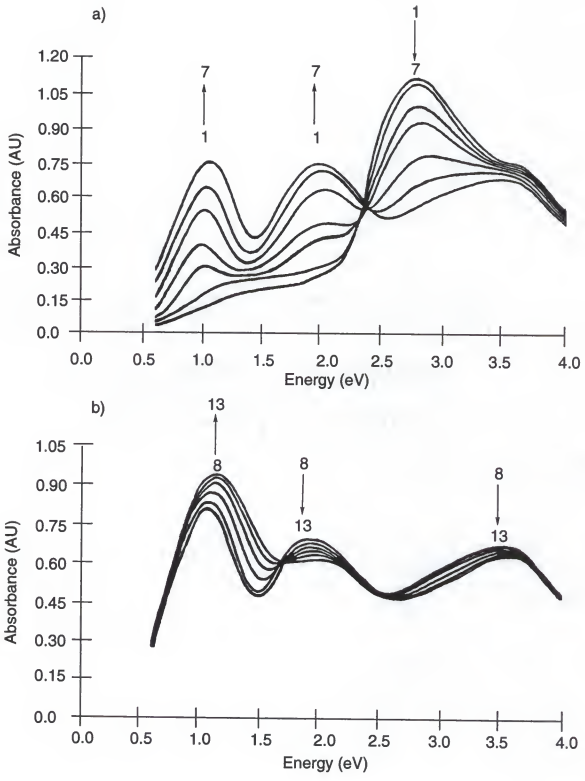

Figure 3.13. Optoelectrochemical spectra for **P13** equilibrated in TBAP/CH_3CN at a): 1) 0.0, 2) 0.4, 3) 0.5, 4) 0.6, 5) 0.7, 6) 0.8, and 7) 0.9 V; b): 8) 0.95, 9) 1.0, 10) 1.05, 11) 1.1, 12) 1.15, and 13) 1.2 V.

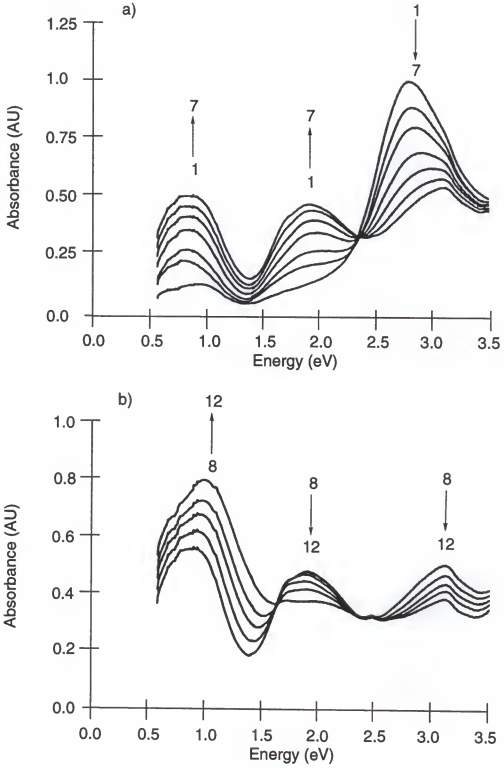

Figure 3.14. Optoelectrochemical spectra for **P15** equilibrated in TBAP/CH_3CN at a): 1) 0.0, 2) 0.6, 3) 0.7, 4) 0.8, 5) 0.9, 6) 0.95, and 7) 1.0 V; b): 8) 1.05, 9) 1.1, 10) 1.15, 11) 1.2, 12) 1.25, and 13) 1.3 V.

electronic levels are created during charge-carrier generation. The alkoxy substituted polymers **P13** and **P15** undergo a further change in the nature of their charge carriers at potentials just below their breakdown voltage. These changes are illustrated in Figure 3.13b and 3.14b for the identical films used in Figure 3.13a and 3.14a respectively as the potential is incrementally stepped above 1.0 V. In the case of **P13** and **P15** at these high doping levels, the peak attributed to the transition between the valence band and the higher energy intragap state decreases in intensity, while the energy of the lowest energy transition shifts to higher energies. This evolution of the optical spectra can be illustrated by the band-structure diagram in Figure 3.15. In the neutral form, the polymer exhibits a simple π to π^* transition with an onset energy at E_g as shown in Figure 3.15a. As the initial charge carriers are formed, likely a combination of polarons and bipolarons (Figure 3.15b and 3.15c), the midgap states are created at the expense of the highest energy states in the valence band. This causes a shift in the π to π^* transition to higher energy. Note that the λ_{max} for this transition in **P13** and **P15** shifts from 2.7 to 3.6 eV and from 2.7 to 3.1 eV respectively during doping. At 1.0 V the polymer contains a high density of bipolarons which can be represented by bands (Figure 3.15d) due to the large number of states possible. At the higher potentials ($1.0\ V \leq E \leq 1.3\ V$) the change in the optical spectra can be attributed to the formation of

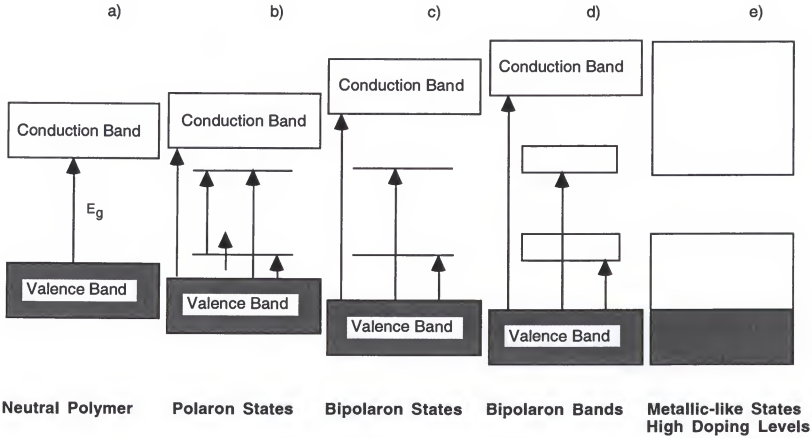

Figure 3.15. Electronic band diagram for nondegenerate ground-state conjugated polymers showing a) neutral state, b) polaron states, c) bipolaron states, d) bipolaron bands, and e) metallic-like bands.

metallic-like charge-carriers.[38,88b,89b] The intragap bipolaron bands become sufficiently broad at high doping levels that they intersect with the valence and conduction bands as illustrated in Figure 3.15e. In this series, this behavior is observed only in the alkoxy-substituted derivatives. At potentials above 1.5 V, each of the polymers undergoes an irreversible degradation due to overoxidation resulting in a pronounced decrease in electroactivity.[175]

The presence of metallic charge carriers in these systems, and their absence in others, can be explained by comparing the monomer and polymer oxidation potentials. Since overoxidation of these conducting polymers involves irreversible structural changes in the polymer backbone,[175] the effect of pendant substituents on the potential for overoxidation will be minimal. Pendant groups have a pronounced effect on the polymer's initial oxidation potential, however, as shown in Table 3-3, the alkoxy-substituted polymers display a significantly lower oxidation potential. At voltages above 1.0, the doping levels for these polymers are significantly higher than for the unsubstituted polymer. In addition to the low oxidation potentials, the long-chain alkoxysubstituted derivatives are able to accommodate a larger number of counterions due to their morphology. The doping levels in the furanyl series have been shown to increase dramatically with the length of the alkoxy chain and reach a level of 0.40 dopants/monomer unit in the diheptoxy-substituted polymer.[176]

3.2.4 EPR/Electrochemistry

The presence of spin-bearing polaron charge carriers at intermediate doping levels has been observed previously in polypyrrole[177] and polythiophene,[95] and in our group for poly[1,4-bis(2-furanyl)-2,5-diheptoxyphenylene] and poly[1,4-bis(2-thienyl)-2,5-diheptoxyphenylene][33b] where the maximum spin concentration is at a potential between the two redox processes observed by cyclic voltammetry. The results discussed above for the polymer with long-alkoxy substituents assumed that the separation of the redox processes is due to the formation of polarons at the first oxidation and their combination into bipolarons at the second redox process.

In order to study further this phenomenon, *in situ* EPR/electrochemistry experiments were carried out. Polymer thin films of **P15** were prepared on a Pt wire by potentiostatic polymerization at 1.3 V vs. Ag wire (1.0 V vs. Ag/Ag^+) from a 0.01 M monomer **15** and 0.1 M TBAP/CH_2Cl_2 solution. The polymerization was stopped when a charge of 50 mC was passed. After washing the polymer with pure CH_2Cl_2, the coated wire was placed in the EPR/electrochemistry cell described in Chapter 2. The polymer was reduced by applying a potential of 0.0 V vs. Ag/Ag^+ in monomer free 0.1 M TBAP/CH_2Cl_2 electrolyte solution and the EPR signal recorded. The potential was subsequently stepped in 50 mV increments and the EPR signal recorded at each potential. Figure 3.16

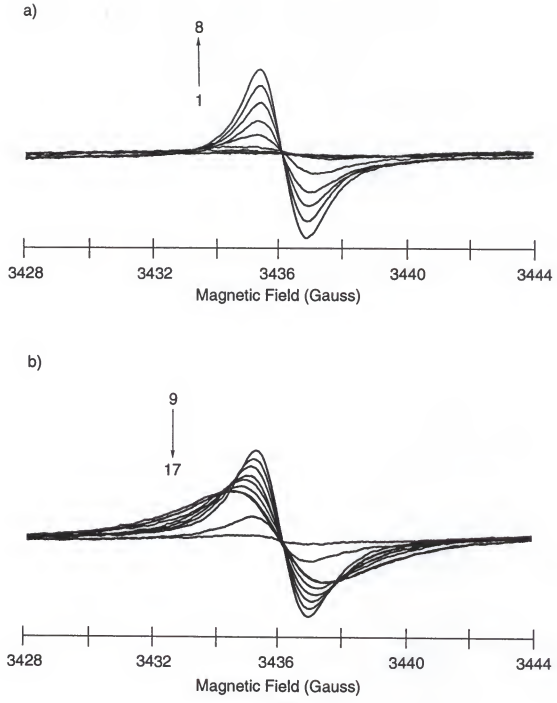

Figure 3.16. Evolution of the EPR signal as a function of the applied potential for **P15** in 0.1 M TBAP/CH_2Cl_2: 1) 0.0, 2) 0.20, 4) 0.25, 5) 0.30, 0.35, 6) 0.40, 7) 0.45, and 8) 0.48, 9) 0.50, 10) 0.55, 11) 0.60, 12) 0.65, 13) 0.70, 14) 0.80, 15) 0.90, 16) 1.0, and 17) 1.3 V.

shows the evolution of the EPR signal as the polymer is oxidized. As can be seen, the magnetic field strength of maximum EPR signal intensity is independent of the potential. A g value of 2.0062 for **P15** was determined using DPPH standard by applying equation (2-1). The g value is close to the free electron value of 2.00232. The EPR signal increased as the polymer is oxidized and reached a maximum value at 0.48 V, as was shown in Figure 3.16a, which is just beyond the first redox process as shown in the cyclic voltammogram in Figure 3.11b. The EPR signal was then observed to decrease upon further oxidation as can be seen in Figure 3.16b. These results corroborate the previous observations in bis(2-heterocycle)-*p*-phenylene polymers with pendant long alkoxy chains,[33b] in which the spin-bearing species are formed at the first oxidation process and dissipated at the second. Although the EPR signal is weak at potentials as high as 1.0 V, the polymer is not diamagnetic, this is likely due to trapped polarons. When the potential is increased to 1.3 V the EPR signal disappears as a result of the overoxidation and degradation of the polymer.

The spin concentration was calculated using equation (2-3) and a DPPH standard as was explained in Chapter 2. The spin concentration for **P15** at 0.48 V (maximum EPR signal) was found to be 0.17 spins per monomer repeat unit, that is equivalent to one spin per 18 rings. This value is similar to the one found in poly[1,4-bis(2-thienyl)-2,5-diheptoxyphenylene] (12 rings/spin) studied previously.[33b]

3.2.5 EQCM Studies

During redox switching, counterions move in and out of the polymer matrix in order to compensate the charge carriers created on the polymer backbone as was explained in Chapter 1. EQCM experiments were carried out to study the ion transport during the redox switching of polymers **P12** and **P13**. The partial solubility of the reduced form of **P14** and **P16** in CH_3CN precluded their study. The high potential needed (1.1 V vs. Ag/Ag^+) for the preparation of **P15** also precluded its study in the gold electrodes used in the EQCM due to Au oxidation at this potential.

The constant potential electropolymerization of **12** and **13** were carried out at 50 mV above the monomer oxidation potentials (0.95 and 0.75 V respectively) in 0.1 M TBAP/CH_3CN electrolyte solution. Frequency (mass) responses at the EQCM were subsequently monitored as the polymer film were deposited. The polymerization was stopped by stepping the electrode potential to 0.0 V, where the polymers were reduced. Figure 3.17 shows the mas response as the polymers were deposited. The electropolymerization was initiated at t=60 s and an immediate linear deposition of polymers (mass increase) was observed. At t=275 s the potential was stepped to 0.0 V and an immediate mass loss due to reductive dedoping was observed. The films were washed with CH_3CN and equilibrated by cycling between their reduced and oxidized states in monomer free 0.1 M TBAP/CH_3CN electrolyte solution

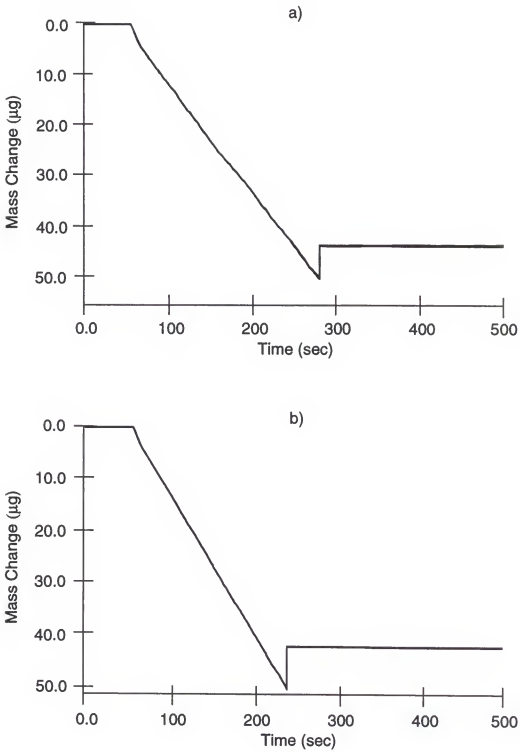

Figure 3.17. Mass change during the potentiostatic electropolymerization in 0.1 M TBAP/CH_3CN of monomers a) **12** and b) **13**.

in order to "break-in" the polymer films and obtain a reproducible current and mass response. Figure 3.18 shows the mass and current response during potential cycling for **P12** and **P13**. During the anodic scan the films are oxidized and a mass increase is observed with an onset potential that corresponds with the oxidation of the polymers. This indicates that ClO_4^- ions (and likely some solvent) are incorporated into the film. During the reductive scan, a mass decrease is observed which is associated with the movement of anions (and solvent) back out of the film. It should be noted that a CV is a non-equilibrium experiment and the films return to their original mass by holding the potential at 0.0 V.

Chronogravimetric studies were also carried out to examine the ion transport properties of **P12** and **P13** films during repeated double-potential step processes. Figure 3.19 shows the mass response vs. time for ten consecutive steps in 0.1 M TBAP/CH_3CN. A relatively reproducible mass gain upon oxidation, and mass loss upon reduction, in agreement with the scanning experiment was observed for both polymers. To examine the ion transport of these polymers further, the EQCM was used to monitor the mass changes during redox switching in several electrolytes having the same anion, ClO_4^- but with different cations. Figure 3.20 shows the mass response during redox switching in 0.1 M solutions of $LiClO_4$, $CsClO_4$ and TBAP in CH_3CN for **P12** and **P13**. The similar mass response in the different electrolytes indicates that the ion

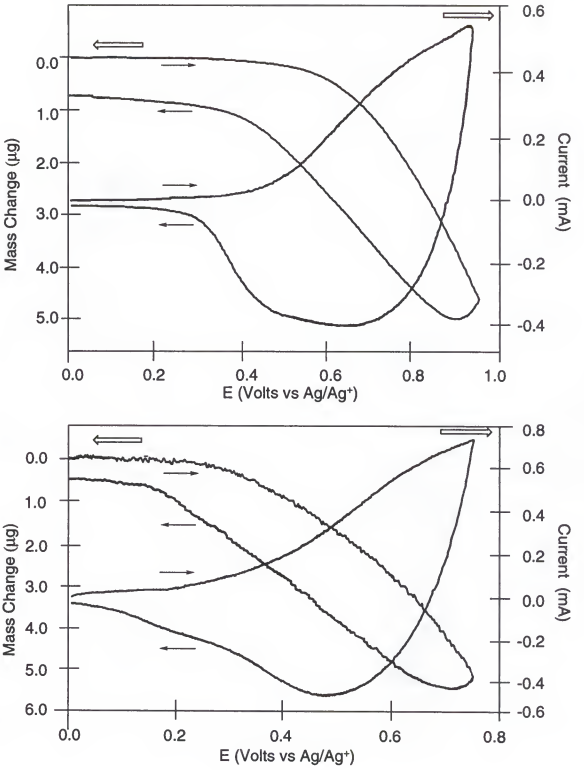

Figure 3.18. Mass and current response during potential cycling at 100 mV/s in 0.1 TBAP/CH_3CN of a) **P12** and b) **P13**.

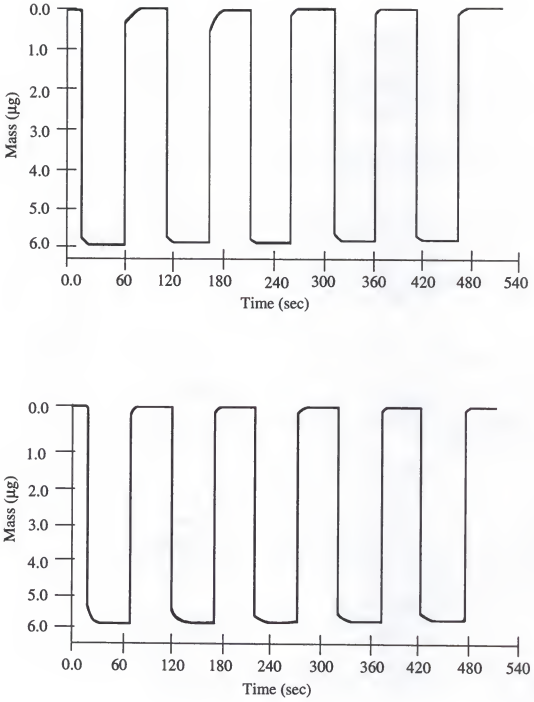

Figure 3.19. Chronogravimetric response for ten potential steps in 0.1 M TBAP/CH_3CN of a) **P12** and b) **P13**.

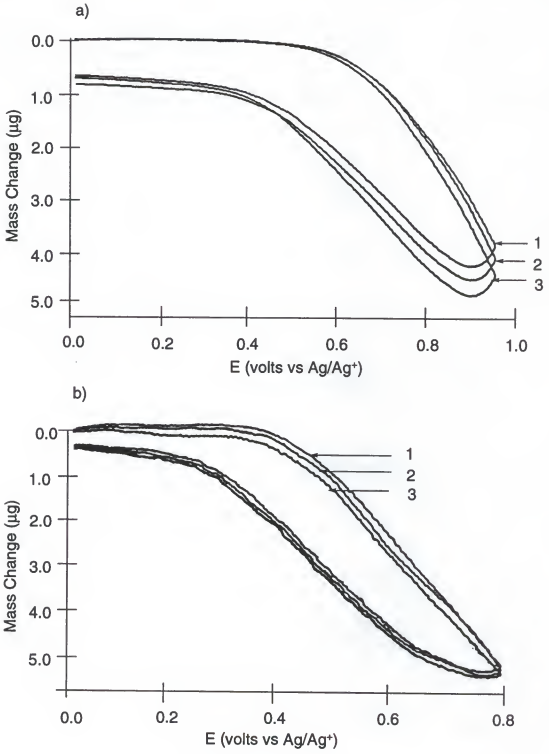

Figure 3.20. Mass response during redox switching of a) **P12** and b) **P13** at 100 mV/s in 0.1 M solution of 1) $LiClO_4$, 2) $CsClO_4$, and 3) TBAP.

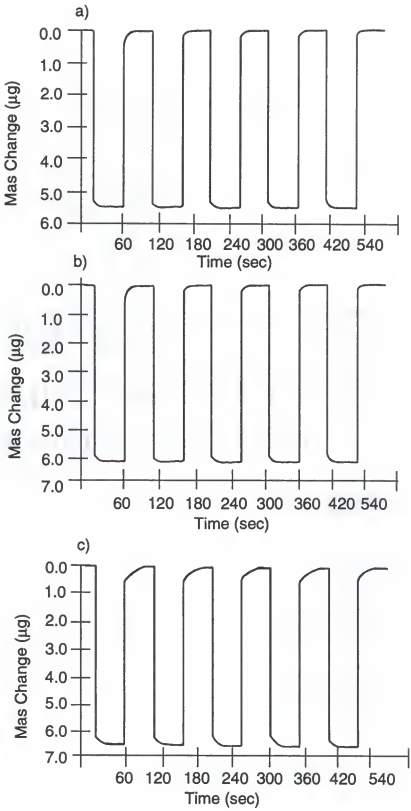

Figure 3.21. Chronogravimetric response of **P13** for ten potential steps in a) $LiClO_4$, b) $CsClO_4$, and c) TBAP.

transport mechanism in these polymers is anion dominant. The small differences can be attributed to the possible contributions from the cations, ion pairs, and solvent. Figure 3.21 shows the corresponding chronogravimetric experiments using different electrolytes in **P13**. Again a reproducible mass response is observed in all cases.

Based on the mass changes during deposition of the polymers and during the double-potential step process, a doping level of 0.33 and 0.48 mol ClO_4^-/mol repeat unit were found for **P12** and **P13** respectively, which are comparable to many polyheterocycles.

3.3 Poly[1,4-bis(2-pyrrolyl)phenylene

In order to study the effect of the heterocycle on the electrochemical and electronic properties of poly(bisheterocycle)-*p*-phenylene polymers, the monomer 1.4-bis-(2-pyrrolyl)benzene (**11**) was electrosynthesized. The monomer was synthesized in the Dr. Katritzky group as is illustrated in Figure 3.22.[20a]

3.3.1 Electropolymerization

Multiple scan cyclic voltammetric polymerization of **11** was carried out to determine monomer oxidation potential along with monitoring the growth of the electroactive film. Figure 3.23 shows the cyclic voltammetric polymerization of **11** in TBAP/CH_3CN, TBAP/PC, LiImide/CH_3CN, LiImide/PC, $LiClO_4/CH_3CN$, and $CsClO_4/CH_3CN$. The solutions were 0.01 M in

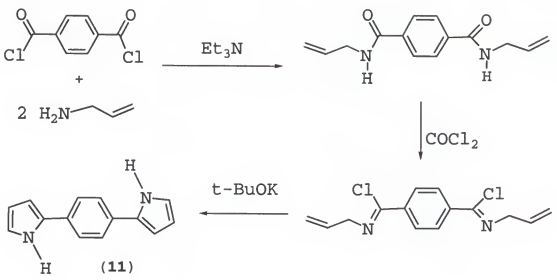

Figure 3.22. Synthetic scheme for 1,4-bis(2-pyrrolyl)benzene.

11 and 0.1 M in the corresponding electrolyte. In each case, during the first anodic scan, the monomer exhibited a low potential current peak due to the formation of the monomer radical-cation as shown in Figure 3.23 and Table 3-4.

Table 3-4. Oxidation potential of monomer **11** obtained by cyclic voltammetry in 0.1 M electrolyte and 0.1 M monomer solution.

	$E_{p,m}$ (V) *	
Electrolyte	CH_3CN	PC
TBAP	0.34	0.34
$TBAPF_6$	0.36	0.36
$LiN(SO_2CF_3)_2$	0.36	0.38
$LiClO_4$	0.37	-
$CsClO_4$	0.39	-
$NaB(Ph)_4$	0.35	-

* All potentials reported vs. Ag/Ag^+.

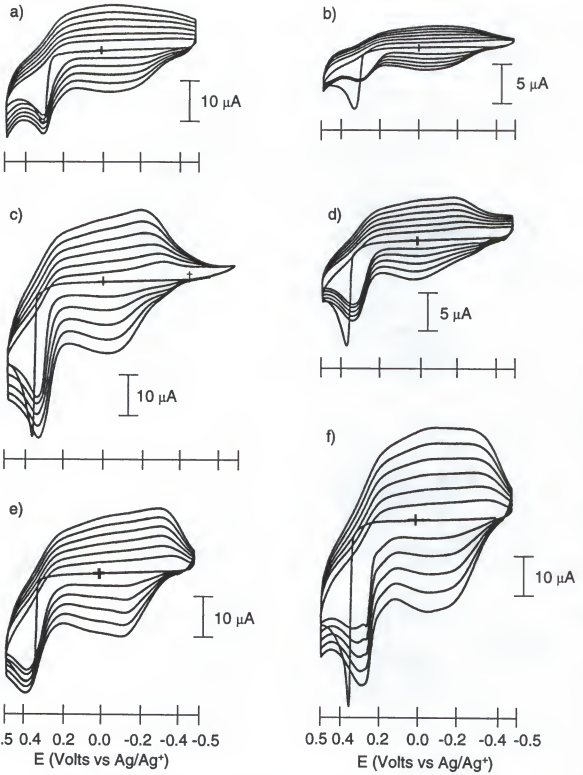

Figure 3.23. Multiple scanning electropolymerization of monomer **11** at 100 mV/s in 0.1 M solution of a) TBAP/CH_3CN, b) TBAP/PC, c) LiImide/CH_3CN, d) LiImide/CH_3CN, e) $LiClO_4$/CH_3CN, and f) $CsClO_4$/CH_3CN.

Upon the reverse scan, a broad cathodic process is observed which is indicative of the reduction of the initially formed oxidized polymer. The second and subsequent scans show an anodic current onset (*ca.* -0.4 V) due to reoxidation of the electroactive polymer followed by further monomer oxidation. The very low oxidation potential of **11** (*ca.* 600 mV lower than monomer **12**) can be attributed to the electron-rich nature of the external pyrrole units when compared to thiophene or furan, which leads to stabilization of the cation-radical intermediates during electropolymerization.

The benefit of the low oxidation potential of **11** is pointed out by its successful electropolymerization in the presence of the easily oxidized electrolyte, sodium tetraphenylborate [$NaB(Ph)_4$]. Figure 3.24b shows the multiple CVs for the scanning polymerization of **11** in 0.1 mM $NaB(Ph)_4$. For comparison, the multiple CVs of a 0.01 M in pyrrole and 0.1 M $NaB(Ph)_4$ are shown in Figure 3.24a. It is evident that, even after 15 scans, no redox processes attributable to polypyrrole can be observed. Scanning to 0.8 V, where pyrrole typically polymerizes, did not yield any deposited polymer as oxidation of $B(Ph)_4^-$ present in higher concentration dominates the anodic current.

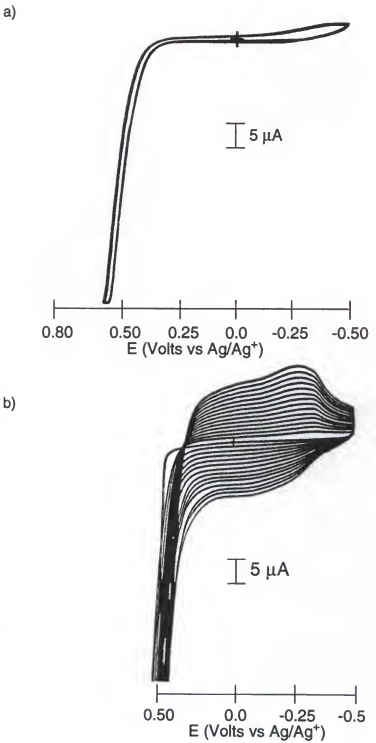

Figure 3.24. Multiple scanning electropolymerization at 100 mV/s in 0.1 M $NaB(Ph)_4/CH_3CN$ of a) pyrrole and b) monomer **11**.

3.3.2 Polymer Electrochemistry

In order to study the redox processes on **P11** formed from the electrochemical polymerization, the working electrodes coated with films were washed thoroughly with pure CH_3CN and subsequently placed into a 0.1 M monomer free electrolyte solution. Figure 3.25 shows the CVs of **P11** in the several electrolyte solutions at various scan rates. The oxidation potentials are summarized in Table 3-5. As can be seen, the potentials of the anodic and cathodic processes of the polymer are relatively close (< 80 mV) indicating a reversible redox process. Also, both current peaks are linearly proportional to the scan rate which is indicative of an electrode supported electroactive film.

Table 3-5. Electrochemical results for **P11** obtained by cyclic voltammetry in 0.1 M electrolyte/CH_3CN.

Electrolyte	$E_{a,p}$ (V)*	$E_{c,p}$ (V)	$E_{1/2}$ (V)
TBAP	-0.03	-0.05	-0.04
$TBAPF_6$	-0.05	-0.18	-0.12
$LiN(SO_2CF_3)_2$	-0.03	-0.15	-0.09
$LiClO_4$	0.09	0.03	0.06
$CsClO_4$	0.07	-0.07	0.00
$NaB(Ph)_4$	0.00	-0.08	-0.04

* All potentials reported vs. Ag/Ag^+.

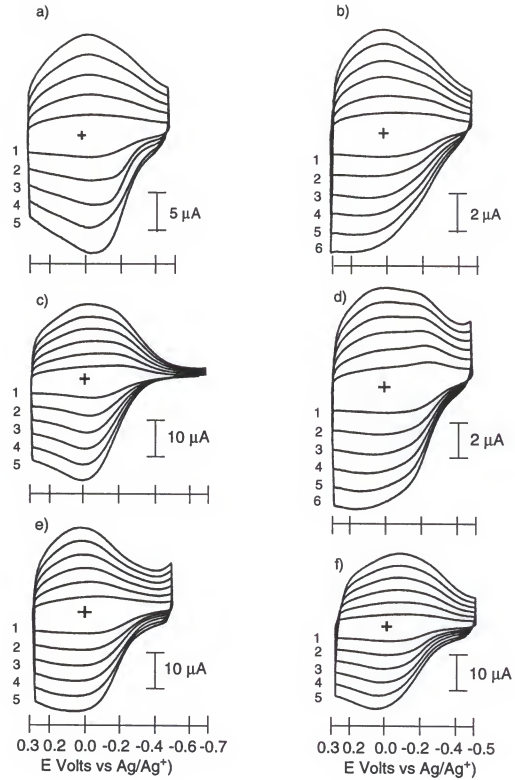

Figure 3.25. Cyclic voltammograms of **P11** electrosynthesized by scanning to $E_{p,m}$, in 0.1 M solution of a) TBAP/CH_3CN, b) TBAP/PC, c) LiImide/CH_3CN, d) LiImide/PC, e) $LiClO_4$/CH_3CN, and f) $CsClO_4$/CH_3CN, carried as a function of scan rate: 1) 25, 2) 50, 3) 75, 4) 100, 5) 125 mV/s, and 6) 150 mV/s.

3.3.3 Optoelectrochemistry

The optoelectrochemistry technique described above was used to elucidate the electronic band structure of **P11**. Figure 3.26 shows the optoelectrochemichal spectra of **P11**. The neutral form of the polymer shows a distintic π to π^* transition with a band gap onset of 2.3 V and a peak at 2.8 eV. This is lower than the values of either polypyrrole or poly-*p*-phenylene (2.7 and 3.0 eV respectively) and equal to the value of poly[1,4-bis(2-thienyl)-*p*-phenylene]. Upon oxidation, the polymer exhibited two new mid-gap transitions (at *ca.* 1 and 2.2 eV) due to the formation of bipolaron bands. At high doping levels these transitions shifted toward higher energies (1.2 and 2.5 eV respectively). This behavior was also observed in the other thienyl polymers and was explained in Chapter 1.

3.3.4 EPR/electrochemistry

The formation of spin-bearing polaronic charge carriers at intermediate doping levels was investigated using the *in situ* EPR/electrochemistry technique described in Chapter 2. Polymer films of **P11** were prepared on a Pt wire by constant potential polymerization at 0.8 V vs. Ag wire (0.5 vs. Ag/Ag^+) from a 0.01 M monomer **11** and 0.1 M TBAP/CH_3CN solution. The polymerization was allow to proceed until a charge of 0.318 C/cm^2 was passed. The polymer was

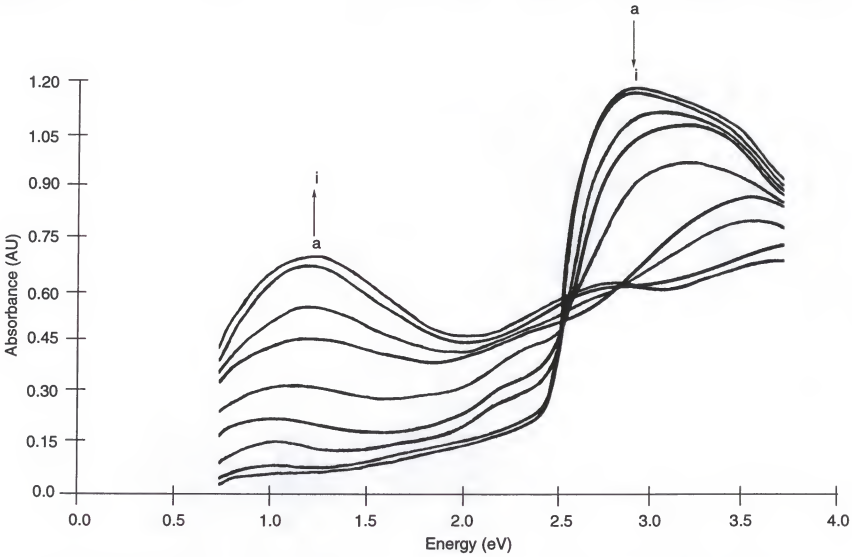

Figure 3.26. Optoelectrochemical spectra for **P11** equilibrated in TBAP/CH_3CN at: a) 0.0, b) 0.4, c) 0.5, d) 0.6, e) 0.7, f) 0.8, g) 0.9, h) 0.95, and i) 1.0 V.

subsequently washed with pure CH_3CN and placed in the EPR/electrochemistry cell. The polymer was reduced by applying a potential of -0.4 V vs. Ag/Ag^+ in monomer free 0.1 M TBAP/CH_3CN electrolyte solution and the EPR spectrum recorded. The potential was subsequently stepped in 50 mV increments and the EPR signal recorded at each potential. Figure 3.27 illustrates the evolution of the EPR signal as the polymer is oxidized. Again the magnetic field strength of maximum EPR signal intensity is independent of the potential, and the g value obtained for **P11** is 2.0052, which is close to the free electron value (g_e=2.00232). The EPR signal increases as the polymer is oxidized until it reaches a maximum value at -0.25 V as can be seen in Figure 3.27a. This is the onset for the oxidation peak observed at -0.03 V in the CV of Figure 3.25a. This result indicate that radical-cations (polarons) are necessarily intermediates in the redox mechanism even though no distinct redox processes are observed in the CVs of the polymers. Figure 3.27b shows the decrease of the EPR signal as the polymer is fully oxidized, until it completely vanishes at 0.3 V due to the combination or further oxidation of polarons to form diamagnetic bipolarons.

The spin concentration was calculated using a DPPH standard as was explained above. The maximum spin concentration (at -0.25 V) for **P11** was 0.22 spins per monomer repeat unit, this is equivalent to one spin per 14 rings.

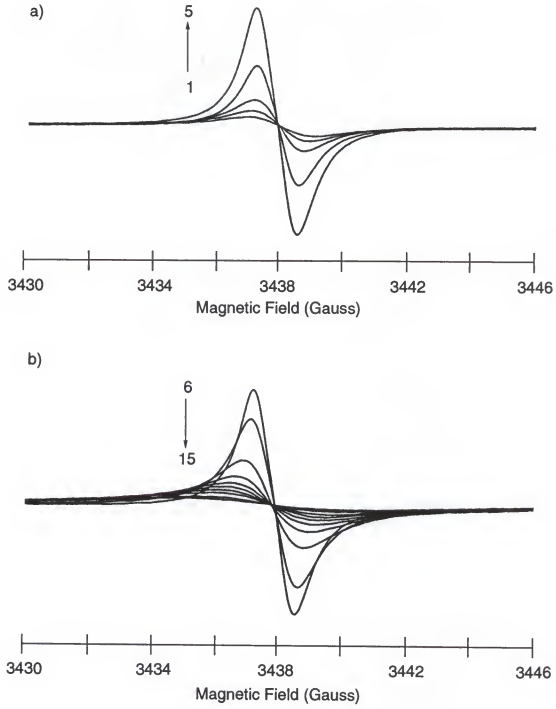

Figure 3.27. Evolution of the EPR signal as a function of the applied potential for **P11** in 0.1 M TBAP/CH_3CN: 1) -0.5, 2) -0.40, 3) -0.35, 4),-0.30 5) -0.25, 6) -0.20, 7) -0.15, 8) -0.10, 9) -0.05, 10) 0.0, 11) 0.05, 12) 0.10, 13) 0.15, 14) 0.20, and 15) 0.30 V.

This value is in the same range of polypyrrole and the other poly[1,4-(2-thienyl)-2,5- dialkylphenylenes] studied before.repeat unit, this is equivalent to one spin per 14 rings. This value is in the same range of polypyrrole and the other poly [1,4-(2-thienyl)-2,5- dialkylphenylenes] studied before. The doping level of the polymer obtained by EQCM experiments (see page 129) was 0.3 mol ClO_4^-/mol repeat unit, that corresponds to one charge per 10 rings. The lower spin concentration is a further indication that the polarons combine into bipolarons when the polymer is oxidized.

3.3.5 EQCM Studies

EQCM experiments were carried out to study the ion transport during redox switching of **P11**. Polymer films were prepared potentiostatically at 50 mV above the monomer oxidation potential (0.4 V vs. Ag/Ag^+). Figure 3.28 shows the mass responses during the polymerization of **11** in 0.1 M TBAP/CH_3CN and 0.1 M $NaB(Ph)_4/CH_3CN$. Again a linear mass deposition was observed during film formation followed by a mass loss during the dedoping of the polymer at the end of polymerization. Note the relatively larger mass loss (38.1% vs. 10.3%) in the case of BPh_4^- which is associated with the much larger mass of this anion compared to ClO_4^- (305.73 g/mol vs. 98.5 g/mol). This is an initial indication that the films are anion dominant. After equilibration, the films were washed with CH_3CN and equilibrated by cycling in monomer free electrolyte solution. Figure 3.29 illustrates the mass and

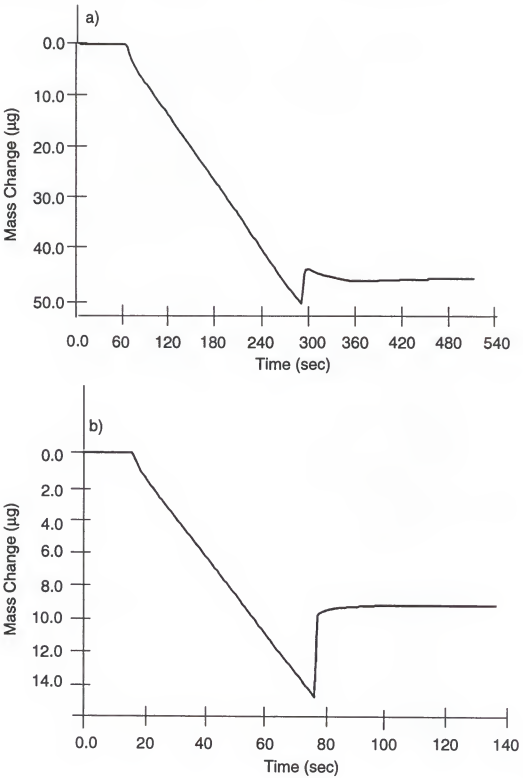

Figure 3.28. Mass change during the potentiostatic electropolymerization of **11** in a) 0.1 M TBAP/CH_3CN, b) $NaB(Ph)_4/CH_3CN$.

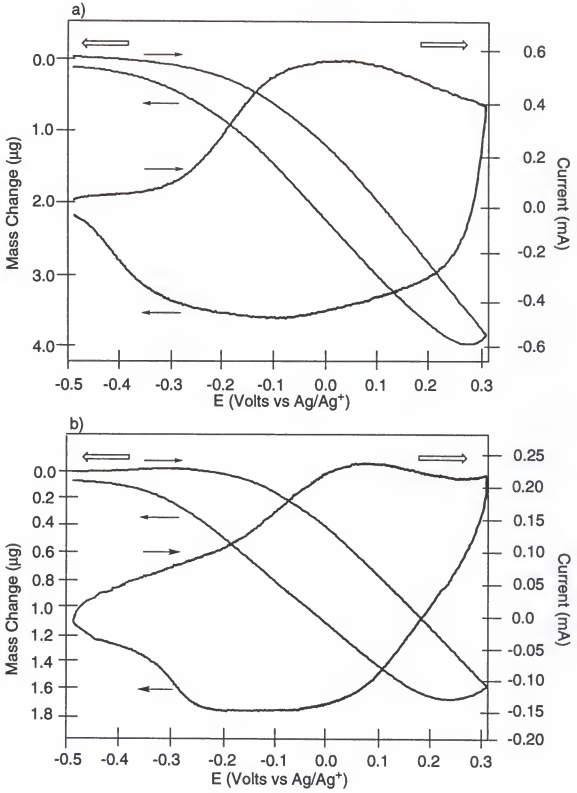

Figure 3.29. Mass and current response during potential cycling of **P11** at 100 mV/s in a) 0.1 TBAP/CH_3CN and b) 0.1 M $NaB(Ph)_4/CH_3CN$.

current response during potential cycling of the polymer. A mass increase is observed as the polymers are oxidized due to incorporation of anions [ClO_4^- and $B(Ph)_4^-$ respectively] into the films, and a mass decrease is observed when the polymers are reduced and anions move back out of the films.

The ion transport properties of **P11**/ClO_4 films during redox switching was also examined in several perchlorate salts having different cations ($LiClO_4$, $NaClO_4$ and $CsClO_4$). Figure 3.30 shows the mass response during redox cycling in 0.1 M solutions of each electrolyte. As can be seen the mass response are very similar indicating that the ion transport mechanism in **P11** is anion dominant with small contributions from the cations.

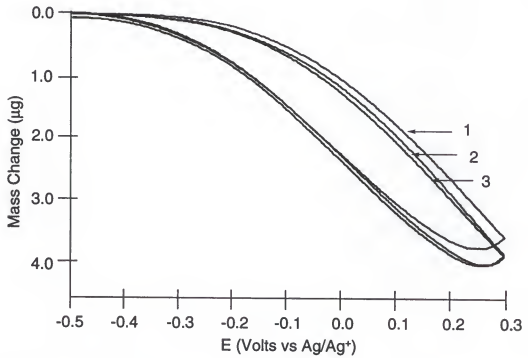

Figure 3.30. Mass response during redox switching of **P11** at 100 mV/s in 0.1 M solutions of 1) $LiClO_4$, 2) $NaClO_4$, and 3) $CsClO_4$.

Chronogravimetric studies were also carried out to study the ion transport properties of **P11** during repeated double-potential switching. Figure 3.31 shows the mass response vs. time for 10 consecutive steps of **P11** in different electrolytes. A reproducible mass gain upon oxidation, and mass loss upon reduction, in agreement with the scanning experiments was observed in all cases. In the case of **P11**/BPh_4, as the mass change is allowed to come to equilibrium in the repeated double-step, a higher change (5.87 μg) is observed than in the scanning experiment

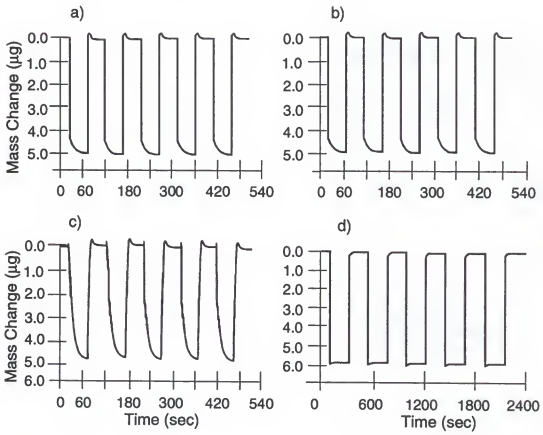

Figure 3.31. Chronogravimetric response of **P11** for ten potential steps in a) $LiClO_4$, b) $NaClO_4$, c) $CsClO_4$, and d) $NaB(Ph)_4$.

(1.56 μg at 0.3 V). The minimum time needed to reach equilibrium is *ca.* 60 s. This relatively slow response compared with the **P11**/ClO_4 films, which attains equilibrium in a few seconds, may be attributed to the larger size of $B(Ph)_4^-$, which reduces the anion mobility in the polymer film.

Based on the mass changes during deposition of the polymers and during the double-potential step process, doping levels of 0.3 mol ClO_4^-/mol repeat unit and 0.4 mol $B(Ph)_4^-$ /mol repeat unit were calculated for **P11**.

In order to determine whether the **P11**/BPh_4 films behave rigidly during the EQCM experiments, conductance spectra were taken before and after deposition of the polymer in its reduced and oxidized states as shown in Figure 3.32. The value of the full width at half height, Δf_{FWHH} of the conductance spectra were *ca.* 63 Hz in all cases indicating that the film is behaving in a rigid manner and that the Sauerbrey relationship is applicable under these conditions.

3.3.6 Conductivity

Films of **P11** were obtained by constant potential electropolymerization at the monomer peak potential (0.35 V vs Ag/Ag^+) for electrical conductivity measurements. The films were handled as was explained in Chapter 2. The conductivity was measured using the four-probe method, and calculated using the equation (1-18). Table 3-6 summarizes the results obtained for **P11** in three different electrolytes.

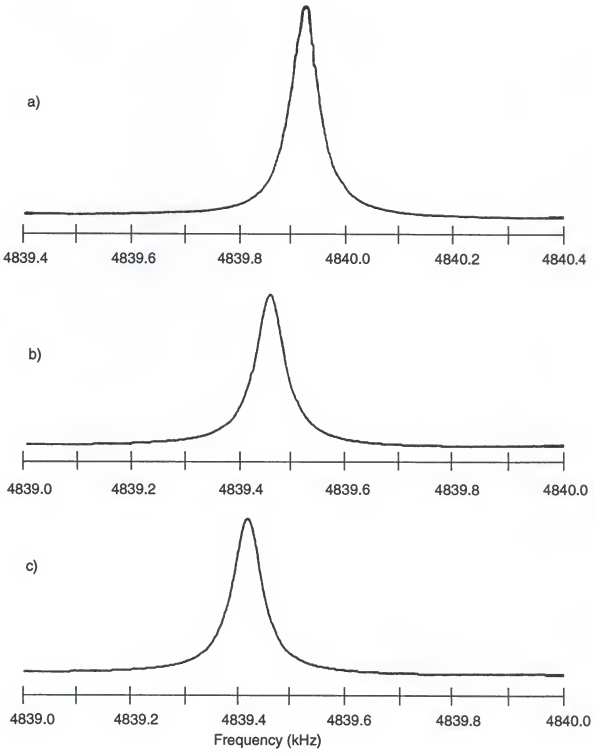

Figure 3.32. Conductance spectra of a) bare quartz crystal, b) quartz crystal plus oxidized **P11**, and c) quartz crystal and reduced **P11**.

Table 3-6. Conductivities of **P11** films prepared in three different electrolyte solutions.

Polymer Film	Q* (C/cm^2)	Electrolyte/solvent	conductivity (S/cm)
P11/ClO_4	2.0	TBAP/CH_3CN	2
P11/TOS	1.5	TEATOS/CH_3CN	1
P11/$N(SO_2CF_3)_2$	1.5	$LiN(SO_2CF_3)_2$/PC	30

* Charge passed during electropolymerization.

The conductivity values are on the same order of magnitude as the conductivities of 1-100 S/cm found in polypyrrole and similar to the ones obtained with poly[1,4-bis(2-thienyl)-2,5-dialkoxyphenylenes].[19,171]

3.4 Poly[bis(2-thienyl)-9,9'-didecylfluorene] and Poly[bis(2-(3,4-ethylenedioxy)thienyl)-9,9'-didecylfluorene]

In order to complement the study of the effect of the terminal heterocycle on the electrochemical and electronic properties of conducting polymers from multi-ring aromatic monomers, the monomers bis(2-thienyl)-9,9'-didecylfluorene (**17**) and bis(2-(3,4-ethylenedioxy)thienyl)-9,9'-didecylfluorene (**18**) were electropolymerized. These monomers were synthesized in the group of Dr. Bruce Reinhardt (US Air Force Wright Laboratory) as illustrated in Figure 3.33.

3.4.1 Electropolymerization

The electropolymerization and concurrent film deposition of **17** and **18** were carried out using multiple scan cyclic

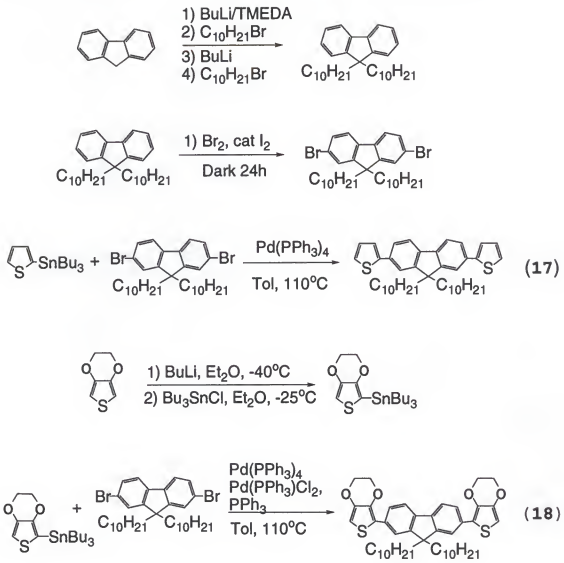

Figure 3.33. Synthetic scheme for monomers **17** and **18**.

voltammetry. Monomer **17** was electropolymerized using mixtures of CH_2Cl_2/CH_3CN different proportions with an optimum composition of 30:70 CH_2Cl_2:CH_3CN yielding a well behaved polymerization and film deposition as illustrated by Figure 3.34. In pure CH_2Cl_2, no polymer deposition was observed at the electrode surface at potentials lower than 1.3 V. Although the monomer oxidation onset is 0.75 V, after several

scans at potentials < 1.2 V the electrolyte solution turns olive green. This behavior can be attributed to a high degree of solubility of the oligomers as they form as was explained above. When the potential was scanned up to 1.4 V (Figure 3.34a), a slow growth of an olive green electroactive polymer was observed on the surface of the working electrode with a redox process evolving at *ca.* 0.7 V. Increasing the polarity of the electrolyte solution with CH_3CN reduces the polymerization potential and increases the rate of polymerization. Figure 3.34b shows the multiple scan cyclic voltammetric polymerization of **17** in a solution 0.1 M TBAP in 30:70 CH_2Cl_2:CH_3CN. In this instance, efficient electropolymerization occurs with scanning to 0.90 V. Evolution of the polymer reduction peak is observed at 0.66 V on the reverse scans, and subsequent polymer reoxidation at 0.69 V. With consecutive scans, the oxidative peak of the polymer shifts to more positive potentials, indicating either increasing resistance as the film increases in thickness or a decreased rate of compensating ion transport. Monomer **18** electropolymerized at significantly lower potentials and more rapidly than **17**. In this instance, the electropolymerization was carried out in 0.1 M TBAP/CH_3CN as the monomer could be fully solubilized (**17** is insoluble in CH_3CN). As shown in the multiple scan cyclic polymerization results in Figure 3.35, the electron donating effect of the alkoxy substituents of the EDOT units reduced the onset for monomer oxidation to 0.51 V allowing the electropolymerization to proceed

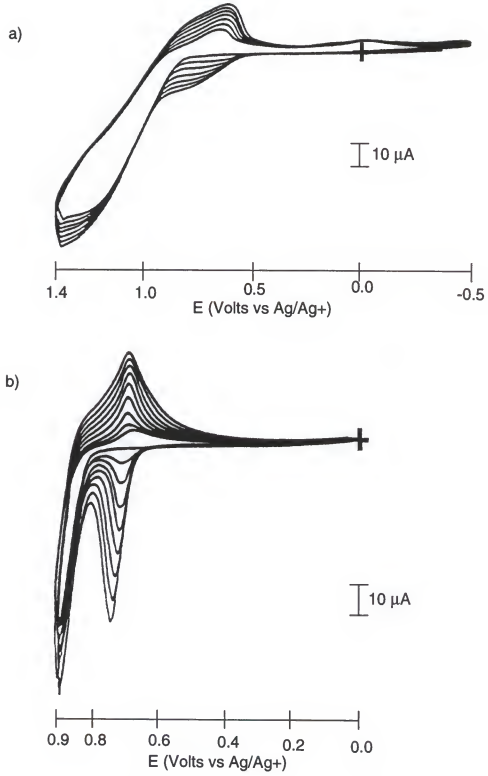

Figure 3.34. Multiple scanning electropolymerization at 100 mV/s of monomer **17** in a) 0.1 M TBAP/CH_2Cl_2, and b) in 0.1 M TBAP/CH_2Cl_2:CH_3CN (30:70).

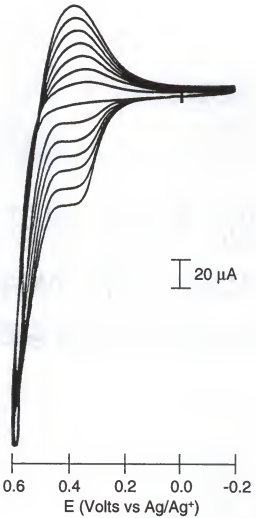

Figure 3.35. Multiple scanning electropolymerization at 100 mV/s of monomer **18** in 0.1 M TBAP/CH_3CN.

efficiently at potentials as low as 0.55 V. This effect of reducing the monomer oxidation potential by changing thiophene to EDOT has also been observed for 1,4-bis(2-thienyl)benzene and 1,4-bis(2-pyrrolyl)benzene and was discussed above. The enhancement in the rate of electroactive polymer deposition is *ca.* 2 times relative to **17** as determined by comparison of the peak currents of the polymer

redox which evolves during the scanning electro-polymerization, and by comparison of the peak currents for redox of the resultant polymers in monomer free electrolyte as showed below.

3.4.2 Polymer electrochemistry

Cyclic voltammograms of the resulting **P17** in monomer free electrolyte show that, after a break in period in which the anodic and cathodic peaks decrease in intensity and move towards slightly higher potentials, they stabilize at 0.81 and 0.74 V respectively. This is illustrated in Figure 3.36a, which shows the scan rate dependence for the current response during redox cycling of **P17** between 0.0 and 0.9 V. It can be seen that both the anodic and cathodic peak currents scale linearly with scan rate. This is as expected for an electrode supported electroactive film. The electrochemical behavior of **P17** ($E_{1/2}$ = 0.78 V) is similar to that of poly[1,4-bis(2-thienyl)benzene] with a broad redox process. At potentials higher than 1.0 V the electroactivity of **P17** decreases rapidly likely due to overoxidation of the polymer. Figure 3.36b shows the scan rate dependence for the redox response of **P18** in monomer free electrolyte. The resulting **P18** shows an $E_{1/2}$ = 0.44 V and again the current response with scan rate is linear. The cyclic voltammograms are reproducible if the potential is not increased to values higher than 0.6 V. At more positive potentials a second irreversible oxidation occurs, decreasing the electroactivity of the film rapidly as

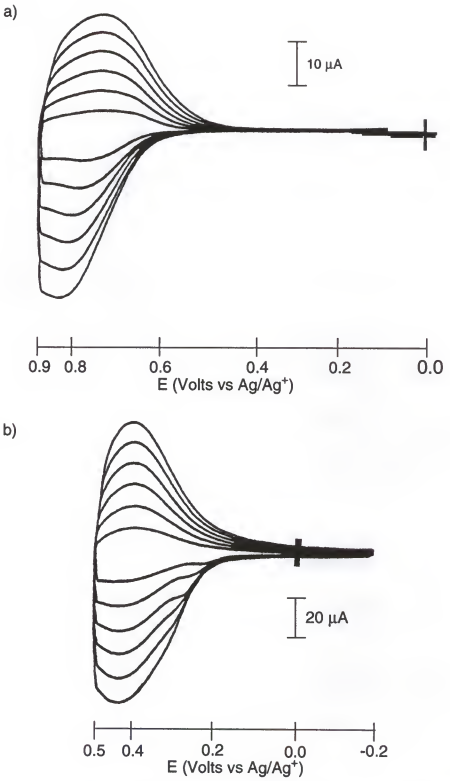

Figure 3.36. Cyclic voltammograms of: a) **P17** b) and **P18** electrosynthesized in a) 0.1 M TBAP/CH_3CN, carried as a function of scan rate: 1) 25, 2) 50, 3) 75, 4) 100, and 5) 125 mV/s.

the polymer overoxidizes. The *ca.* 400 mV decrease in $E_{1/2}$ attained by utilizing EDOT as the electropolymerizable unit yields a significantly more stable oxidized and conducting state, along with more facile redox switching avoiding high potential derived side reactions.

3.4.3 Optoelectrochemistry

The electronic properties of **P17** and **P18** were studied by optoelectrochemistry after potentiostatic synthesis onto transparent ITO coated glass electrodes at the $E_{p,m}$ of the monomers. The spectra were initially obtained in the fully reduced state in order to determine the band gap of the polymer, which is defined as the onset of the π to π^* transition for the conjugated backbone. The potential applied to the polymer coated electrodes was then sequentially increased to higher potentials to oxidize the polymers and monitor the creation of the charge carriers.

As shown by spectrum 1 in Figure 3.37, **P17** exhibits a band gap of 2.4 eV and an absorption maximum at 3.1 eV when the potential is held at 0.0 V vs Ag/Ag^+. In the fully reduced state, films of **P17** are olive green which convert to a dark green upon oxidation. At intermediate levels of oxidation, up to an applied potential of 0.9 V, two absorbance peaks evolve at 0.8 and 1.8 eV due to the formation of bipolaronic charge carriers as was explained above. These two new low energy transitions grow in intensity at the expense of the π to π^* transition, but in the case of

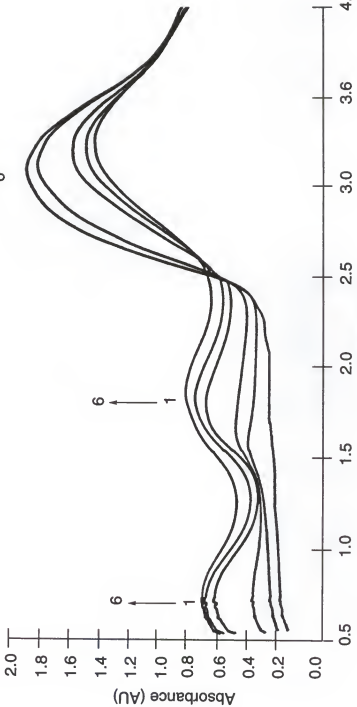

Figure 3.37. Optoelectrochemical spectra for **P17** equilibrated in TBAP/CH_3CN at a): 1) 0.0, 2) 0.5, 3) 0.6, 4) 0.7, 5) 0.8, 6) 0.9 V.

P17, it should be noted that even at 0.9 V there is a significant amount of absorption remaining due to the interband transition. At the same time, the intensity of the bipolaronic transitions are weak. At potentials higher than 1.0 V, the intensity of all transitions decreases rapidly. This indicates that the polymer does not dope to a high level before the overoxidation process occurs leading to degradation of the polymer's redox activity.

During electropolymerization, **P18** forms a dark blue film in the oxidized form. Electrochemical reduction, even at potentials as low as -1.0 V, does not fully reduce the film as evidenced by low energy absorbances (< 2 eV) due to trapped charged states. In order to fully reduce **P18**, the films were first reduced electrochemically at -0.5 V and subsequently reduced chemically by exposure to a dilute solution of hydrazine *ca.* 1% in CH_3CN. As shown in Figure 3.38, in the fully reduced state, **P18** is reddish-tan and the spectrum shows a broad onset at 2.2 eV with a peak at 2.6 eV corresponding to the intergap transition of the neutral polymer. It is worth noting that the high energy peak observed at 3.4 eV is also present in the monomer. Oxidation of **P18** leads to the formation of bipolaronic states as characterized by two new transitions at 1.1 and 2.1 eV and the polymer converts back to a dark blue. As in **P17**, these two transitions increase in intensity at the expense of the interband transition with increased potential, but in this instance the intragap transitions of **P18** are more intense in

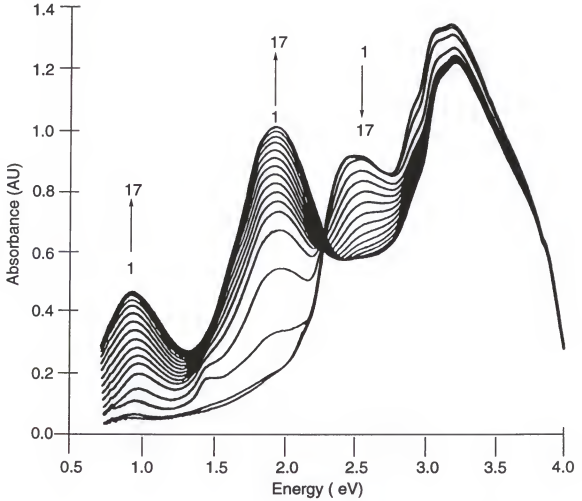

Figure 3.38. Optoelectrochemical spectra for **P17** equilibrated in TBAP/CH_3CN at a): 1) -0.5, 2) -0.3, 3) -0.2, 4) -0.1, 5) 0.0, 6) 0.05, and 7) 0.1 V; 8) 0.15, 9) 0.2, 10) 0.25, 11) 0.30, 12) 0.35, 13) 0.4, 14) 0.45, 15) 0.5, 16) 0.55, and 17) 0.60 V.

the fully oxidized state and the interband transition disappears. This is further indication that **P18** reaches higher doping levels without being overoxidized, which is a consequence of its lower redox potential.

3.4.4 EQCM studies

The mass transport characteristics of **P17** and **P18** films, synthesized potentiostatically at the $E_{p,m}$, were studied using the EQCM. Figure 3.39a shows the polymerization of **17** at 0.9 V vs. in 0.1 M TBAP CH_2CH_2:CH_3CN (30:70) and Figure 3.39b shows the polymerization of **18** at 0.6 V in 0.1 M TBAP/CH_3CN. The linear mass deposition was allow to proceed until a *ca.* 35 μg were deposited, again the mass loss at the end of the polymerization corresponds to the dedoping of the polymer when it is reduced at -0.3 V. The films were washed thoroughly with distilled CH_3CN, and placed in monomer free 0.1 M TBAP/CH_2Cl_2:CH_3CN (30:70) solution for **P17** and 0.1 M TBAP/CH_3CN for **P18**. The polymer films were cycled ten times between the reduced and oxidized states at 100 mV/s to equilibrate the redox response. Figure 3.40 shows the mass response during a cyclic scan for a film of **P17**.During the anodic scan the film is oxidized and a mass increase is observed with an onset potential (*ca.* 0.60 V) that corresponds with the oxidation of the polymer. This indicates that the ClO_4^- ions (and likely some solvent) are incorporated into the film. During the cathodic scan, a mass decrease is observed, which is associated with the movement of anions

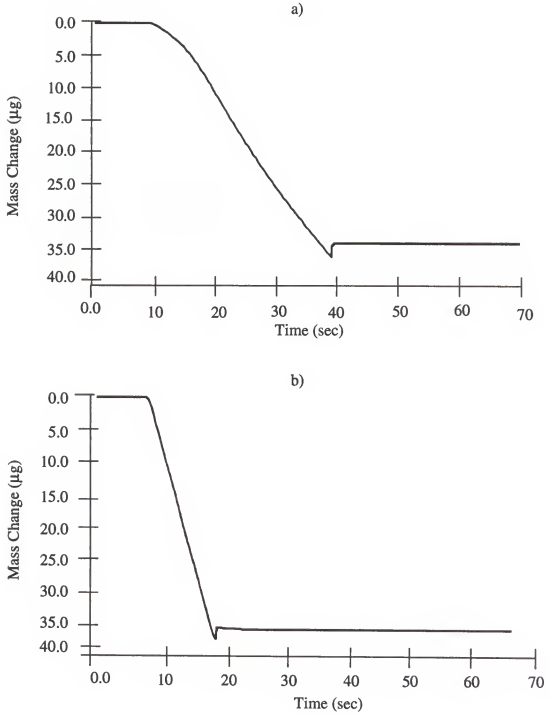

Figure 3.39. Mass change during the potentiostatic electropolymerization of a) momomer **17**, and b) monomer **18**.

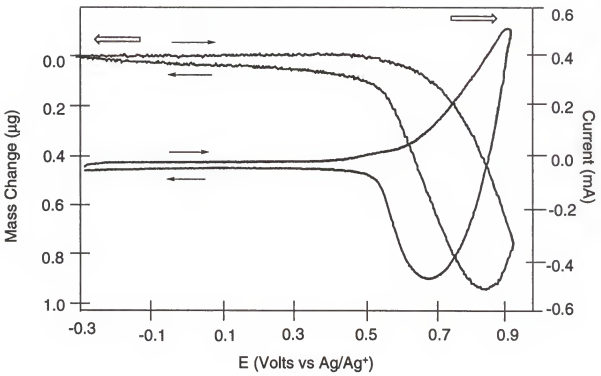

Figure 3.40. Mass and current response during potential cycling of **P17** at 100 mV/s in 0.1 TBAP/CH_2l_2:CH_3CN (30:70).

(and solvent) back out of the film. Some hysteresis in the mass response is observed during the initial part of the reverse scan (0.9 to 0.6 V) due to the non-equilibrium nature of the cyclic voltammetric experiment, but the film returns to its original mass when the potential applied is low enough (*ca.* -0.3 V) to reduce the film completely. Due to problems associated with incomplete electrochemical reduction of **P18**, reproducible mass transport characteristics during switching could not be obtained.

A chronogravimetric experiment was subsequently carried out on the same **P17** film to examine the mass transport properties of the film during a double potential step process

from -0.3 to 0.9 V. Figure 3.41 shows the mass response as a function of time for 10 consecutive potential steps. A relatively reproducible mass response is obtained for approximately 20 redox switches. The observed increase of mass upon oxidation and decrease upon reduction are in agreement with the scanning experiments. However, as the mass change is allowed to come to equilibrium in the repeated double potential step experiment, a higher mass change (2.25 μg) is observed than in the scanning experiment (0.80 μg at 0.9 V). Based on the mass changes observed during deposition of the polymer and during the double step process, and assuming that the amount of solvent incorporated is

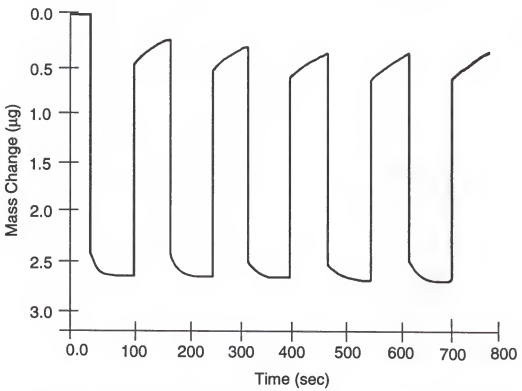

Figure 3.41. Chronogravimetric response of **P17** in 0.1 M TBAP/CH_2Cl_2:CH_3CN.

negligible, a molar ratio of 0.46 mol ClO_4^- per mol repeat unit of **17** is found. This corresponds to a doping level of 0.12 charges per ring along the polymer backbone. These results indicate that **P17** has an anion dominant behavior when it is switched between its reduced and oxidized forms. Conductance spectra were taken before and after deposition of **P17** in its reduced and oxidized state as illustrated in Figure 3.42. The values of the full width at half height, Δf_{fwhh} of the conductance were 46 and 42 Hz for the reduced and oxidized film respectively. These very close values indicate that the film is behaving in a rigid manner and that the Sauerbrey relationship is applicable under these conditions.

3.4.5 Conductivity and Morphology

Room temperature conductivities for **P17** and **P18** were measured on films synthesized potentiostatically at the monomer peak potentials, $E_{p,m}$ (0.9 and 0.6 V respectively). The films were washed thoroughly with distilled CH_3CN, and placed in monomer free 0.1 M TBAP/CH_2Cl_2:CH_3CN (30:70) solution for **P17** and 0.1 M TBAP/CH_3CN for **P18**. Conductivities up to $1x10^{-4}$ S/cm for **P17** and $6x10^{-4}$ S/cm for **P18** were observed. Both polymers are insoluble in common organic solvents in both their oxidized and reduced forms. Scanning electron micrographs were obtained of oxidized and reduced films of **P18** prepared by repeated scanning

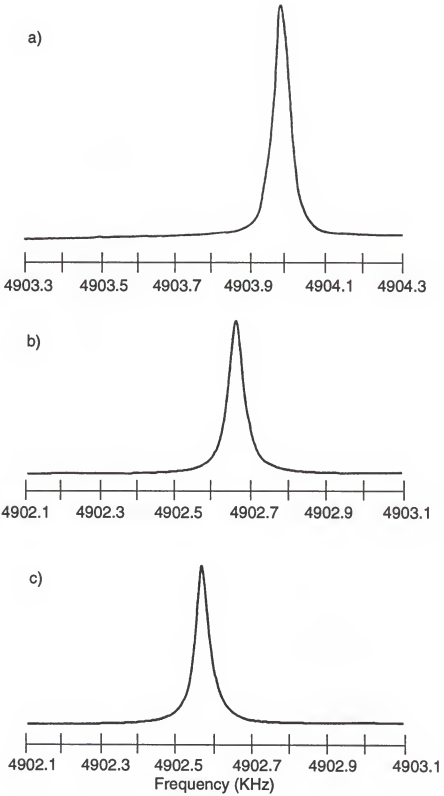

Figure 3.42. Conductance spectra of a) bare quartz crystal, b) quartz crystal plus oxidized **P17**, and c) quartz crystal plus reduced **P17**.

a)

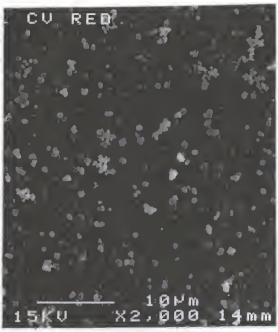

b)

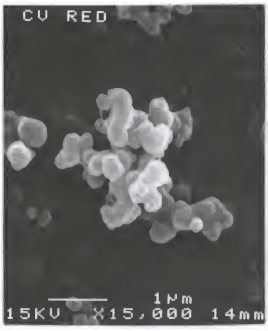

c)

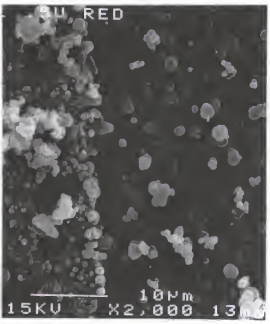

d)

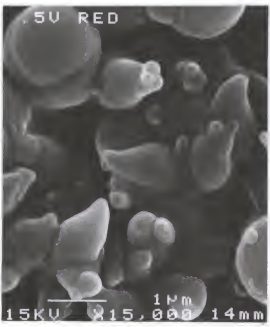

Figure 3.43. Scanning electron micrographs of: a) and b) reduced **P18** prepared by repeated scanning up to 0.6 V at 100 mV/s; c) and d) reduced **P18** prepared by constant potential polymerization at 0.5 V.

e)

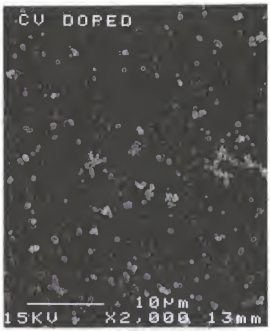

f)

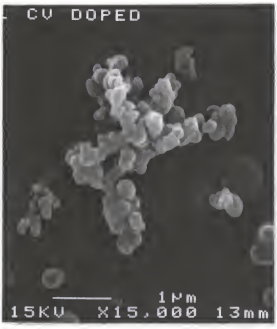

g)

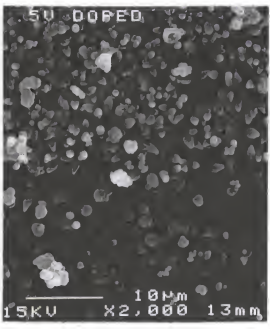

h)

Figure 3.43 (continuation). e) and f) oxidized **P18** prepared by repeated scanning up to 0.6 V at 100 mV/s; g) and h) oxidized **P18** prepared by constant potential polymerization at 0.5 V.

polymerization and potentiostatic synthesis at 0.5 V as shown in Figure 3.43. The morphology of the films is characterized for the presence of nodular deposits scattered over the entire area on top of a smoother surface. The density of the nodular deposits is higher in the films obtained by repeated scanning polymerization and the size of the nodules is smaller indicating a more compact film.

3.5 Conclusions

The electrochemical and electronic properties in a series of substituted poly[1,4-bis(2-heterocycle)-*p*-phenylenes] and poly(3,12-(2-heterocycle)-9,9-dialkylfluorenes] have found to be highly substituent dependent. Alkoxy substitution on the phenylene rings, through a combination of electro-donating and steric factors, results in a marked decrease in monomer and polymer oxidation potentials and a decrease in the electronic band gap. Substitution with long-chain alkoxy groups results in the formation of stable paramagnetic charge carriers at intermediate doping levels, and metallic charge carriers at high doping levels.

Changing the nature of the heterocycle, decreases further the monomer and polymer oxidation potentials. The presence of electron rich heterocycles (e.g., pyrrole and EDOT) as terminal electropolymerizable moieties on the multi-ring conjugated monomers leads to stabilization of the cation radical intermediates allowing the electropolymerization to

proceed at low potentials even in the presence of easily oxidized electrolytes. The ion transport results indicate that these polymers have an anion dominant behavior.

CHAPTER 4
POLYPYRROLE AS A SOLID ELECTROLYTE FOR TANTALUM CAPACITORS

4.1. Introduction

The development of conducting polymers has now led to a number of materials available for practical application in a number of systems of industrial interest.[24-30] One of the more highly developed applications is in the field of solid electrolyte capacitors,[136] where polypyrrole (PPy) as been used to replace MnO_2, and TCNQ as the counter electrode due to its higher conductivity, long term stability, and ease of preparation by both chemical[165] and electrochemical[6a] methods. PPy doped with several counterions has been previously applied as a solid electrolyte in aluminum and tantalum capacitors using chemical and electrochemical synthetic procedures.[136d] In addition, capacitors prepared using a combination of MnO_2 and PPy have been studied.[136c]

In this chapter, a study of PPy as a solid electrolyte for Ta capacitors, prepared using a combination of chemical and electrochemical methods, is presented. Anthraquinone-2-sulfonate (AQS) was used as the charge compensating dopant ion in PPy due to its good thermal and long term stability. The properties of the PPy's synthesized were analyzed before and after the re-anodization process used in the preparation

of the capacitors. In addition, the dielectric properties of the capacitors prepared under various conditions were measured in order to determine the optimum conditions for PPy solid electrolyte deposition.

4.2. Preparation of Tantalum Solid Electrolyte Capacitors

4.2.1. PPy Prepared by Chemical Polymerization Followed by Electropolymerization

Ta/Ta_2O_5 pellets of 1 and 2 μF used in the experiments were provided by AVX, which were regular anodes vacuum sintered and subsequently anodized in 1% phosphoric acid at 85 ^0C. In order to eliminate possible damages to the dielectric layer upon handling, the anodes were re-anodized at the formation voltage of 125 V. Pyrrole was purified by passing through a Pasteur pipette filled with activated alumina until colorless prior to use. After rinsing the pellets with double distilled water, they were dipped into a solution of 70 mM $FeCl_3$, 0.1 M NaAQS, and 30 mM pyrrole in water to form the chemically polymerized PPy as a coating on the Ta_2O_5 throughout the capacitor. An excess amount of AQS^- was used in order to force aromatic sulfonates to be the dominant dopant ions important for high conductivity. The optimum reaction time was *ca.* 24 hours. The PPy coated anodes were subsequently washed with double distilled water and dried at 80 ^0C for 15 minutes. The anodes were re-anodized at room temperature in a solution of 1% H_3PO_4 or 0.1 M H_3BO_3/SSA

or $PhB(OH)_2$/SSA starting with an initial potential of 5 V and sequentially increasing the potential up to 50 V, where the leakage current was 1-2 μA/anode. The electropolymerization of pyrrole was carried out galvanostatically (current density=2 mA/anode) by using an external electrode to contact the conductive layer of the chemically deposited PPy as is shown in Figure 4.1. The electrolytic solution was 0.1 M pyrrole, and 0.1 M sodium tosylate (NaTos) in water. The electropolymerization was carried out until the anodes were fully coated with PP, *ca.* 30 minutes.

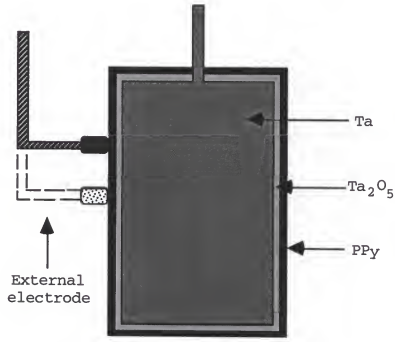

Figure 4.1. schematic design for the electropolymerization of pyrrole on a Ta/Ta_2O_5 pellet previously coated with chemically prepared PPy.

After washing with double distilled water and drying at 80 ^{0}C, the capacitors were finished by applying layers of graphite and silver paste.

4.2.2. PPy Coating Prepared by Multi-Step chemical Polymerization

After the initial chemical coating with PPy as described above, the thickness of the PPy layer was increased by a repeated dipping process where the pyrrole monomer, $FeCl_3$, and NaAQS are premixed in the proportions mentioned above. The anodes were subsequently re-anodized at room temperature to reduce the leakage current. This process was repeated until the anodes were fully covered with PPy. After washing and drying, graphite and Ag pastes were applied in sequence to form the electrical contact.

4.3. Characterization of the PPy Solid Electrolyte Capacitors

Cyclic voltammetry was used to study the electrochemical properties of PPy prepared chemically and electrochemically. PPy films were prepared on ITO electrodes as the working electrodes using the same conditions as in the preparation of the capacitors for both the chemically and electrochemically synthesized PPy. An Ag/AgCl reference electrode and a platinum foil counter electrode were employed.

XPS spectra were obtain as was explained in chapter 2 in order to obtain the doping levels of the PPy films.

UV-Vis spectra of the re-anodization solution were obtained to check if spontaneous ion-exchange occurred during the re-anodization process.

The characterization of the capacitors was carried out using an HP 4263A LCR meter measuring capacitance, dissipation factor (DF), and equivalent series resistance (ESR).

4.4. Results and Discussion

Figure 4.2 shows a schematic of a solid electrolytic tantalum capacitor where the high surface area sintered anode body has been covered by a continuous dielectric layer of

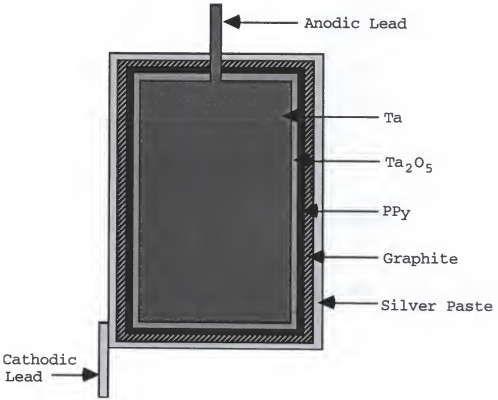

Figure 4.2. Schematic of a solid electrolytic Ta capacitor.

Ta_2O_5, subsequently coated with PPy, and layers of graphite and silver paste to complete the capacitor. It is essential that the solid electrolyte, in this case PPy, covers the whole dielectric layer in order to achieve full capacitance. It was found that full capacitance, indicative of full surface coverage of the anodes by the PPy, can be achieved regardless of the preparation procedure. Figure 4.3 shows the Ta/Ta_2O_5 pellets before and after impregnation with PPy. These capacitors also have a low eqivalent series resistances, ESR, suggesting that the PPy layer formed on the dielectric is highly conductive. This is demonstrated in Figure 4.4, in which a comparison is made between a PPy/Ta capacitor with a standard commercial MnO_2 coated capacitor. The replacement of MnO_2 with PPy reduces the ESR about 50% at high frequency. Figure 4.5 shows the capacitance retention of Ta capacitors as function of frequency for capacitors prepared under different conditions. The PPy/Ta capacitors retain about 87% of the design capacitance value at 100 kHz, while their MnO_2 counterparts retain less than 70% of their original value. At frequencies higher than 100 kHz, the PPy based capacitors reach the resonance frequency, where they behave as inductors and the capacitance is not well defined. This behavior has already been observed with MnO_2 coated capacitors,[136d] but the phenomenon begins at lower frequencies (*ca.* 0.1-1 kHz). This is due to the fact that MnO_2 has a lower conductivity than PPy and indicates that PPy is the better material for high frequency applications.

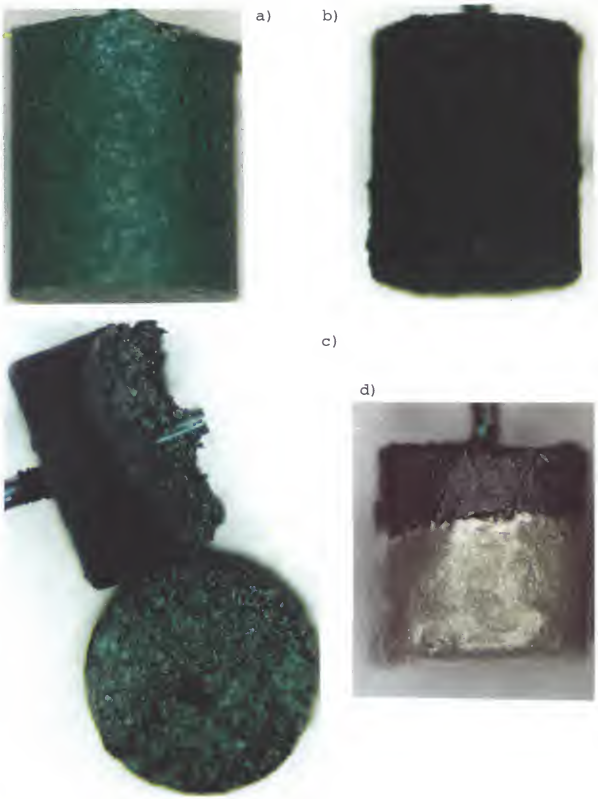

Figure 4.3. a) Ta/Ta_2O_5 pellet before impregnation with PPy, b) Ta/Ta_2O_5 coated with PPy, c) internal view of Ta/Ta_2O_5 coated with PPy, and d) finished PPy/Ta capacitor.

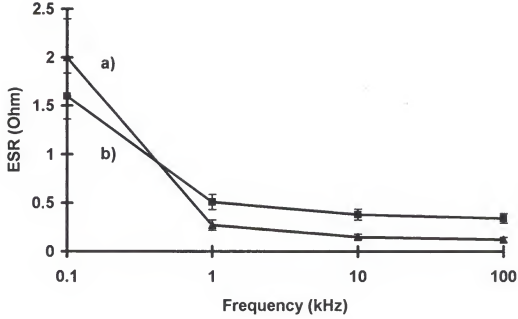

Figure 4.4. ESR vs. frequency for a) PPy/Ta capacitor and b) MnO_2/Ta capacitor.

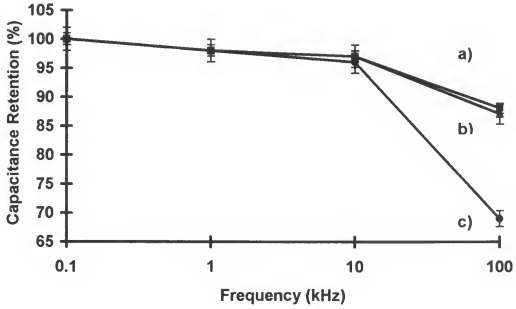

Figure 4.5. Capacitance vs. frequency for a) PPy/Ta capacitors prepared with chemically synthesized PPy, b) PPy/Ta capacitors prepared with chemical plus electrochemical synthesized PPy, and c) MnO_2/Ta capacitors.

Other impregnation methods were also evaluated, such as the exposure of anodes precoated with oxidants to pyrrole vapor and the dipping of anodes in oxidant and pyrrole solutions in sequence, for their effectiveness and capacitor performance. These approaches do not to yield satisfactory results, likely due to the formation of oligomers during the polymerization where the monomer/oxidant reactions are limited by the interfacial diffusion.

One key issue in manufacturing tantalum capacitors is to build up a robust outer layer for the anode to protect it from possible mechanical damage. One drawback of the PPy/Ta capacitors made using the multiple dipping process is the fragility of the parts due to the powdery nature of chemically synthesized PPy. In order to overcome this problem, an electrodeposition process is used to electrochemically polymerize PPy onto the anodes after partial coverage with chemically formed PPy. There are no significant differences in the dielectric properties of the capacitors prepared using either chemically formed PPy or electrochemically deposited PPy. This suggests that the electrical properties of the PPy's, especially conductivity, are similar. These results were confirmed by a CV experiment, where chemically prepared PPy on ITO was compared to electrochemically prepared PPy as shown in Figure 4.6 and Table 4.1. It is clear that during chemical polymerization the positions of the anodic and cathodic peaks are unaffected

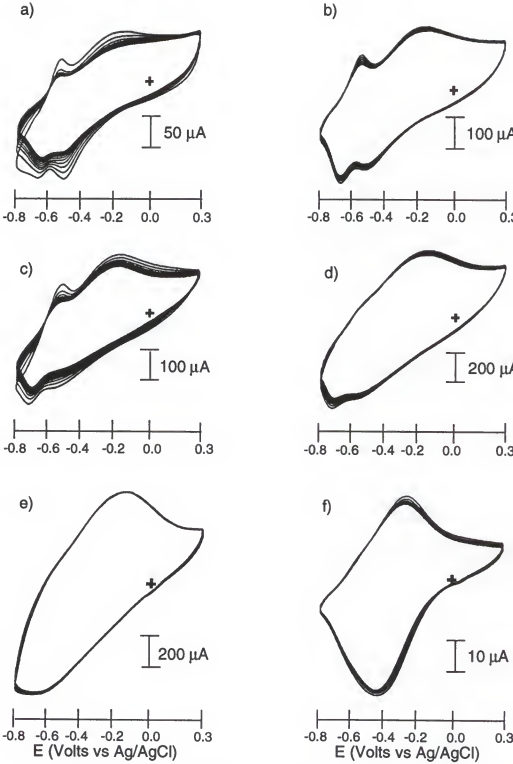

Figure 4.6. Cyclic voltammograms of chemically synthesized PPy on ITO at different reactions times: a) 10 min, b) 30 min, c) 1 hour, d) 2 hours, e) 4 hours, and f) PPy electrosynthesized.

Table 4.1. Cyclic voltammetry results for PPy prepared chemically and electrochemically.

Reaction Time	$E_{p,m}$ (V)*	$E_{p,c}$ (V)
10 minutes	-0.54, -0.19	-0.52, -0.67
30 minutes	-0.55, -0.19	-0.53, -0.69
1 hour	-0.53, -0.18	-0.57, -0.73
2 hours	-----, -0.18	-0.59, -0.73
4 hours	-----, -0.17	-----, -0.67
PPy electrosynthesized	-----, -0.30	-----, -0.46

* All potentials reported vs. Ag/AgCl.

by the reaction time. However, as the polymer films become thicker, the resolution observed in the CV's decreases and the two redox processes converge into one broad band. This is possibly due to a broadening in the distribution of the conjugation length in the polymer chains. As can be seen in Table 4.1, the difference in the E_p values for the main redox process of the thick chemically and the electrochemically synthesized PP are on the order of 0.1-0.2 V, indicating that the polymers have similar electrochemical properties.

The electrolytes used to re-anodize the anodes are important. For example, re-anodization in H_3PO_4 results in a much higher dissipation factor (DF) than in H_3BO_3/SSA or $PhB(OH)_2$/SSA solutions as is presented in Figure 4.7. This is due to the fact that the doping level of PPy is affected by the process. These results were complemented by XPS analysis of the PP films deposited on Ta/Ta_2O_5 foils. The XPS spectra

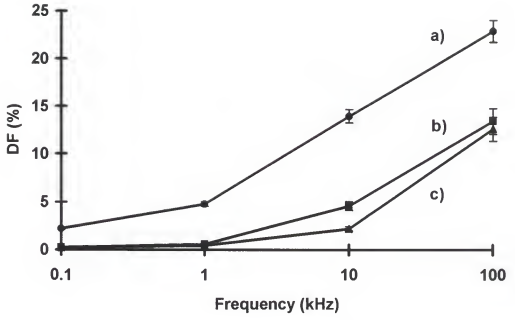

Figure 4.7. DF vs. voltage for capacitors prepared with chemically synthesized PPy and re-anodized at different conditions: a) in 1% H_3PO_4, b) in 0.1 M $PhB(OH)_2$/SSA, and c) in 0.1 M H_3BO_3/SSA.

are shown in Figure 4.8 and the results are summarized in Table 4.2. These results indicate that $H_2PO_4^-$ is incorporated as the dopant ion in the matrix, as evidenced by the decrease of the sulfur to nitrogen (S/N) ratio and an increase of the phosphorous to nitrogen (P/N) ratio, while the total doping level (S + P/N ratio) remained unchanged. The doping level (S/N ratio) is not affected by the re-anodization process carried out in H_3BO_3/SSA or $PhB(OH)_2$/SSA electrolytes, indicating that the AQS^- is retained as the dopant ion. This was subsequently confirmed by UV-Vis spectroscopy. Figure 4.9 shows the spectra of the re-anodization solution before and

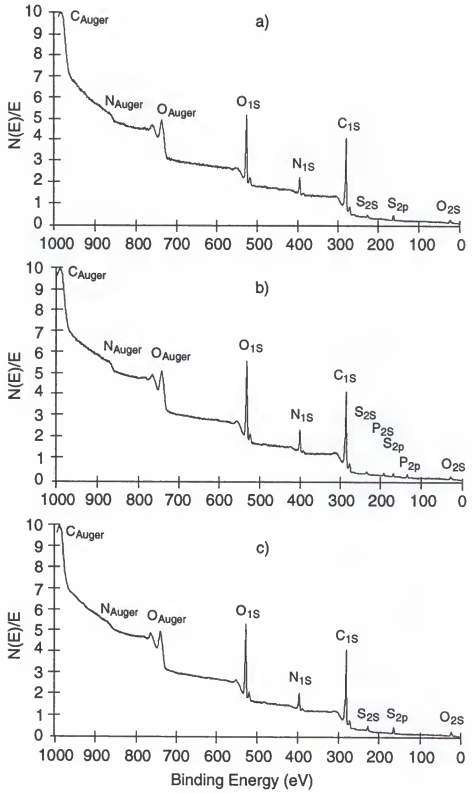

Figure 4.8. XPS spectra of $Ta/Ta_2O_5/PPy$ foils: a) before re-anodization, b) after re-anodization in H_3PO_4, and c) after re-anodization in H_3BO_3.

Table 4.2. XPS results for PPy/AQS films.

Sample	S/N	P/N	S+P/N
Ta/Ta_2O_5/PP before re-anodization	0.237	--	--
Ta/Ta_2O_5/PP after re-anodization in H_3PO_4	0.0852	0.153	0.238
Ta/Ta_2O_5/PP after re-anodization in H_3BO_3	0.245	--	--

after the re-anodization process in H_3BO_3/SSA and H_3PO_4. As can be seen the spectra in Figures 4.9a and 4.9b are almost identical showing that no AQS^- has been released to the electrolytic solution (absence of the characteristic peak at 255 nm), while the spectra in Figure 4.9c shows the presence of AQS^- in the solution after been release from the PPy/AQS coating film of the capacitors.

The DF is also affected by the synthetic conditions used for the preparation of PPy as illustrated in Figure 4.10. This work confirms previous observations that low temperature, and the addition of *p*-nitrophenol, yields the best conditions under which to synthesize PPy and obtain capacitors with optimum performance.[178]

Figure 4.11 show the leakage current (LC) as a function of the applied voltage for capacitors prepared chemically and re-anodized under different conditions. These results shows that the LC is higher and increases more quickly for

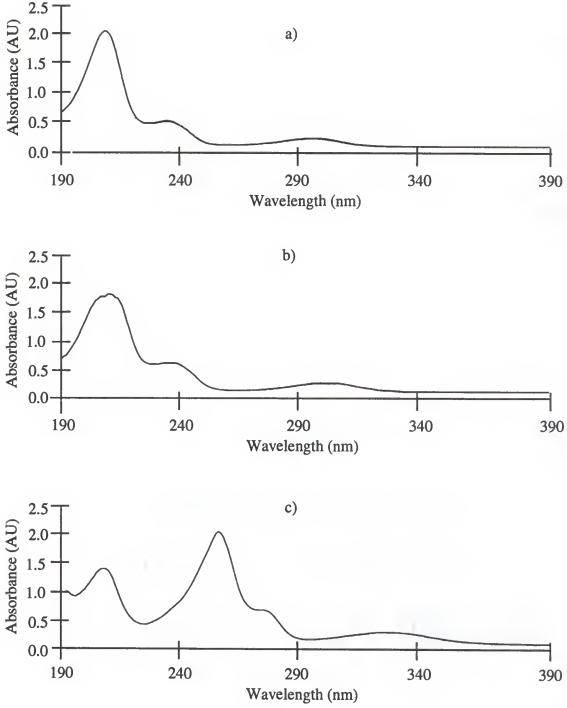

Figure 4.9. UV-Vis spectra of a) 0.1 M H_3BO_3/SSA solution before re-anodization, b) solution after re-anodization in 0.1 M H_3BO_3/SSA, and c) solution after re-anodization in 1% H_3PO_4.

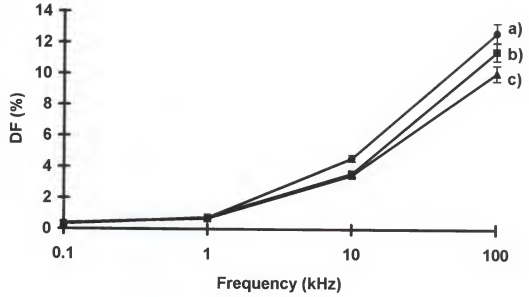

Figure 4.10. DF vs. frequency for capacitors prepared with chemically synthesized PPy under different synthetic conditions: a) room temperature, b) room temperature and *p*-nitrophenol, and c) 3-5 °C and *p*-nitrophenol.

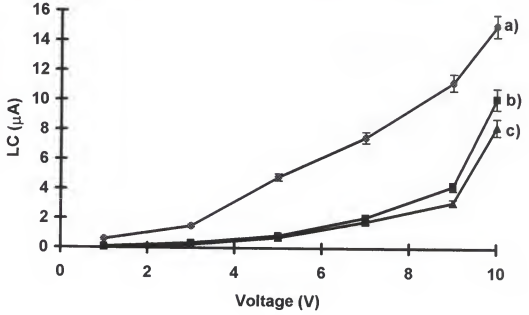

Figure 4.11. LC vs. voltage for capacitors prepared with chemically synthesized PPy and re-anodized at different conditions: a) in 1% H_3PO_4, b) in 0.1 M $PhB(OH)_2$/SSA, and c) in 0.1 M H_3BO_3/SSA.

capacitors re-anodized in H_3PO_4 than for capacitors re-anodized in H_3BO_3 or $PhB(OH)_2$. This is in agreement with the behavior of the DF discussed above. Figure 4.12 shows that there is a minor difference in LC properties between capacitors prepared with and without the electrochemical coating. This further confirms the similarities of the electrochemical properties of both PPy's. Figure 4.13 shows the LC as a function of the applied voltage for capacitors prepared chemically under different conditions, the results indicate that a PPy with better properties is obtained at low temperature and with the addition of *p*-nitrophenol. This is confirmed by the lowest series resistance, shown in Figure 4.14, for the PPy obtained at low temperature and with the addition of *p*-nitrophenol. It is evident that a higher conductivity of the PPy prepared under the conditions leads to enhanced capacitor performance.

Finally, the stability of the capacitors were tested by measuring the dielectric properties at 100 Hz as a function of time. Figure 4.15 shows the changes of capacitance and DF with time. The capacitance and DF increase only slightly during a period of 90 days. The almost constant capacitance is attributed to the high stability of PPy doped with aromatic sulfonates, and the small increase is attributable to a slight amount of moisture intake of the capacitors.

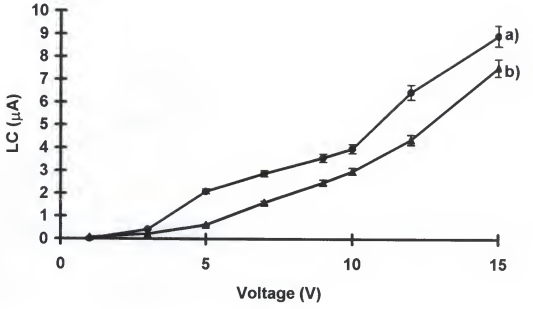

Figure 4.12. LC vs voltage for capacitors: a) prepared with chemically synthesized PPy ,and b) with prepared with chemically plus electrochemically synthesized PPy.

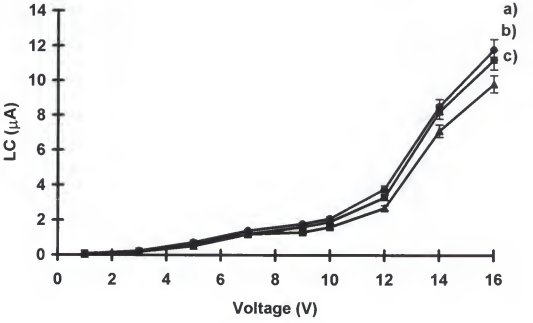

Figure 4.13. LC vs. voltage for capacitors prepared with chemically synthesized PPy under different synthetic conditions: a) room temperature, b) room temperature and *p*-nitrophenol, and c) 3-5 °C and *p*-nitrophenol.

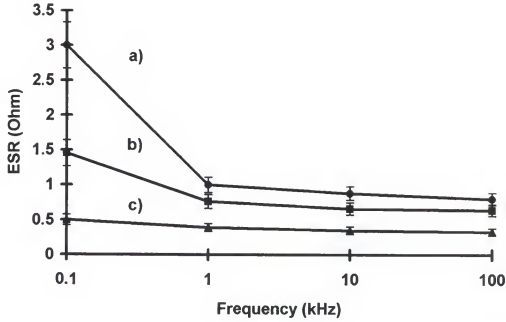

Figure 4.14. ESR vs. frequency for capacitors prepared with chemically synthesized PPy under different synthetic conditions: a) room temperature, b) room temperature and *p*-nitrophenol, and c) 3-5 °C and *p*-nitrophenol.

4.5. Conclusions

Conductive polymer tantalum solid electrolyte capacitors have been prepared with good high frequency performance and stability. The replacement of MnO_2 with PPy significantly reduces ESR due to the higher conductivity of PPy. The PPy capacitors show similar performance using PPy prepared either chemically or electrochemically, indicating that the elimination of an electrochemical coating process is possible without detrimental effects on capacitors properties. The re-anodization conditions are important in order to obtain

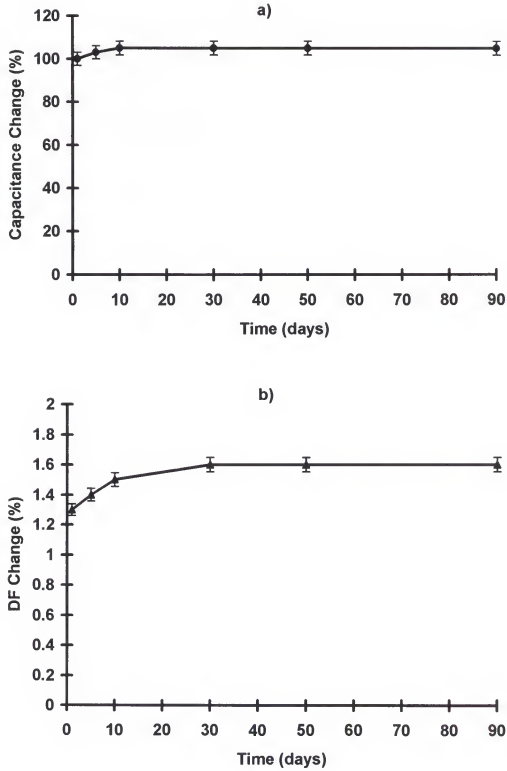

Figure 4.15. Stability of capacitors as a function of time: a) capacitance retention, and b) DF retention.

capacitors with stable properties. It is essential that the re-anodization process does not affect the doping level of the PP as is the case with H_3BO_3/SSA acid electrolytes. Finally, the addition of *p*-nitrophenol and the use of low temperatures during the synthesis of PP are useful in order to obtain a PP coating with better conductivity and consequently capacitors with lower ESR.

LIST OF REFERENCES

1) a) Chiang, C.K.; Park, Y.W.; Heeger, A.J.; Shirakawa, H.Louis, E.J.; MacDiarmid, A.G., *Phys. Rev. Lett.* **1977**, 39, 1098.
b) MacDiarmid, A.G.; Heeger, A.J. *Synth. Met.* **1978**, 1, 1013.

2) Ito, T.; Shirakawa, H.; Ikeda, S. *J. Polym. Sci., Pol. Chem.* **1974**, 12, 11.

3) a) White, D.; Bott, D.C. *Polym. Commun.* **1984,** 25, 98.
b) Edwards, J.H.; Feast, W.J.; Bott, D.C. *Polymer* **1984**, 25, 395.
c) Baker, G.L; Bates, F.S. *Macromolecules* **1984**, 17, 2619.
d) Feast, W.J.; Winter, J.N. *J. Chem. Soc., Chem. Commun.* **1985**, 202.
e) Naarmann, H. *Synth. Met.* **1987**, 17, 223.
f) Tanaka, H.; Danno, T. *Synth. Met.* **1987**, 17, 545.
g) Klaveter, F.L.; Grubbs, R.H. *J. Am. Chem. Soc.* **1988**, 110, 7807.
h) Stowell, J.A.; Amass, A.J.; Beevers, M.S.; Farren, T.R. *Makromol. Chem.* **1987**, 188, 1635.
i) Swager, T.M.; Dougherty, D.A.; Grubbs, R.H. *J. Am. Chem. Soc.* **1988**, 110, 2973.
j) Ginsburg, E.J.; Gorman, C.B.; Marder, S.R.; Grubbs, R.H. *J. Am. Chem. Soc.* **1989**, 111, 7621.
k) Gorman, C.B.; Ginsburg, E.J.; Grubbs, R.H. *J. Am. Chem. Soc.* **1993**, 115, 1397.
l) Akagi, K.; Sakamaki, K.; Shirakawa, H. *Synth. Met.* **1993**, 55, 779.
m) Reibel, D.; Nuffer, R.; Mathis, C. *Synt. Met.* **1993**, 55, 791.

4) Reynolds, J.R. *Chemtech.* **1988**, 18, 440.

5) a) MacDiarmid, A.G.; Heeger, A.J. *Synth. Met.* **1979**, 1, 101.
b) Wegner, G. *Angew. Chem. Int. Ed. Eng.* **1981**, 20, 361.
c) Baughman, R.H. *Contemp. Topics in Pol. Sci.* **1984**, 5, 321.
d) Greene, , R.L.; Street, G.B. *Science*, **1984**, 226, 651.
e) Reynolds, J.R. *J. Mol. Elec.* Dekker: New York, **1986**, vol 1 & 2, 757.
f) *Handbook of Conducting Polymers,* Skotheim, T.A., Ed. Marcel Dekker: New York, **1986**, vol 1 & 2.

g) Patil, A.O.; Heeger, A.J.; Wudl, F. *Chem. Rev.* **1988**, 88, 183.
h) Kanatzidis, M.G. *Chem. Eng. News* **1991**, 68 (49), 36.
i) Reynolds,J.R.; Child, A.D.; Gieselman, M.B. *Kirk-Othmer Encyclopedia of Chemical Technology*. Wiley: New York, 4th ed., vol. 9, **1993.** p. 61-87.
j) Toshima, N.; Hara, S. *Prog. Polym. Sci.* **1995,** 20, 155.

6) a) Diaz, A.F.; Kanazawa, K.K.; Gardini, G.P. *J. Chem. Soc., Chem. Commun.* **1979**, 635.
b) Kanazawa, K.K.; Diaz, A.F.; Geiss, R.H.; Gill, W.D.; Kwak, J.F.; Logan, J.A.; Rabolt, J.F.; Street, G.B. *J. Chem. Soc., Chem. Commun.* **1979**, 854.
c) Diaz, A.F.; Martinez, A.; Kanazawa, K.K.; Salmon, M. *J. Electroanal. Chem.* **1981**, 130, 181.
d) Asavapiriyanont, G.K.; Chandler, G.K.; Gunawardena, G.A.; Pletcher, D. *J. Electroanal. Chem.* **1984**, 177, 229.
e) Otero, T.F.; Tejada, R.; Elola, A.S. *Polymer* **1987**, 28, 651.

7) a) Tourillon, F.; Garnier, F. *J. Electroanal. Chem.* **1982**, 135, 173.
b) Tourillon, F.; Garnier, F. *J. Electroanal. Chem.* **1984**, 161, 407.

8) a) Jen, K.Y.; Jow, T.R.; Elsenbaumer, R.L. *J. Chem. Soc., Chem. Commun.* **1987**, 1113.
b) Nishioka, Y.; Wang, S.; Yoshino, K. *Synth. Met.* **1991**, 41-43, 815.
c) Glenis, S.; Benz, M.; LeGoff, E.; Schindler, J.L.; Kannewurf, C.R.; Kanatzidis, M.G. *J. Am. Chem. Soc.* **1993**, 115, 12519.

9) a) Diaz, A.F.; Logan, J.A. *J. Electroanal Chem.* **1980**, 111, 111.
b) MacDiarmid, A.G.; Chiang, J.C.; Halpern, M. Huang, H.S.; Mu, S.L.; Somarisi, N.L.D.; Wu, W.; Yaniger, S.I. *Mol. Cryst. Liq. Cryst.* **1985**, 121, 181.
c) Genies, E.M.; Tsintavis, C.; Syed, A.A. *Mol. Cryst. Liq. Cryst.* **1985**, 121, 181.
d) Genies, E.M.; Tsintavis, C. *J. Electroanal. Chem.* **1985**, 195, 109.
e) Lacroix, J.C.; Kanazawa, K.K.; Diaz, A.F. *J. Electrochem. Soc.* **1989**, 136, 1308.

10) Bargon, J.; Mohamed, S.; Waltman, K.J. *Mol. Cryst. Liq. Cryst.* **1983**, 93, 279.

11) Waltman, R.J.; Bargon, J.; Diaz, A.F. *J. Phys. Chem.* **1984**, 88, 4343.

12) Bargon, J.; Mohamed, S.; Waltman, R.J. *IBM J. Res. Develop.* **1983**, 27, 330.

13) a) Waltman, R.J.; Bargon, J. *Can. J. Chem.* **1986**, 64, 76.
b) Fukuda, M.; Sawada, K.; Morita, S.; Yoshino, K. *Synth. Met.* **1991**, 41-43, 855.
c) Berthelot, J.R.; Simonet, J. *J. Electrochem. Soc.* **1985**, 182, 187.

14) a) Ivory, P.M.; Miller, G.G.; Sowa, J.M.; Shacklette, L. W.; Chance, R.R.; Baughman, R.H. *J. Chem. Phys.* **1979**, 71, 1506.
b) Eckhardt, H.; Shacklette, L.W.; Elsenbaumer, R.L. *J.Chem. Phys.* **1989**, 91. 1303.

15) Zotti, G.; Schiavon, G. *Synt. Met.* **1992**, 47, 193.

16) Dietrich, M.; Heinze, J.; Heywang, G.; Jonas, F. *J. Electroanal. Chem.* **1994**, 369, 87.

17) a) Waltman, R.J.; Diaz, A.F.; Bargon, J. *J. Electrochem. Soc.* **1984**, 31, 1452.
b) Andrieux, C.P.; Audebert, P. *J. Electroanal. Chem.* **1990**, 285, 163.
c) Torres, W.; Fox, M.A. *Chem. Mat.* **1990**, 2, 158.
d) Delabouglise, D.; Roncali, J.; Lemaire, M.; Garnier, F. *J. Chem. Soc., Chem. Commun.* **1989**, 475.
e) Ruiz, J.P.; Child, A.D.; Nayak, K.; Marynick, D.S.; Reynolds, J.R. *Synth. Met.* **1991**, 41-43, 783.
f) Musmanni, S.; Ferraris, J.P. *J. Chem. Soc., Chem. Commun.* **1993**, 172.

18) a) Sato, M.; Tanaka, S.; Kaeriyama, K. *J. Chem. Soc., Chem. Commun.* **1986**, 873.
b) Elsenbaumer, R.L., Jen, K.Y.; Miller, G.G.; Schacklette, L.W. *Synth. Met.* **1987**, 18, 277.
c) Roncali, J. *Chem. Rev.* **1988**, 92, 711.

19) Reynolds, J.R.; Ruiz, J.P.; Child, K.; Nayak, K.; Marynick, D.S. *Macromolecules* **1991**, 24, 678.

20) a) Reynolds, J.R.; Katritzky, A.R.; Soloducho, J.; Belyakov, S.; Sotzing, G.A.; Pyo, M. *Macromolecules* **1994**, 27, 7225.
b) Irvin, J.A.; Reynolds, J.R., *Polym. Prep.* **1996**, 37, 682.
c) Reddinger, J.L.; Sotzing, G.A.; Reynolds, J.R. *Chem. Commun.* **1996**, 1777.
d) Sotzing, G.A.; Reynolds, J.R.; Steel, P.J. *Chem. Mat.* **1996**, 8, 882.

21) Naoi, K.; Lien, M.; Smyrl, W.H. *J. Electrochem. Soc.*, **1991**, 138, 440.

22) John, R.; Wallace, G.G. *J. Electroanal. Chem.*, **1993**, 354,145.

23) Reynolds, J.R.; Pyo, M.; Qiu, Y.J. *Synth. Met.*, **1993**, 55-57, 1388.

24) Baughman, R.H. *Makromol. Chem., Macromol. Symp.*, **1991**, 51, 193.

25) a) Schacklette, L.W.; Jow, T.R.; Maxfield, M.; Hatami, R.H. *Synth. Met.*, **1989**, 28, C655.
b) Matsunaga, T.; Daifuku, H.; Nakajima, T.; Kawagoe, T. *Polymers for Adv. Technol.* **1990**, 1, 33.

26) Baughman, R.H.; Schacklette, L.W.; Elsenbaumer, R.L.; Plichta, E.; Becht, C. *Conjugated Polymeric Materials: Opportunities in Electronics, Optoelectronics and Molecular Electronics*, Bredas, J.L. Chance, R.R., Eds. Kluwer: Boston, **1990.** p. 559-82.

27) a) Akhtar, M.H.; Weaklien, W.; Paiste, R.M.; Gaughan, K. *Synth. Met.* **1988**, 26, 203.
b) Yoneyama, H.; Wakamoto, K.; Tamura, H. *Materials Chemistry and Physics* **1986**, 15, 917.
c) Sapp, S.; Sotzing, G.A.; Reddinger, J.L.; Reynolds, J.R. *Polym. Prep.* **1996**, 37, 797.
d) Panero, S.; Passerini, S.; Scrosati, B. *Mol. Cryst. Liq. Cryst.* **1993**, 229, 97.
e) Hyodo, K. *Electrochim. Acta* **1994**, 39, 265.
f) Potomber, R.S.; Hoffman, R.C.; Hu, H.S.; Coccihiaro, J.E.; Viands, C.A.; Murphy, R.A.; Poehler, T.O. *Polymer* **1987**, 28, 574.

28) Colaneri, N.F.; Schaklette, L.W. *IEEE Trans. Intr. Meas.*, **1992**, 41, 291.

29) a) Shimidzu, T.; Ohtani, A.; Honda, K. *J. electroanal. Chem.* **1988**, 251, 323.
b) Deinhammer, R.; Shimazu, K.; Porter, M.R. *Anal. Chem.* **1991**, 63, 1989.
c) Ge, H.; Gilmore, K.; Ashrab, A.; Too, C.O.; Wallace, G.G.; *J. Liq. Chromatog.* **1993**, 16, 95.
d) Zinger, B.; Miller, L.L. *J. Am. Chem. Soc.* **1984**, 106, 6861.

30) a) Nishizawa, M.; Matsue, T.; Uchida, I. *Anal. Chem.* **1992**, 64, 2642.
b) Teasdale, P.R.; Wallace, G.G. *Analyst* **1993**, 118, 329.
c) Schuhmann, W. *ACS Symp. Ser.* **1994**, 556, 110.
d) Barlett, P.N.; Birkin, P.R. *Anal. Chem.* **1994**, 66, 1552.

31) a) Wipf, D.; Kristensen, E.; Deakin, M.R.; Wightman, R.M. *Anal. Chem.* **1988**, 60, 306.
b) Andrieux, C.P.; Audebert, P.; Hapiot, P.; Saveant, J.M. *J. Am. Chem. Soc.* **1990**, 112, 2439.

32) Heeger, A.J. *Mol. Cryst. Liq. Cryst.* **1985**, 125, 289.

33) a) Oudard, J.F.; Allendoerfer, R.D.; Osteryoung, R.A. *J. Electroanal. Chem.*, **1988**, 241, 231.
b) Child, A.D.; Reynolds, J.R. *J. Chem. Soc., Chem. Commun.* **1991**, 24, 1780.

34) Buttry, D.A.; Ward, M.D. *Chem. Rev.* **1991**, 92, 1355

35) Reynolds, J.R.; Hsu, S.G. *J. Polym. Sci.: Part B: Polym. Physics* **1989**, 27, 2081.

36) Wielder, H.H. Mat. *Sci. Monographs 2*, Elsevier, Amsterdam, **1979**. p. 6-12.

37) a) Hoffmann, R. *Angew. Chem. Int. Ed. Engl.* **1987**, 220, 351.
b) Chance, R.R.; Boudreaux, D.S.; Bredas, J.L.; Silbey, R. in *Handbook of Conducting Polymers*, Skothein, T.A., Ed. Dekker: New York, **1986**, vol. 2. p. 285.

38) Bredas, J.L.; Street, G.B. *Acc. Chem. Res.* **1985**, 18, 309.

39) Ikehata, S.; Kaufer, J.; Woerner, T.; Pron, A.; Dury, M.A.; Sivak, A.; Heeger, A.J.; MacDiarmid, A.G. *Phys. Rev. Lett.* **1980**, 45, 423.

40) a) Peo, M.; Roth, S.; Dransfeld, K.; Tieke, B.; Hocker, J.; Gross, H.; Grupp, A.; Sixl, H. *Solid State, Commun.* **1980**, 35, 119.
b) Kaufman, J.H.; Colaneri, N.; Scott, J.C.; Kanazawa, K.K.; Street, G.B. *Mol. Cryst. Liq. Cryst.* **1985**, 118, 171.

41) a) Scott, J.C.; Krounbi, M.; Pfluger, P.; Street, G. B. *Phys. Rev. B.* **1983**, 28, 2140.
b) Scott, J.C.; Bredas, J.L.; Pfluger, P.; Yakushi, K.; Street, G.B. *Synth. Met.* **1984**, 9, 154.

42) Scott, J.C.; Bredas, J.L.; Kaufman, J.H.; Pfluger, P.; Street, G.B.; Yakushi, K. *Mol. Cryst. Liq. Cryst.* **1985**, 118, 163.

43) Zotti, G.; Shiavon, G. *Chem. Mat.* **1991**, 3, 62.

44) Bredas, J.L. *Synth. Met.* **1987**, 17, 115.

45) Su, W.P. in *Handbook of Conducting Polymers*, Skothein, T.A., Ed. Dekker: New York, **1986**, vol. 2. p. 757.

46) a) Heeger, A.J.; Kivelson, S.; Schriffer, J.R.; Su, W.P. *Rev. Mod. Phys.* **1988**, 60, 781.
b) Bredas, J.L. *Mol. Cryst. Liq. Cryst.* **1985**, 118, 49.

c) Bredas, J.L.; Themans, B.; Andre, J.M. *Phys. Rev. B.* **1983**, 27, 7827.

47) Gardini, G.P. *Adv. Heterocyclic Chem.* **1973**, 15, 767.

48) a) Street, G.B.; Clarke, T.C.; Krounbi, M.; Kananzawa, K. K.; Lee, V.; Pfluger, P.; Scott, J.C.; Weiser, G. *Mol. Cryst. Liq. Cryst.* **1982**, 83, 1285.
b) Shimidzu, T.; Othani, A.; Iyoda, T.; Honda, K. *J. Chem. Soc., Chem. Commun.* **1986**, 1414.

49) Warren, L.F.; Walker, J.A.; Anderson, D.P.; Rhodes., C.G.; Buckley, L.J. *J. Electrochem. Soc.* **1989**, 136, 2286.

50) Baughman, R.H. *Makromol. Chem., Macromol. Symp.* **1991**, 51, 193.

51) Satoh, M.; Kaneto, K.; Yoshino, K. *Synth. Met.* **1986**, 14, 286.

52) a) Rosseinsky, D.R.; Morse, N.J.; Slade, R.C.; Hix, G.B.; Mortimer, R.J.; Walton, D.J. *Electrochim. Acta* **1991**, 36, 733.
b) Schlenoff, J.D.; Xu, H. *J. Electrochem. Soc.* **1992**, 139, 2397.

53) Haimerl, A.; Mertz, A. *J. Electroanal. Chem.* **1987**, 220, 55.

54) Zinger, B. *J. Electroanal. Chem.* **1988**, 244, 115.

55) LaCroix, J.C.; Diaz, A.F. *J. Electrochem. Soc.* **1988**, 135, 1457.

56) Heywang, G.; Jones, F. *Adv. Mat.* **1992**, 4, 116.

57) a) Otero, T.F.; Rodriguez, J. *Synth. Met.* **1992**, 51, 307.
b) Downard, A.J.; Pletcher, D. *J. Electroanal. Chem.* **1986**, 206, 139.

58) Diaz, A.F.; Bargon, J. in *Handbook of Conducting Polymers*, Skothein, T.A., Ed. Dekker: New York, **1986**, vol. 1. p. 82.

59) Salmon, M.; Diaz, A.F.; Logan, A.J. Krounbi, M. *Liq. Cryst.* **1982**, 83, 265.

60) a) Baker, C.K.; Qiu, Y.J.; Reynolds, J.R. *J. Phys. Chem.* **1991**, 95, 4446.
b) Qiu, Y.J.; Reynolds, J.R. *Pol. Eng. Sci.* **1991**, 31, 417.
c) Qui, Y.J.; Reynolds, J.R. *J. Pol. Sci. Pol. Chem.* **1992**, 30, 1315.

61) a) Wernet, W.; Monkenbush, M. Wegner, G. *Mol. Cryst. Liq. Cryst.* **1985**, 118, 193.
b) Kiani, M.S.; Mitchell, G.B. *Synth. Met.* **1992**, 48, 203.
c) Wynne, K.J.; Street, G.B. *Macromolecules*, **1985**, 18, 2361.
d) Belanger, D.; Laperriere, G.; Gravel, L. *J. Electrochem. Soc.* **1990**, 137, 395.
e) Ye, F.; Noftle, R.E.; DesMarteau, D.D. *Synth. Met.* **1993**, 60, 141.

62) Reynolds, J.R.; Hsu, S.G.; Arnott, H.J. *J. Pol. Sci. Pol. Phys.* **1989**, 27, 2081.

63) a) Bates, N.; Cross, M.; Lines, R.; Walton, D.J. *J. Chem. Soc., Chem. Commun.* **1985**, 871.
b) Shimidzu, T.; Ohtani, A.; Iyoda, T.; Honda, K. *J. Chem. Soc., Chem. Commun.* **1986**, 1415.
c) Noftle, R.E.; Pletcher, D. *J. Electroanal. Chem.* **1987**, 227, 229.
d) Gieselman, M.B.; Reynolds, J.R. *Macromolecules* **1990**, 23, 3118.
e) Fan, F.F.; Bard, A.J. *J. Electrochem. Soc.* **1987**, 133, 301.
f) Glatzhofer, D.T.; Ulanski, J.; Wegner, G. *Polymer* **1987**, 134, 101.
g) Miller, L.L.; Zhou, Q.X.; *Macromolecules*, **1987**, 20, 1554.
h) Warren, L.F.; Anderson, D.P. *J. Electrochem. Soc.* **1987**, 134, 101.
i) Buckly, L.J.; Roylance, D.K.; Wnek, G.E. *J. Pol. Sci. B.* **1987**, 25, 2178.
j) Kuwabata, S. Okamoto, K.; Yoneyama, H. *J. Chem. Soc. Faraday Trans.* **1988**, 84, 2317.

64) a) Raymond, D.E.; Harrison, D.J. *J. Electroanal. Chem.* **1993**, 361, 65.
b) Tanaka, K.; Shichiri, T.; Wang, S.; Yanabe, T. *Synth. Met.* **1988**, 24, 203.
c) Andrieux, C.P.; Audebert, P.; Hapiot, P.; Savéant, J.M. *J. Am. Chem. Soc.* **1990**, 112, 2439.
d) Andrieux, C.P.; Audebert, P.; Hapiot, P.; Savéant, J.M. *Synth. Met.* **1991**, 41-43, 2877.
e) John, R.; Wallace, G.G. *J. Electroanal. Chem.* **1991**, 306, 157.

65) a) Scharifker, B.R.; Garcia-Paztoriza, E.; Marino, W. *J. Electroanal. Chem.* **1991**, 300, 85.
b) Lowen, S.V.; Van Dike, J.D. *J. Pol. Sci. Pol. Chem.* **1990**, 28, 451.

66) a) Waltman, R.J.; Bargon, J. *Tetrahedron* **1984**, 40, 3963.
b) Tanaka, K.; Shichiri, T.; Toriumi, M.; Yamabe, T. *Synth. Met.* **1989**, 30, 271.

67) Genies, E.M.; Bidan, G.; Diaz, A.F. *J. Electrochem. Soc.* **1983**, 149, 101.

68) a) Fermin, D.J.; Scharifker, B.R. *J. Electroanal. Chem.* **1993**, 357, 273.
b) Scharifker, B.R.; Fermin, D.J. *J. Electroanal. Chem.* **1994**, 365, 35.

69) a) Bruckenstein, S.; Sharkey, J.W. *J. Electroanal. Chem.* **1988**, 241, 211.
b) Raymond, D.E.; Harrison, D.J. *J. Electroanal. Chem.* **1991**, 306, 157.

70) Fletcher, S.; Halliday, C.S.; Gates, D.; Westcott, M.; Lwin, T.; Nelson, G. *J. Electroanal. Chem.* **1983**, 159, 267.

71) Hillman, A.R.; Mallen, E.F. *J. Electroanal. Chem.* **1987**, 220, 351.

72) Onoda, M.; Nakayama, H.; Morita, S.; Yoshino, K. *Synth. Met.* **1993**, 55, 1343.

73) Okano, M.; Fujishima, A.; Honda, K. *J. Electroanal. Chem.* **1985**, 185, 393.

74) a) Fu, B.;Bakker, E.; Yun, Yang, V.C.; Meyerhofff, M.E. *Anal. Chem.* **1994**, 66, 2250.
b) Pyo, M.; Reynolds, J.R. *Chem. Mat.* **1996**, 8, 128.

75) Reynolds, J.R.;Pyo, M.; Qiu, Y.J.; *J. Electrochem. Soc.* **1994**, 141, 35.

76) a) Kaufmann, J.H.; Kanazawa. K.K.; Street, G.B. *Phys. Rev. Lett.* **1984**, 53, 2461.
b) Genies, E.M.; Pernaut, J.M. *Synth. Met.* **1984**, 10, 117.
c) Inoue, M.B.; Nebesny, K.W.; Fernando, Q.; Castillo-Ortega, M.A. *Synth. Met.* **1990**, 38, 205.
d) Miller, L.L.; Zinger, B.; Zhou, Q.X. *J. Am. Chem. Soc.* **1987**, 109, 2267.

77) a) Zhou, Q.Z; Kolaskie, C.J.; Miller, L.L. *J. Electroanal. Chem.* **1987**, 223, 283.
b) Lee, I.C. *J. Electroanal. Chem.* **1992**, 340, 333.
c) John, R.; Wallace, G.G. *J. Electroanal. Chem.* **1993**, 354, 145.
d) Shinonara, H.; Kojima, J.; Aizawa, M. *J. Electronal. Chem.* **1989**, 266, 297.
e) Hillman, A. R.; Swann, M.J.; Bruckenstein, S. *J. Electroanal. Chem.* **1990**, 291, 147.
f) Bruckenstein, S.; Wilde, C.P.; Shay, M.; Hillman, A.R. *J. Phys. Chem.* **1990**, 94, 787.

g) Hillman, A.R.; Loveday, D.C.; Swann, M.J.; Bruckenstein, S.; Wilde, C.P. *J. Chem. Soc. Faraday Trans.* **1991**, 87, 2047.
h) Lasky, S.; Buttry, D.A. *J. Am. Chem. Soc.* **1988**, 110, 6258.
i) Lien, M.; Smyrl, W.H. *J. Electroanal. Chem.* **1991**, 309, 333.
j) Zhong, C.; Dooblhofer, K. *Electrochim. Acta* **1990**, 35, 1971.
k) Chesher, D.A.; Christensen, P.A.; Hammett, A. *J. Chem. Soc. Faraday Trans.* **1993**, 89, 303.
l) Novak, P.; Kotz, R.; Hass, O. *J. Electrochem. Soc.* **1993**, 140, 37.
m) Barbero, C.; Miras, M.C.; Kotz, R. *Electrochim. Acta* **1992**, 37, 429.

78) a) Curtin, L.S.; Koplin, G.C.; Pietro, W. *J. Phys. Chem.* **1988**, 92, 12.
b) Tsai, E.W.; Pajkossy, T.; Rajeshwar, K.; Reynolds, J.R. *J. Phys. Chem.* **1988**, 62, 3560.
c) Schlenoff, J.B.; Chien, J.C.W. *J. Am. Chem. Soc.* **1987**, 109, 6269.

79) a) Hagen, G.; Thoresen, A.H.; Sunde, S.; Hesjevik, S.M.; Odegard, R. *Mol. Cryst. Liq. Cryst.* **1990**, 189, 213.
b) Abruna, H. *Coord. Chem. Rev.* **1988**, 86, 135.

80) a) Evans, D.H.; O'Connell, K.M.; Petersen, R.A.; Kelly, M.J. *J. Chem. Edu.* **1983**, 60, 291.
b) Kissinger, P.T.; Heineman, W.R. *J. Chem. Edu.* **1983**, 60, 703.

81) a) Bard, A.J.; Faulkner, L.R. *Electrochemical Methods, Fundamentals and Applications*, John Wiley & Sons, Inc.: New York, **1980**, p. 213-220.
b) Sawyer, D.T.; Sobkowiak, A.; Roberts, J.L. *Electrochemistry for Chemists*, 2nd Ed., John Wiley & Sons, Inc., New York, **1995**, p. 68-78.

82) a) Lane, R.F.; Hubbard, A.T. *J. Phys. Chem.* **1973**, 77, 1401.
b) Laviron, E. *J. Electroanal. Chem.* **1972**, 39, 1.

83) a) Laviron, E. *J. Electroanal. Chem.* **1979**, 105, 35.
b) Brown, A.P.; Anson, F.C. *Anal. Chem.* **1977**, 49, 1589.
c) Smith, D.F.; William, K.; Kuo, K.; Murray, R.W. *J. Electroanal. Chem.* **1979**, 95, 217.

84) Lennox, J.C.; Murray, R.W. *J. Am. Chem. Soc.* **1978**, 100, 3710.

85) a) Zhou, Q.X.; Miller, L.L.; Valentine, J.R. *J. Electroanal. Chem.* **1989**, 261, 147.

b) Daum, P.; Lenhard, J.R.; Rolison, D.R.; Murray, R.W. *J. Am. Chem. Soc.* **1980**, 102, 4649.
c) Laviron, E. *J. Electroanal. Chem.* **1980**, 112, 1.
d) Buttry, D.A.; Anson, F.C. *J. Electroanal. Chem.* **1981**, 130, 333.
e) Buttry, D.A.; Anson, F.C. *J. Am. Chem. Soc.* **1982**, 104, 4842.
f) Anson, F.C.; Saveant, J.C.; Shigehara, K. *J. Am. Chem. Soc.* **1983**, 105, 1096.
g) Martin, C.R.; Rubinstein, I.; Bard, A.J. *J. Am. Chem. Soc.* **1982**, 104, 4817.
h) Harrison, K.A.; Daube, K.A.; Wrigthon, M.S. *J. Electronal Chem.* **1984**, 163, 93.

86) a) Christie, J.; Lauer, G.; Osteryoung, R.A. *J. Electroanal. Chem.* **1964**, 7, 60.
b) Anson, F.C. *Anal. Chem.* **1966**, 38, 54.

87) West, K.; Jacobsen, T.; Zachau-Christiansen, B.; Careem, M.A.; Shaarup, S. *Synth. Met.* **1993**, 55, 1412.

88) a) Feldblum, A.; Kaufman, J.H. Etemad, S.; Heeger, A.J.; Chung, T.C.; MacDiarmid, A.G. *Phys. Rev. B.* **1982**, 26, 815.
b) Chung, T.C.; Kaufman, J.H.; Heeger, A.J.; Wudl, F. *Phys. Rev. B.* **1984**, 30, 702.
c) Glidle, A.; Hillman, A.R. *Chemistry in Britain* **1990**, 255.
d) Patil, A.O.; Heeger, A.J.; Wudl, F. *Chem. Rev.* **1988**, 88, 183.

89) a) Heeger, A.J. *Mol. Cryst. Liq. Cryst.* **1985**, 125, 289.
b) Sun, Z.W.; Frank, A.J. *J. Chem. Phys.* **1991**, 94, 4000.

90) a) McKinney, T.M. in Bard, A.J. (Ed.), *Electroanalytical Chemistry*. Marcel Dekker, New York, **1977**, vol. 10, p. 97.
b) Heineman, W.R.; Kissinger, P.T. *Laboratory Techniques in Electroanalytical Chemistry*, 2nd ed. Marcel Dekker, Inc.: New York, **1996**. p. 901-960.

91) a) Wertz, J.E.; Bolton, J.R. *Electron Spin Resonance, Elementary Theory and Practical Applications*. Chapman and Hall: New York, **1986**.
b) Drago, R. in *Physical Methods for Chemists*, 2nd ed. Saunders College Pub: Ft. Worth, **1992**, p. 360-363.

92) a) Genoud, M.; Guglielmi, M.; Nechtschein, M.; Genies, E.; Salmon, M. *Phys. Rev. Lett.* **1985**, 55, 118.
b) Nechtschein, M.; Devreux, F.; Genoud, F.; Vieil, E.; Pernault, J.M.; Genies, E. *Synth. Met.* **1986**, 15, 59.
c) Oudard, J.M.; Allendoerfer, R.D.; Osteryoung, R.A. *J. Electroanal. Chem.* **1988**, 241, 231.
d) Kruszka, J.; Nechtschein, M.; Sartier, C. *Rev. Sci. Instrum.* **1991**, 62, 695.

93) Saunders, B.R.; Fleming, R.J.; Murray, K.S. *Chem. Mat.* **1995**, 7, 1082.

94) a) Monkman, A.P.; Bloor, D.; Stevens, G.C.; Stevens, J.C.H.; Wilson, P. *Synth. Met.* **1989**, 29, E277.
b) Anand, J.; Palaniappan, S.; Sathyanarayama, D.N. *Synth. Met.* **1994**, 63, 43.
c) Anand, J.; Palaniappan, S.; Sathyanarayama, D.N. *J. Phys. Chem.* **1995**, 99, 10324.

95) Zotti, G.; Shiavon, G. *Synth. Met.* **1989**, 31, 347.

96) a) Ward, M.D.; Buttry, D.A. *Science*, **1990**, 249, 1000.
b) Buttry, D.A. in *Electroanalytical Chemistry. A Series of Advances*, Bard, A.J., Ed. Marcel Dekker: New York, **1991**, vol. 17. p. 1-85.
c) Schumacher, R. *Angew. Chem., Int. Ed. Engl.* **1990**, 29, 329.
d) Buttry, D.A.; Ward, M.D. *Chem. Rev.* **1992**, 92, 1355.

97) a) Guilbault, G.G.; Jordan, J.M. *CRC Crit. Rev. Anal. Chem.* **1988**, 19, 1.
b) Guilbault, G.G. *Ion Selective Rev.* **1980**, 2, 3.
c) McCallum, J.J. *Analyst* **1989**, 114, 1173.

98) a) Roederer, J.E.; Bastiaaans, G. J. *Anal. Chem.* **1983**, 55, 2333.
b) Ngwainbi, N.J.; Foley, P.H. Kuan, S.S.; Guilbault, G.G. *J. Am. Chem. Soc.* **1986**, 108, 5444.
c) Ebersole, R.C.; Ward, M.D. *J. Am. Chem. Soc.* **1988**, 110, 8623.
d) Lasky, S.J.; Buttry, D.A. *ACS Symp. Ser.* **1989**, 403, 237.
e) Ebersole, R.C.; Miller, J.A.; Moran, J.R.; Ward, M.D. *J. Am. Chem. Soc.* **1990**, 112, 3239.

99) a) Bruckenstein, S.; Swathirajan, S. *Electrochim. Acta* **1985**, 30, 851.
b) Schumacher, R.; Muller, A.; Stockel, W.J. *J. Electroanal. Chem.* **1987**, 219, 311.
c) Melroy, O.; Kanazawa, K.K.; Gordon, J.G.; Buttry, D.A. *Langmuir*, **1987**, 2, 697.
d) Deankin, M.R.; Melroy, O. *J. Electronal. Chem.* **1988**, 239, 321.

100) Ward, M.D. *J. Electroanal. Chem.* **1989**, 273, 79.

101) Baker, C.K.; Reynolds, J.R. *J. Electroanal. Chem.* **1988**, 251, 307.

102) a) Orata, D.; Buttry, D.A. *J. Am. Chem. Soc.* **1987**, 109, 3574.

b) Reynolds, J.R. Sundaresan, N.S.; Pomerantz, M.; Basak, S.; Baker, C.K. *J. Electroanal. Chem.* **1988**, 250, 355.
c) Borjas, R.; Buttry, D. *Chem. Mat.* **1991**, 3, 872.
d) Hillman, A.R.; Loveday, D.C.; Swann, M.J.; Bruckenstein, S.; Wilde, C.P. *Analyst* **1992**, 117, 1251.

103) Sauerbrey, G. *Z. Phys.* **1959**, 155, 206.

104) Ullevig, D.M.; Evans, J.M.; Albrecht, M.G. *Anal. Chem.* **1982**, 54, 2341.

105) Lu, C.S.; Lewis, O. *J. Appl. Phys.* **1972**, 43, 4385.

106) Kanazawa, K.K.; Gordon, J.G. *Anal. Chem.* **1985**, 57, 1770.

107) Bruckenstein, S.; Shay, M. *Electrochim. Acta* **1985**, 30, 1295.

108) Martin, S.J.; Granstaff, V.E.; Frye, G.C. *Anal. Chem.* **1991**, 63, 2272.

109) a) Benje, M.; Eiermann, M.; Pitterman, U.; Weil, K.G. *Ber. Bunsen-Ges. Phys. Chem.* **1986**, 90, 435.
b) Benje, M.; Hoffman, U.; Pitterman, U.; Weil, K.G. *Ber. Bunsen-Ges. Phys. Chem.* **1988**, 92, 1257.

110) a) Hager, H.E.; Ruedisueli, R.D.; Buehler, M.E. *Corrosion* **1986**, 42, 345.
b) Grzeyorzewski, A.; Hensler, K.E. *J. Electroanal. Chem.* **1987**, 228, 455.

111) Deakin, M.; Li, T.; Melroy, O. *J. Electroanal. Chem.* **1988**, 243, 343.

112) a) Gabrielli, C.; Huet, F.; Keddan, M.; Sahar, A. *J. Appl. Electrochem.* **1989**, 19, 617.
b) Gabrielli, C.; Huet, F.; Keddan, M.; Sahar, A. *J. Appl. Electrochem.* **1989**, 19, 683.

113) Ward, M.D. *Synth. Met.* **1988**, 27, B211.

114) a) Freund, M.S.; Brajter-Toth, A.; Ward, M.D. *J. Electroanal. Chem.* **1990**, 289, 127.
b) Larew, L.A.; Gordon, J.S.; Hsiao, Y.L.; Johnson, D.C.; Buttry, D.A. *J. Electrochem. Soc.* **1990**, 137, 3071.

115) a) Donohue, J.J.; Buttry, D.A. *Langmuir* **1989**, 5, 671.
b) Nordyke, L.; Buttry, D.A. *Langmuir* **1991**, 7, 380.
116) Kaufman, J.N.; Kanazawa, K.K.; Street, G.B. *Phys. Rev. Lett.* **1984**, 53, 2461.

117) a) Varinean, P.T.; Buttry, D.A. *J. Phys. Chem.* **1987**, 91, 1292.

b) Bruckenstein, S.; Hillman, A.R. *J. Phys. Chem.* **1988**, 92, 4837.
c) Hillman, A.R.; Loveday, D.C.; Bruckenstein, S. *Langmuir* **1991**, 7, 191.
d) Bruckenstein, S.; Wilde, C.P.; Shay, M.; Hillman, A.R.; Loveday, D.C. *J. Electroanal. Chem.* **1989**, 258, 457.

118) a) Hillman, A.R.; Loveday, D.C.; Bruckenstein, S.; Wilde, C.P. *J. Chem. Soc., Faraday Trans.* **1990**, 86, 437.
b) Bruckenstein, S.; Wilde, C.P.; Shay, M.; Hillman, A.R. *J. Phys. Chem.* **1990**, 94, 787.
c) Hillman, A.R.; Swann, M.J.; Bruckenstein, S. *J. Phys. Chem.* 1991, 95, 3271.
d) Bruckenstein, S.; Wilde, C.P. Hillman, A.R. *J. Phys. Chem.* **1990**, 94, 6458.
e) Bruckenstein, S.; Hillman, A.R.; Swann, M.J. *J. Electrochem. Soc.* **1990**, 137, 1323.

119) a) Feldman, B.J.; Melroy, O.R.; *J. Electroanal. Chem.* **1987**, 234,213.
b) Aoki, K.; Miyamoto, T.; Oshawa, Y. *Bull. Chem. Soc. Jpn.* **1989**, 62, 1658.
c) Deakin, M.R.; Byrd, H. *Anal. Chem.* **1989**, 61, 290.
d) Humphrey, B.D.; Sinha, S.; Bocarsly, A.B. *J. Phys. Chem.* **1984**, 88, 736.

120) Baker, C.K.; Reynolds, J.R. *Synth. Met.* **1989**, 28, C21.

121) a) Glarum, S.H.; Marshall, J.H.; *J. Phys. Chem.* **1986**, 90, 6076.
b) Daifuku, H.; Kawagoe, T.; Tamamoto, N.; Ohsaka, T.; Oyama, N. *J. Electroana. Chem.* **1989**, 274, 313.
c) Cordoba-Torresi, S.; Gabrielli, C.; Keddan, M.; Takenuoti, H.; Torresi, R. *J. Electroanal. Chem.* **1990**, 290, 269.
d) Rubinstein, I.; Rishpan, J.; Sabatini, E.; Redondo, A; Gottesfeld, S.; *J. Am. Chem. Soc.* **1990**, 112, 6135.
e) Orata, D.O.; Buttry, D.A. *J. Electroanal. Chem.* **1988**, 257, 71.

122) a) Servagent, S.; Vieil, E. *J. Electroanal. Chem.* **1990**, 280, 227.
b) Hillman, A.R.; Swann, M.J.; Bruckenstein, S. *J. Electroanal. Chem.* **1990**, 291, 147.
c) Hillman, A.R.; Swann, M.J. Bruckenstein, S. *J. phys. Chem.* **1991**, 95, 3271.

123) a) Borjas, R.; Buttry, D.A. *J. Electroanal. Chem.* **1990**, 280, 73.
b) Kipling, A.L.; Thompson, M. *Anal. Chem.* **1990**, 280, 73.

c) Vorotyntsev, M.A.; Daikhis, L.I.; Levi, M.D. *J. Electroanal. Chem.* **1994**, 364, 37.
d) Noel, M.A.; Topart, P.A. *Anal. Chem.* **1994**, 66, 484.

124) Lee, R.E. in *Scanning Electron Microscopy and X-Ray Microanalysis*. PRT Prentice Hall, Inc: Englewood Cliffs, NJ, **1993**.

125) Lawes, G. in *Scanning Electron Microscopy and X-Ray Micronalysis*, James, A., Ed. John Wiley & Sons: Chichester, **1987**.

126) a) Tourrillon, G.; Garnier, F. *J. Pol. Sci. Pol. Phys.* **1984**, 22, 33.
b) Tourrillon, G.; Garnier, F. *J. Phys. Chem.* **1984**, 88, 5281.

127) Ko, J.M.; Rhee, H.W.; Park, S.M.; Kim, C.Y. *J. Electrochem. Soc.* **1990**, 137, 905.

128) Cheung, K.M.; Bloor, D.; Stevens, G.C. *Polymer*, **1988**, 29, 1709.

129) Diaz, A.F.; Castillo, J.I.; Logan, J.A.; Lee, W.Y. *J. Electroanl. Chem.* **1981**, 88, 5281.

130) Wielder, H.H. in *Mat. Sci. Monographs 2*. Elsevier: Amsterdam, **1979**, p. 2-20.

131) a) Gregory, R.V.; Kimbell, W.C.; Kuhn, H.H. *Synth. Met.* **1989**, 28, C823.
b) Gregory, R.V.; Kimbell, W.C.; Kuhn, H.H. *J. Coated Fabrics* **1991**, 20, 1.

132) a) Thackery, J.W.; White, H.S.; Wrighton, M.S. *J. Phys. Chem.* **1985**, 89, 5133.
b) White, H.S.; Kittlesen, G.P.; Wrighton, M.S. *J. Am. Chem. Soc.* **1984**, 106, 5375.
c) Kittlesen, G.P.; White, H.S.; Wrigthon, M.S. *J. Am. Chem. Soc.* **1984**, 106, 7389.
d) Bloor, D. *Nature* **1991**, 349, 378.

133) a) Burroughs, J.H.; Bradley, D.D.C.; Brown, A.R.; Marks, R.N.; MacKay, K.; Friend, R.H.; Burns, P.L.; Holmes, A.B. *Nature* **1990**, 374, 539.
b) Burn, P.L.; Holmes, A.B.; Kraft, A.; Bradley D.D.C.; Brown, A.R.; Friend, R.H.; Gymer, R.W. *Nature* **1992**, 356, 47.
c) Gustafsson, G.; Cao, Y.; Treacy, G.M.; Klaveter, F.; Colaneri, N; Heeger, A.J. *Nature* **1992**, 357, 477.

134) McLean, D.A.; Power, F.S. *Proc. IRE*, **1965**, 44, 872.

135) Niwa, S. *Synth. Met.* **1987**, 18, 665.

136) a) Fukuyama, M.; Kudoh, Y.; Nanai, N.; Yoshimura, S. *Mol. Cryst. Liq. Cryst.* **1993**, 224, 61.
b) Yamamoto, H.; Fukuda, M. Isa, I.; Yoshino, K. *Mol. Cryst. Liq. Cryst.* **1993**, 227, 255.
c) Kudoh, Y.; Tsuchida, S.; Kojiyama, T.; Fukuyama, M.; Yoshimura, S. *Synth. Met.* **1991**, 41-43, 1133.
d) Krings, L.H.M.; Havinga, E.E.; Donkers, J.J.T.M.; Vork, F.T.A. *Synth. Met.* **1993**, 54, 453.

137) a) Nigrey, P.; MacDiarmid, A.G.; Heeger, A.J. *J. Am. Chem. Soc., Chem. Commun.* **1979**, 594.
b) Nigrey, P. MacInnes, D.; Nairns, D.D.; MacDiarmid, A.G. *J. Electrochem. Soc.* **1981**, 128, 1651.
c) Kaneto, K.; Maxfield, M. Nairns, D.P.; MacDiarmid, A.G. *J. Chem. Soc., Faraday Trans. I* **1982**, 78, 3417.
d) Kaner, R.; MacDiarmid, A.G., *J. Chem. Soc., Faraday Trans. I* **1984**, 80, 2109.

138) Nakajima, T.; Kawagoe, T. *Synth. Met.* **1989**, 28, C629.

139) Munstedt, H.; Kohker, G.; Monwald, H.; Naegele, D.; Bittin, R.; Ely, G.; Meissner, E. *Synth. Met.* **1987**, 18, 259.

140) Shacklette, L.W.; Maxfield, M.; Gould, S.; Wolf, J.F.; Jow, T.R.; Baughman, R.H. *Synth. Met.* **1987**, 18, 611.

141) Bjorklund, R.; Anderson, S.; Allenmark, S.; Lundstrom, I. *Mol. Cryst. Liq. Cryst.* **1985**, 121, 263.

142) a) Kobayashi, T.; Yoneyama, H.; Tamura, H. *J. Electroanal. Chem.* **1984**, 177, 281.
b) Kobayashi, T.; Yoneyama, H.; Tamura, H. *J. Electroanal. Chem.* **1984**, 117, 293.

143) a) Gustafsson, J.C.; Inganas, O.; Anderson, A.M. *Synth. Met.* **1994**, 62, 17.
b) Druy, M.A.; Seymour, R.J. *J. Phys. Col.* **1983,** C3, 595.
c) Mastragostino, A.; Marinangeli, A.M.; Conadidi, A.; Giacobbe, S. *Synth. Met.* **1989**, 28, C501.

144) Sotzing, G.A.; Reynolds, J.R.; Steel, P. *Chem. Mat.* **1996**, 8, 882.

145) a) Janata, J. *Anal. Chem.* **1994**, 66 207R.
b) Zotti, G. *Synth. Met.* **1992**, 51, 373.
c) Teasdale, P.R.; Wallace, G.G. *Analyst* **1993**, 118, 329.

146) a) Foulds, N.C.; Lowe, C.R. *J. Chem. Soc., Faraday Trans I* **1986**, 82, 1259.
b) Schuhmamm, W.; Krantz, C; Huber, J.; Wohlschlager, H. *Synth. Met.* **1993**, 61, 31

147) Umana, M.; Waller, J. *Anal. Chem.* **1986**, 58, 2979.

148) a) Schuhmann, W. *Synth. Met.* **1991**, 41-43, 1551.
b) Schuhmann, W. *Adv. Mat.* **1993**, 5, 124.
c) Lowe, C.R. *Anal. Chem.* **1992**, 64, 1541.

149) Schuhmann, W. *ACS Symp. Ser.* **1994**, 556, 112.

150) Ikariyama, Y.; Heineman, W.R. *Anal. Chem.* **1986**, 58, 1803.

151) a) Dong, S.; Sun, Z.; Lu, Z. *Analyst* **1988**, 113, 1525.
b) Pearson, J.F.; Slater, J. *Analyst* **1992**, 177, 188.
c) Okada, T. *Anal. Chim. Acta* **1992**, 266, 89.

152) Matsue, T.; *Trends in Anal. Chem.* **1993**, 12, 100.

153) a) Thackeray, J.; Wrighton, M.S. *J. Phys. Chem.* **1986**, 90, 6674.
b) Uchida, I. *Synth. Met.* **1991**, 45, 241.

154) Matsue, T. *J. Electronal, Chem.* **1991**, 300, 111.

155) Barlett, P.; Birkin, P. *Anal. Chem.* **1994**, 66, 1552.

156) Nishizama, M.; Matsue, T.; Uchida, I. *Anal. Chem.* **1992**, 64, 2642.

157) Miller, L.L.; Blankespoor, R.L.; Zinger, B. *U.S. Patent # 4,585,652,* **1984**.

158) a) Miller, L.L. *Mol. Cryst. Liq. Cryst.* **1988**, 160, 297.
b) Miller, L.L. in *Funct. Polym., Proc. Am. IUCCP Symp.* Bergreister, D.E., Ed. Plenum Press: New York, **1988**, p. 61-68.

159) a) Blankespoor, R.L.; Miller, L.L. *J. Am. Chem. Soc, Chem. Commun* **1985**, 90.
b) Zhou, Q.X.; Kolaski, C.J.; Miller, L.L. *J. Electroanal. Chem.* **1987**, 223, 283.
c) Miller, L.L.; Zinger, B.; Zhou, Q.X. *J. Am. Chem. Soc.* **1987**, 109, 2267.
d) Chang, A.C.; MIller, L.L.; *J. Electroanal. Chem.* **1988**, 247, 173.

160) a) Miller, L.L. Zhou, Q. X. *Macromolecules* **1987**, 20, 1594.
b) Valentine, J.R. Miller, L.L. *Pol. Prep.* **1988**, 29, 446.

c) Zhou, Q.X.; Miller, L.L.; Valentine, J.R. *J. Electroanal. Chem.* **1989**, 261, 147.

161) Hepel, M.; Fajalek, Z. *ACS Symp. Ser.* **1994**, 545, 79.

162) Pyo, M.; Maeder, G.; Kennedy, R.T.; Reynolds, J.R. *J. Electroanal. Chem.* **1994**, 368, 329.

163) Chiarelli, P.; DeRossi, D.; Della Santa, A.; Mazzoldi, A. *Polymer Gels and Networks* **1994**, 2, 289.

164) a) Chen, L.Y.; Zang, Z. L.; Yao, J.J.; Thomas, D.C.; MacDonald, N.C. *Microelectromechanical Systems, Proc. IEEE*, Ed. Jacobsen, S.C.; Petersen, K.E. **1989**. p. 82-87.
b) Pei, Q.; Inganas, O. *Synth. Met.* **1993**, 55-57, 3718.
c) DeRossi, D.; Chiarelli, P. *ACS Symp. Ser.* **1994**, 548, 517.

165) a) Diaz, A.F.; Crowly, J.; Bargon, J.; Gardini, G.P.; Torrance, J.B. *J. Electrochem. Soc.* **1981**, 121, 355.
b) Ferraris, J.P.; Skiles, G.D. *Polymer* **1987**, 28, 179.
c) Laguren-Davison, L.; Van Pham, C.; Zimmer, H.; Mark, H.B. *J. Electrochem. Soc.* **1988**, 135, 1406.
d) Hillman, A.R.; Swann, M. *J. Electrochim. Acta* **1988**, 33, 1303.
e) Ferraris, J.P.; Hanlon, T.R. *Polymer*, **1989**, 30, 1319.
f) Ferraris, J.P.; Andrus, R.G; Hrncir, D.C. *J. Chem. Soc., Chem. Commun.*, **1989**, 1318.
g) Raymond, D.E.; Harrison, D.J. *J. Electroanal. Chem.* **1990**, 296, 269.
h) Souto Maior, R.M.; Hinkelmann, K.; Eckert, H.; Wudl, F. *Macromolecules* , **1990**, 23, 1268.
i) Roncali, J.; Giffard, M.; Jubault, M.; Gorgues, A. *J. Electroanal. Chem.*, **1993**, 361, 185.
j) Glenis, S.; Benz, M.; LeGoff, E.; Schindler, J.L.; Kannewurf, C.R.; Kanatzidis, M.G. *J. Am. Chem.* **1993**,.115, 12519.
k) Joshi, M.V.; Cava, M.P.; Bakker, M.G.; McKinley, J.A.; Cain, J.L.; Metzger, R.M. *Synth. Met.* **1993**, 55-57, 948.
l) Musmanni, S.; Ferraris, J.P. *J. Chem. Soc., Chem. Commun.* **1993**, 172 .

166) Rehan, M.; Schluter, A.D.; Wegner, G.; Feast, W.J. *Polymer* **1989**, 30, 1060.

167) a) Reynolds, J.R.; Poropatic, P.A.; Toyooka, R.L. *Macromolecules* **1987**, 20, 958.
b) Bryce, M.R.; Chissel, A.D.; Smith, N.R.M.; Parker, D. *Synth. Met.* **1988**, 26, 153.
c) Sundaresan, N.S.; Basak, S.; Pomerantz, M.; Reynolds, J.R. *J. Chem. Soc., Chem. Commun.* **1987**, 621.

168) a) Souto-Maiour, R.; Wudl, F. *Synth. Met.* **1989**, 28, C281 .
b) Patil, A.O.; Ikenoue, Y.; Wudl, F. A.J. Heeger, *J. Am. Chem. Soc.* **1987**, 109, 1858.

169) a) Sato, M.; Tanaka, S.; Kaeriyama, K. *J. Chem. Soc. Chem., Commun.* **1986**, 15, 169.
b) Kobayashi, K.; Yin, X.H.; Ozaki, M.; Kawai, T.; Yoshino, K. *Synth. Met.* **1995**, 69, 597.
c) Gu, H.B.; Morita, S.; Yin, X.H.; Kawai, T.; Yoshino, K. *Synth. Met.* **1995**,.69, 449.

170) Hong, S.Y.; Marinick, D.S. *Macromolecules* **1992**, 25, 3591.

171) Ruiz, J.P.; Dharia, J.R.; Reynolds, J.R. Buckley, L.F. *Macromolecules* **1992**, 25, 849.

172) Reynolds, J.R.; Pomerantz, M.P. in *Electroresponsive Molecular and Polymeric Systems*. Marcel Dekker, Inc.: New York, **1991**, p. 187.

173) Roncali, J.; Garreau, R.; Yassar, A.; Marque, P.; Garnier, F.; Lemaire, M. *J. Phys. Chem.* **1987**, 91, 6706.

174) a) Leclerc, M; Diaz, F.M.; Wegner, G. *Makromol. Chem.* **1989**, 190, 3105.
b) Kaeriyama, K.; Tanaka, S.; Sato, M.; Hamada, M. *Synth. Met.* **1989**, 28, C611.
c) Roncali, J.; Shi, L.H.; Garreau, R.; Garnier, F.; Lemaire, M. *Synth. Met.* **1990**, 36, 267.

175) Tsai, E.W.; Basak, S.; Ruiz, J.P.; Reynolds, J.R.; Rajeshwar, K. *J. Electrochem. Soc.* **1989**, 136, 3683.

176) Reynolds, J.R.; Child, A.D.; Ruiz, J.P.; Hong, S.Y.; Marinick, D.S. *Macromolecules* **1993**, 26, 2095.

177) Marque, P.; Roncali, J. *J. Phys. Chem.* **1990**, 94, 8614.

178) a) Rapi, S.; Bocchi V.; Gardini, G.P. *Synth. Met.* **1988**, 24, 217.
b) Fukuzama, M.; Nanai, N.; Kojima, T.; Kudoh, K.; Yoshimura, S. *Synt. Met.* **1993**, 58, 367.

BIOGRAPHICAL SKETCH

Fernando E. Larmat Gonzalez was born on May 31, 1958, in Santa Fe de Bogotá, Colombia. In the spring of 1978 he began his undergraduate education in chemistry at Universidad del Valle in Cali, Colombia. In 1984 he obtained his B.S.in chemistry. In the spring of 1985 he began his graduate studies and obtained his M.S. degree in physicalchemistry in 1987. Before entering the Ph.D. program at the University of Florida, he was employed at Universidad del Valle as an instructor and then as an assistant professor. Mr. Larmat will complete his Ph.D at the University of Florida in the spring of 1997 and will return to Universidad del Valle to continue his academic career.

I certify that I have read this study and that in my opinion it conforms to acceptable standards of scholarly presentation and is fully adequate, in scope and quality, as a dissertation for the degree of Doctor of Philosophy.

John R. Reynolds, Chair
Professor of Chemistry

I certify that I have read this study and that in my opinion it conforms to acceptable standards of scholarly presentation and is fully adequate, in scope and quality, as a dissertation for the degree of Doctor of Philosophy.

Anna Brajter-Toth
Associate Professor of Chemistry

I certify that I have read this study and that in my opinion it conforms to acceptable standards of scholarly presentation and is fully adequate, in scope and quality, as a dissertation for the degree of Doctor of Philosophy.

Kenneth B. Wagener
Professor of Chemistry

I certify that I have read this study and that in my opinion it conforms to acceptable standards of scholarly presentation and is fully adequate, in scope and quality, as a dissertation for the degree of Doctor of Philosophy.

James D. Winefordner
Graduate Research Professor of Chemistry

I certify that I have read this study and that in my opinion it conforms to acceptable standards of scholarly presentation and is fully adequate, in scope and quality, as a dissertation for the degree of Doctor of Philosophy.

Joseph H. Simmons
Professor of Material Sciences

This dissertation was submitted to the Graduate Faculty of the Department of Chemistry in the College of Liberal Arts and Sciences and to the Graduate School and was accepted as partial fulfillment of the requirements for the degree of Doctor of Philosophy.

May, 1997

_____

Dean, Graduate School